

Expression, Enzymatic Activity, and Inhibition of MMP-3 in C6-13 Rat Glioma Cells

By

Alisha Poole

Thesis submitted in partial fulfilment of the requirements for the degree of
Master of Science
Environmental and Life Sciences
Brandon University

© Alisha Poole
2018

Brandon University
FACULTY OF SCIENCE

The undersigned certify that they have read, and recommended to the Senate for acceptance, a **MASTER'S THESIS** entitled:

Expression, Enzymatic Activity, and Inhibition of MMP-3 in C6-13 Rat Glioma Cells

Submitted by: **Alisha Poole**

In partial fulfillment for the requirements for the degree of

MASTER OF SCIENCE (ENVIRONMENTAL AND LIFE SCIENCES)

Date:

12 - 21 - 2018

Month - Day - Year



Supervisor: Dr. V. Chen

Date:

12 - 21 - 2018

Month - Day - Year



Committee Member: Dr. M. Majumder

Date:

12 - 21 - 2018

Month - Day - Year



Committee Member: Dr. B. Hill

Date:

12 - 21 - 2018

Month - Day - Year

Jorg Stetefeld

Digitally signed by Jorg Stetefeld
DN: cn=Jorg Stetefeld, o=University of
Manitoba,
email=jorg.stetefeld@umanitoba.ca, c=CA
Date: 2019.01.02 17:31:24 -06'00'

External Examiner: Dr. J. Stetefeld

Abstract

Glioblastoma multiforme is the most aggressive form of brain cancer due to high rates of reoccurrence. Although >95% of a tumor can be removed with surgery, the invasiveness of gliomas frequently leads to the formation of tumors at secondary sites. The invasiveness of gliomas is in part due to their ability to secrete proteolytic enzymes, including members of the matrix metalloproteinase (MMP) family, that are involved with the remodeling of the extracellular matrix. In this study, MMP-3 expression and activity was found to be upregulated in C6-13 rat glioma cells that exogenously express the promigratory protein Cx43. Based on these findings, a panel of synthesized inhibitors were proposed and benchmarked against ilomastat, a known inhibitor of MMP-3. Binding ability of inhibitors to the MMP-3 active site was performed using in silico molecular docking. Ilomastat was chosen for further activity studies, in which MMP-3 was significantly inhibited. Findings presented in this thesis indicate that MMP-3 activity is upregulate in C6-13 rat glioma cells and can be significantly inhibited. MMP-3 inhibition may contribute to decreasing invasive potential of glioma cells.

Acknowledgements

These two years of my masters will be an experience I will never forget. First off, I would like to thank my supervisor Dr. Vincent Chen for accepting me into the lab, your excitement and dedication to research are inspiring and helped to motivate me to keep pushing through the tough times. I want to thank Dr. Bryan Hill for guiding me through the synthesis schemes and reaction mechanisms, I am always amazed at how effortlessly you can think of reaction mechanisms. To my final committee member Dr. Mousumi Majumder, thank you for all your support and guidance. Thank you to Dr. Eric Bushnell and Chris Sitko for your work on the in silico molecular docking. I would like to acknowledge the Canadian Institute for Health Research (CIHR) for providing funding to make this thesis possible via a Banting and Best CGS-M fellowship.

I could not have asked for a better lab group to be a part of. Thank you Emmanuel Ojefua for always being there to help bounce ideas off of and aid in solidifying protocols. Caitlin Le thank you for all of your help in the lab during the summer, your eagerness to learn motivated me to work harder myself. Nguyen Nguyen thank you for your stories, laughter, and also being the most amazing cook.

A major contributor to making my masters journey an amazing adventure were the MELS graduate students themselves. I entered the MELS program with an incredible group of people, I couldn't be prouder of the community and friendships we built. Thank you to Brandice Hollier, Alex Lowe, Mark Klapheke, Markus Sudermann, and Jillian Perreux for making this experience memorable, I can't wait for our MELS reunions. Special thanks to Gustavo Diaz Cruz, from teaching me about photography to teaching me how to become a better researcher, your endless support and friendship means the world to me.

I would also like to thank my boyfriend Graham Gilbert, who I met at the beginning of my masters. You have been incredibly patient and understanding throughout the struggles that accompany any masters. I look forward to whatever the future has in store for us.

Finally, I would like to thank my family, in particular my mom Debbie and sister Elise. You are both the most incredible, intelligent, independent, strong women I know. Every day I strive to be more and more like the both of you.

Preface

My role in this thesis was to further investigate the activity of MMP-3, design and synthesize novel MMP-3 inhibitors, and monitor the change MMP-3 activity upon inhibition. The cell lines used in this thesis (parental C6 and C6-13) were provided by Dr. Christian Naus at the University of British Columbia. I wrote the methods for the experiments I carried out, with the exception of the zymography protocol which was assisted by Emmanuel Ojefua. I used ImageJ to quantify Western blot, zymography, and scratch wound data. I interpreted the data I produced. I wrote the results and discussion for the data acquired. I made the figures pertaining to the experiments I performed.

Chapter 2: MMP-3 Expression & Activity in C6WT and C613 Cell Lines

All of the experiments in Chapter 2 were carried out by myself with the exception of the experiments described in Figure 2.1.2. These experiments were performed by Q. Aftab, M. Mesnil and V. Chen (***“Cx43-associated secretome and interactome reveal synergistic mechanisms for glioma migration and MMP3 activation (In Review)”***), Q. Aftab, M. Mesnil, E. Ojefua, A. Poole, J. Noordenbos, C. Sitko, C. Le, P.O. Strale, N. Stoynov, L.J. Foster, W.C. Sin, C.C. Naus, V.C. Chen, currently *in revision*). The remainder of the experiments were designed by me under the guidance of Dr. Vincent Chen. I carried out SDS-PAGE/Western blots and data analysis of MMP-3 in C6/C6-13 outlined (Figure 2.3.2). The NFF-3 assay was carried out by myself to analyze MMP-3 activity in conditioned media of C6 and C6-13 cells.

Chapter 3: Synthesis of Matrix Metalloproteinase 3 Inhibitors

The synthesis, and biological assay we carried out by me with the exception of the in silico molecular docking. The molecular docking was done in collaboration with members of the Bushnell Lab at Brandon University (Dr. Eric Bushnell and Chris Sitko). The synthesis reactions were designed by myself and Dr. Bryan Hill. The NFF-3 assay was designed by myself under the guidance of Dr. Vincent Chen. The synthesis reactions were carried out by myself, along with the NFF-3 assay.

Chapter 4: Chapter 4: Biological Effects of MMP-3 Inhibition by Ilomastat

All of the experiments in Chapter 4 were performed by myself. The experiments were designed by myself and Dr. Vincent Chen. The aim of this chapter was monitor the effect of ilomastat inhibition on MMP-3 activity. I carried out the flow cytometry cytotoxicity, NFF-3, and zymography experiments in addition to the scratch wound assay. I carried out the zymography assay, with protocol assistance from Emmanuel Ojefua.

Table of Contents

Abstract.....	iii
Acknowledgements.....	iv
Preface.....	vi
Table of Contents.....	viii
List of Tables.....	xii
List of Figures.....	xiii
List of Abbreviations.....	xv
Chapter 1: General Introduction.....	1
1.1 Glioblastoma Multiforme.....	1
1.1.1 Glioblastoma Multiforme Classification.....	5
1.1.2 Glioblastoma Multiforme Subtypes.....	8
1.2 Glioblastoma Multiforme Migration.....	11
1.2.1 Molecular Mechanisms of Cell Migration.....	13
1.2.2 Glioblastoma Multiforme Microenvironment & Extracellular Matrix.....	17
1.3 Matrix Metalloproteinases and Collagen ECM Substrates.....	18
1.4 Matrix Metalloproteinases in Cancer.....	25
1.5 A Summary: Hypothesis, Objectives, and Aims.....	26
Chapter 2: MMP-3 Expression & Activity in C6 and C6-13 Cell Line.....	28
2.1 Introduction.....	28
2.1.1 Methods to study MMPs.....	32

2.2 Materials & Methods.....	34
2.2.1 C6 Glioma Culture and Protein Precipitation.....	34
2.2.2 Bicinchoninic Acid Protein Assay.....	34
2.2.3 Peptide Sample Preparation and Analysis.....	35
2.2.4 Western Blot.....	36
2.2.5 ImageJ Analysis.....	37
2.2.6 NFF-3 Fluorescence Assay.....	37
2.3 Results & Discussion.....	38
2.3.1 Secretome Analysis of C6 and C6-13 Cells.....	38
2.3.2 Western Blot of C6 and C6-13.....	39
2.3.3 C6 and C6-13 NFF-3 Fluorescence Assay.....	41
2.4 Conclusion.....	42
 Chapter 3: Synthesis of Matrix Metalloproteinase 3 Inhibitors.....	43
3.1 Introduction.....	43
3.2 Materials & Methods.....	49
3.2.1 Chemistry: General Procedures.....	50
3.2.1.1 Compound B.....	50
3.2.1.2 Compound C.....	50
3.2.1.3 Compound D (Leu-Trp).....	51
3.2.1.4 Compound E (AP-1).....	51
3.2.1.5 Compound F (AP-2).....	51

3.2.2	In Silico Molecular Docking.....	52
3.2.3	NFF-3 Fluorescence Assay.....	53
3.3	Results & Discussion.....	53
3.3.1	Synthesis of Ilomastat Derivatives.....	53
3.3.2	Molecular Docking of Ilomastat Derivatives.....	57
3.3.3	NFF-3 of Ilomastat and Synthesized Compounds.....	58
3.4	Conclusion.....	61
Chapter 4:	Biological Effects of MMP-3 Inhibition by Ilomastat.....	62
4.1	Introduction.....	62
4.2	Materials & Methods.....	65
4.2.1	Flow Cytometry Cell Death Assay.....	66
4.2.2	NFF-3 Fluorescence Assay.....	67
4.2.3	Gelatin Zymography.....	67
4.2.4	ImageJ Analysis.....	68
4.2.5	Scratch Wound Assay.....	69
4.3	Results & Discussion.....	69
4.3.1	Flow Cytometry Cell Death Assay.....	69
4.3.2	NFF-3 Fluorescence Assay.....	74
4.3.3	Gelatin Zymography.....	76
4.3.4	Scratch Wound Assay.....	78
4.4	Conclusion.....	85
Chapter 5:	Overview of Research and Future Directions.....	86

5.1 Overview of Research.....	86
5.2 Future Research into MMP-3 and C6-13 Secretome.....	88
References.....	91
Appendix 1.....	103
Appendix 2.....	104
Appendix 3.....	105

List of Tables

Table 1.1.1: WHO grading of Central Nervous System Tumors.....	5
Table 1.2.1: Characteristics of Mesenchymal Migration Phenotype.....	16
Table 2.1.1: Matrix Metalloproteinase 3 extracellular matrix substrates, non-matrix substrates, and cellular sources of MMP-3.....	29
Table 2.2.1: Liquid Chromatography, Mass Spectrometry, and Mascot Search Parameters.....	35

List of Figures

Figure 1.1.1: Common mutations and effected signaling pathways in GBM.....	2
Figure 1.1.2: Top 30 frequently mutated genes in GBM.....	4
Figure 1.1.3: Tissue sections of different grade gliomas following WHO classification.....	7
Figure 1.1.4: Common genetic changes in primary GBM subtypes.....	10
Figure 1.1.5: Summary of GBM Classification.....	11
Figure 1.2.1: The five steps of migration.....	15
Figure 1.2.2: Model of ECM proteins.....	17
Figure 1.3.1: Five categories of matrix metalloproteinases.....	19
Figure 1.3.2: MMP propeptide cleavage mechanism.....	22
Figure 1.3.3: Mechanism of MMP peptide cleavage.....	24
Figure 2.1.1: MMP-3 domains.....	28
Figure 2.1.2: Scratch wound assay and secretome changes in C6 versus C6-13 cells.....	31
Figure 2.1.3: Mechanism behind fluorogenic substrates.....	33
Figure 2.3.1: Comparison of MMP-3 chromatographic (XIC) peak area of peptide SANAELMYPVYK (retention time 84.0) from secretome of C6 & C6-13	39
Figure 2.3.2: Western blot analysis of MMP-3 in C6 and C6-13 secretome.....	40
Figure 2.3.3: NFF-3 assay of MMP-3 activity in C6 and C6-13 secretome.....	42
Figure 3.1.1: Interaction of Batimastat with MMP active site.....	45
Figure 3.2.1: General synthesis scheme for derivatives.....	49
Figure 3.3.1: Proposed ilomastat derivatives.....	54
Figure 3.3.2: Interaction diagrams for ilomastat, Leu-Trp, AP-1, and AP-2.....	55

Figure 3.3.3: Interaction diagrams for AP-3, AP-4, AP-5, AP-6, and AP-7.....	56
Figure 3.3.4: Inhibition of MMP-3 activity detected by NFF-3 assay.....	60
Figure 4.1.1 Flow cytometry mechanism.....	63
Figure 4.3.1: Cytotoxicity of ilomastat after 24 hours.....	71
Figure 4.3.2: Cytotoxicity of ilomastat after 72 hours.....	73
Figure 4.3.3: Inhibition of MMP-3 activity by varying ilomastat concentrations.....	75
Figure 4.3.4: Gelatin zymography of varying ilomastat treatments.....	77
Figure 4.3.5: Low glucose media migration for control, 25 μ M, and 50 μ M at 0, 24, and 48 hours.....	79
Figure 4.3.6: Low glucose media migration for 75 μ M, and 100 μ M at 0, 24, and 48 hours...	80
Figure 4.3.7: High glucose media migration for control, 25 μ M, and 50 μ M at 0, 24, and 48 hours.....	81
Figure 4.3.8: High glucose media migration for 75 μ M, and 100 μ M at 0, 24, and 48 hours...	82
Figure 4.3.9: Relative migration of each ilomastat treatment for low glucose and high glucose media at 24 and 48 hours.....	83
Figure 5.2.1: MMP-3 active site with amino acid preference for each subsite.....	90

List of Abbreviations

BCA	Bicinchoninic Acid
BSA	Bovine Serum Albumin
CM	Conditioned Media
COSMIC	Catalogue of Somatic Mutations in Cancer
DCM	Dichloromethane
DIC	N,N'-Diisopropylcarbodiimide
DMF	Dimethylformamide
DMSO	Dimethyl Sulfoxide
Dnp	<i>N</i> -2,4-dinitrophenyl
DTT	Dithiothreitol
ECL	Enhanced Chemiluminescence
ECM	Extracellular Matrix
EtOH	Ethanol
FBS	Fetal Bovine Serum
Fmoc	Fluorenylmethyloxycarbonyl
GBM	Glioblastoma Multiforme
IDH	Isocitrate dehydrogenase
LC-MS/MS	Liquid Chromatography Mass Spectroscopy/Mass Spectroscopy
M	Molarity
Mca	(7-methoxycoumarin-4-yl)acetyl
MeOH	Methanol
mL	Milliliter
MMP	Matrix Metalloproteinase
MMPI	Matrix Metalloproteinase Inhibitor
MOE	Molecular Operating Environment
MS	Mass Spectroscopy
NMR	Nuclear Magnetic Resonance

PBS	Phosphate Buffered Saline
PDB	Protein Data Bank
PI	Propidium Iodide
TBST	Tris-buffered Saline with Tween 20 (Polysorbate 20)
TCGA	The Cancer Genome Atlas
THF	Tetrahydrofuran
TLC	Thin Layer Chromatography
TNBS	2, 4, 6 – trinitrobenzenesulfonic acid
Tp53	Tumor protein 53
SDS	Sodium Dodecyl Sulfate
SILAC	Stable Isotope Labeling with Amino Acids in Cell Culture
UV	Ultraviolet
WHO	World Health Organization
WR	Working Reagent
ZBG	Zinc Binding Group

Chapter 1: General Introduction

Cancer is a disease that has an impact on the lives of many humans. The World Health Organization (WHO) estimates the number of cancer cases rising from 1.3 to 2.1 million from 2012 to 2030, in North and South America alone.¹ In addition, the number of Canadians diagnosed with cancer within their lifetime is approximately 1 in 2.² Cancer is the uncontrolled division of cells resulting in tumor formation. The cause of this uncontrolled division is due to genetic mutations, may that be due to environmental conditions, lifestyle, or genetic predisposition to given mutations. Given that cancer is a disease that will have an impact on our lives directly or indirectly, it is important for continuing research on the mechanisms of cancer, including causation, progression, invasion, and treatment. This thesis will focus on the protease matrix metalloproteinase 3 and the inhibition of the protease through development of peptide-based inhibitors. The development of these compounds may offer insight into the mechanism of cancer invasion while providing new avenues to inhibit the malignant tumours of the brain.

1.1 Glioblastoma Multiforme

Glioblastoma Multiforme (GBM) is an aggressive and most common form of primary brain tumor. Occurring mostly within the cerebral hemisphere, GBM may also occur in other regions of the brain, as well as the brain stem and spinal cord. GBM, a high grade glioma, can arise from neural stem cells, differentiated glial cells that have acquired stem-cell like properties, and through de-differentiation of astrocytes, oligodendrocytes and ependymal cells.³ Classified as the highest grade (grade IV), GBM has an incidence of 3-4/100,000 with the incidence increasing with age.⁴ Survival after GBM diagnosis is still short, with majority of patients surviving between 15 -18

months after diagnosis, and only approximately 10% surviving past five years.⁴ The short term survival of patients is due to ill-defined tumors, tumor reoccurrence, and resistance to therapy. The causation of GBM is most likely due to genetic mutation and its aggressiveness due to the expression of these mutations.

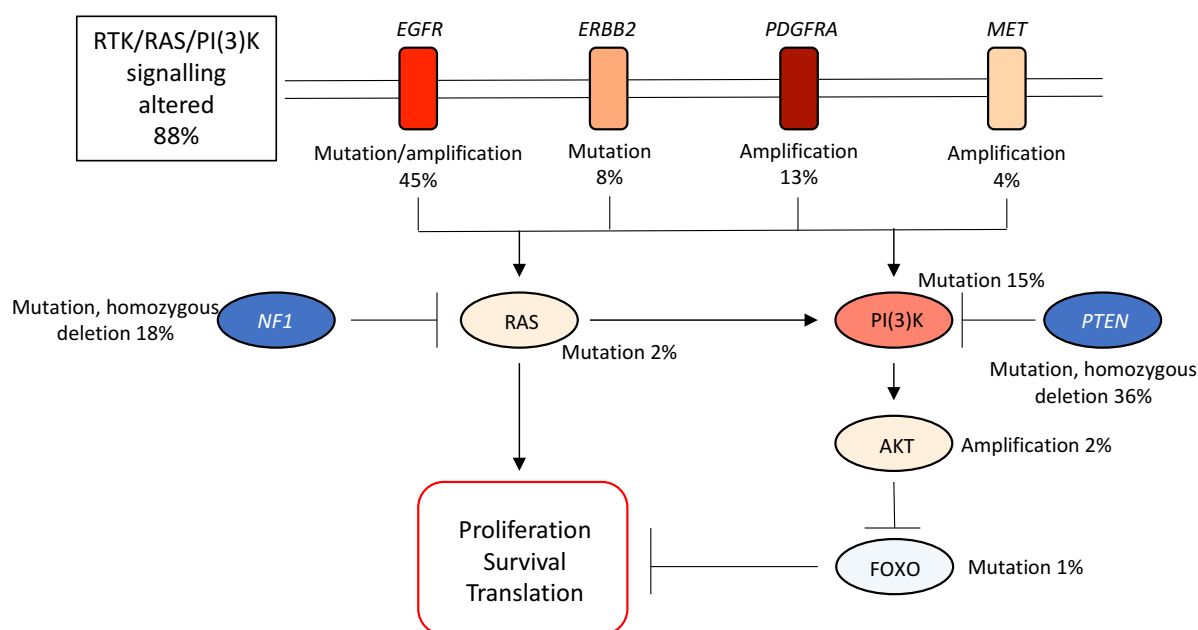


Figure 1.1.1: Common mutations and effected signaling pathways in GBM. Adapted from McLendon et al. 2008.⁵

In order for any type of cancer to develop, key genetic events must occur. In GBM, the most common genetic events include: (1) inactivation of the p53 mutation and retinoblastoma tumor suppressor pathway leading to uncontrolled proliferation; (2) activation of phosphatidylinositol-3-OH kinase (PI3K) pathway (PTEN is a PI3K pathway antagonist and most common mutation Figure 1.1.2); and (3) mutational activation and amplification of receptor tyrosine kinase (RTK) leading to the dysregulation of growth factor signaling, such as epidermal

growth factor receptor (EGFR) (Figure 1.1.1).^{5,6} The commonly mutated genes, TP53, RB1 (tumor suppressor), PIK3R1 (PI3K pathway), PTEN, and EGFR are all within the top 30 of the frequently mutated genes (Figure 1.1.2) from The Cancer Genome Atlas (TCGA) project TCGA-GBM.⁷ The number and type of genetic mutations produce varying tumors, which can be classified to give general tumor malignancy.

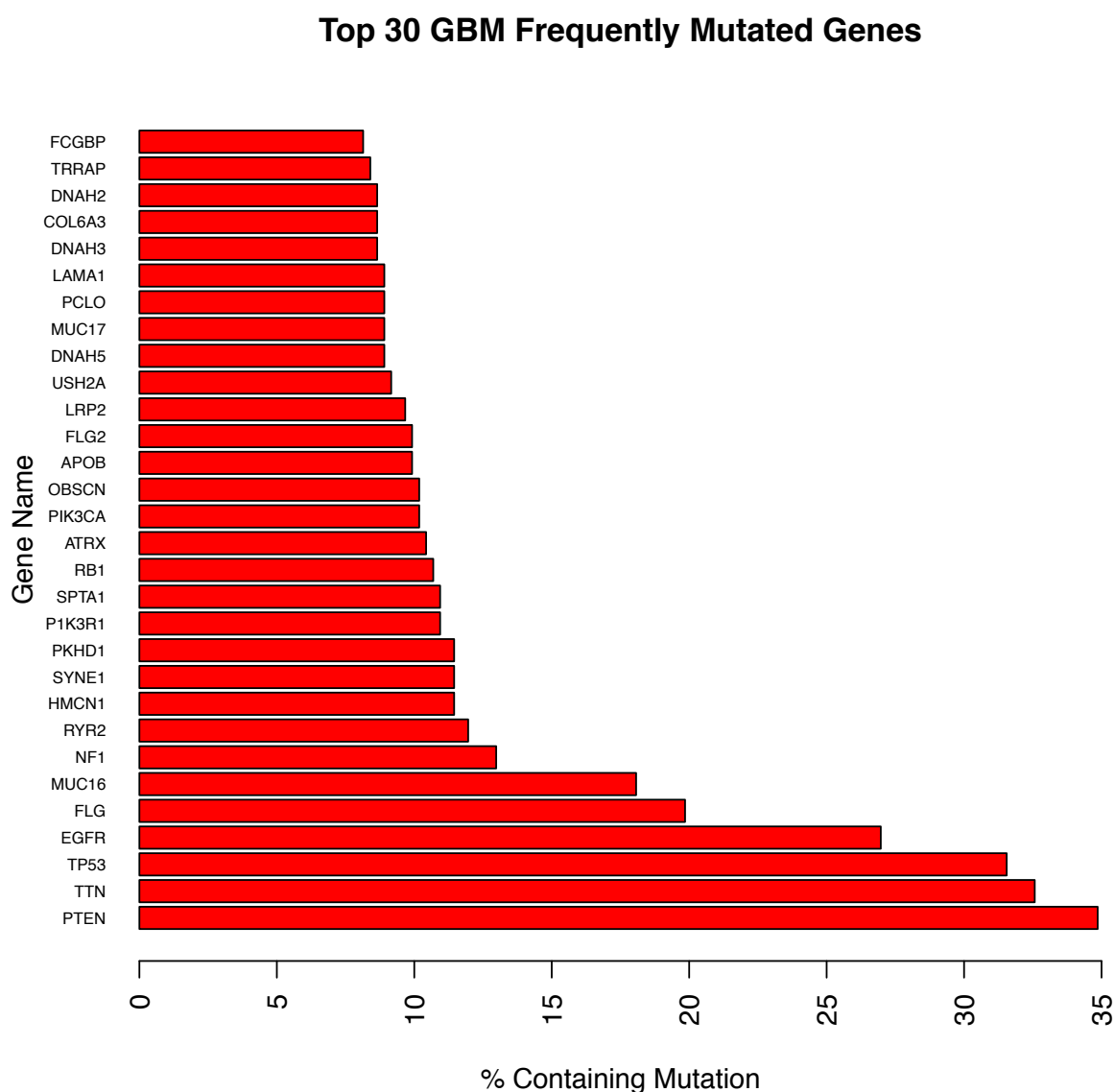


Figure 1.1.2: Top 30 frequently mutated genes in GBM. The top 30 out of 17449 most frequently mutated genes in GBM. Data was from TCGA and plotted as a percentage of mutations detected from the total number of samples acquired.⁷

1.1.1 Glioblastoma Multiforme Classification

The WHO uses a grading system to classify gliomas through characteristics to predict tumor malignancy. Gliomas are classified based upon the cellular morphology of the tumor cells, which may include tumors such as astrocytoma, ependymoma, oligoastrocytoma, and oligodendroglioma. In addition to classifying gliomas based upon cell type, tumors are graded based on the biological behavior and morphology of the tumor, giving a malignancy scale of the tumor. The WHO uses a scale from grade I to grade IV, with malignancy increasing as the grade increases (Table 1.1.1). A summary of the grading scale and an example of an astrocytic tumor of that grade is outlined in Table 1.1.1.

Table 1.1.1: WHO grading of Central Nervous System Tumors^{8,9}

Grade	Characteristic	Astrocytic Tumor
I	Non-malignant/least malignant Low proliferative potential Normal cell morphology Minimal reoccurrence Generally long-term survival	Pilocytic Astrocytoma
II	Generally infiltrates nearby tissue Low-level proliferation Slightly abnormal morphology May recur as higher grade Survival of more than 5 years	Diffuse Astrocytoma
III	Infiltrates and affects nearby tissue Proliferative Abnormal morphology Reoccurrence, often as higher grade Survival of 2-3 years	Anaplastic Astrocytoma
IV	Invasive, blood vessel formation Highly proliferative Very abnormal morphology Reoccurrence, necrosis Fatal outcome (approximately 1 year)	Glioblastoma

The WHO classification of gliomas is the most widely used classification system and overall provides a means of placing tumors into specific categories. However, classification schemes that are based upon visual characteristics (Figure 1.1.3), dependent on the observer, and can be difficult to place into one grade.¹⁰ Furthermore, the WHO classification does not predict the aggressiveness, therapeutic response, and survival of individual patients.¹⁰ The alternative route for classification is separating tumors based upon genetic mutations.

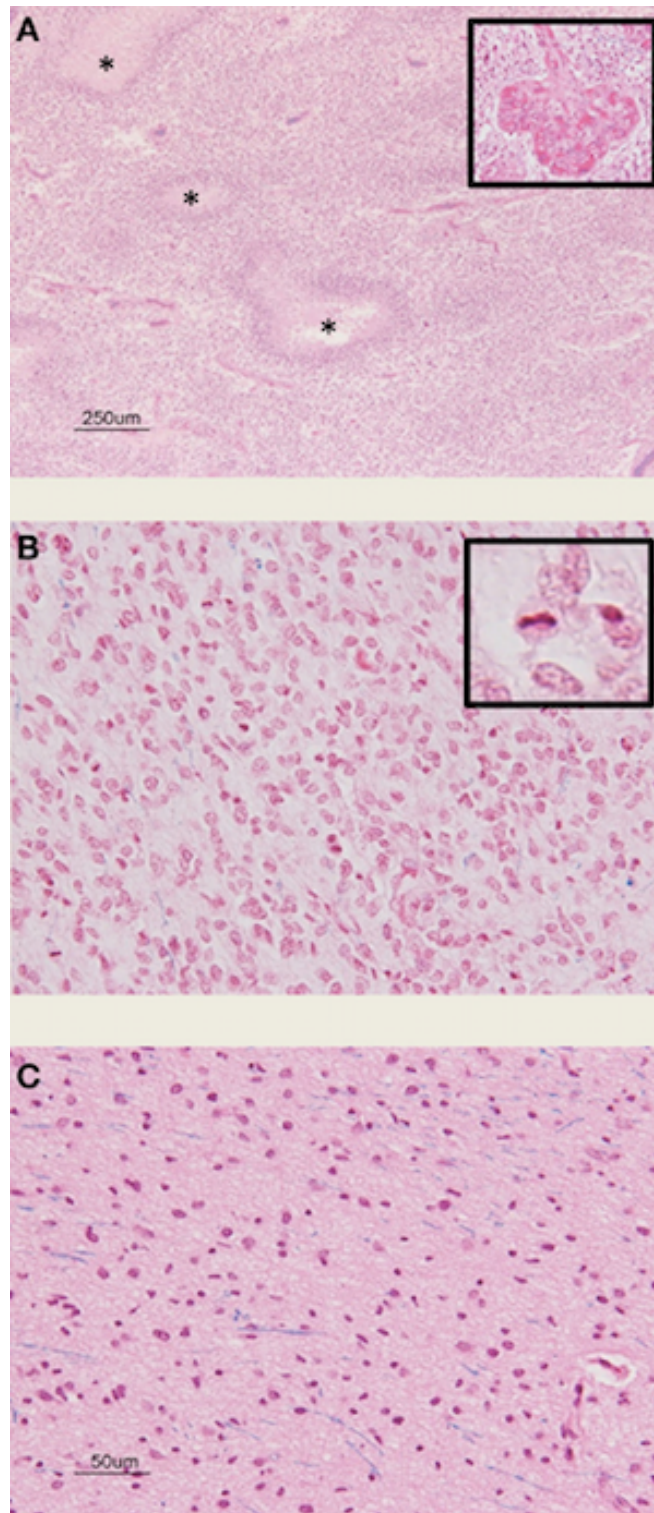


Figure 1.1.3: Tissue sections of different grade gliomas following the WHO classification system. Classification of glioma grade based upon visual characteristics. A) Glioblastoma (Grade IV), B) Anaplastic Astrocytoma (Grade III), C) Diffuse Astrocytoma (Grade II). Variation of classification can be different from observer to observer as visual observation varies between individuals. Adapted from Buczkowicz et al. 2015.¹¹

GBM can be divided into two types, primary or secondary, with the primary GBM occurring de novo, and the secondary GBM progressing from a lower grade glioma (grade II or III) to grade IV GBM. Patients in the primary glioblastoma group account for 90% of glioblastoma cases, and occurs primarily in patients over the age of 55.¹² Secondary glioblastoma accounts for about 10% of GBM cases, and is generally associated with younger patients¹² Another distinguishing characteristic between primary and secondary GBM is the mutational status of isocitrate dehydrogenase (IDH), with primary GBM maintaining the wild type version of the IDH gene and secondary GBM having the IDH-mutant gene.¹³ IDH is an enzyme of the citric acid cycle that might play a role in cellular defense against oxidative stress, which may account for the better outcome of patients that carry this mutation.¹⁴ Patients diagnosed with primary glioblastoma (IDH wild type) have a median survival of 11 – 13 months, whereas patients with secondary glioblastoma (IDH mutation) survival is 27 – 31 months.¹⁵ While the tumors may be divided into primary or secondary GBM based upon GBM progression (de novo or progressive) and IDH mutation status, morphologically and clinically these two are indistinguishable. The inability to distinguish morphology results in difficulties with diagnosis and treatment. However, due to the advances in genomic sequencing, GBM can be divided into molecular subclasses.

1.1.2 Glioblastoma Multiforme Subtypes

Until recently gliomas were classified based upon histological criteria. In 2006, molecular subclasses or subtypes were developed to better predict outcome and the clinical response to treatment. These subtypes were developed based upon the key molecular events that occur in

tumor development, such as changes in signaling pathways and gene expression.¹⁶ The subtypes were defined by clustering of the expression of survival-related genes, resulting in three discrete subtypes.¹⁶ A set of 35 signature genes were derived to be used by clustering techniques to assign high grade glioma tumors to an appropriate subtype, these subtypes being: proneural, proliferative, and mesenchymal.¹⁶ Adding on to the work done by Philips et al. (2006), a further subtype was identified by using 200 GBM and two normal brain samples to identify 210 signature genes per subtype.¹⁷ The four subtypes redefined as proneural, neural, classical, and mesenchymal.

The proneural subtype is generally found in younger patients with secondary GBM, and have characteristics similar to oligodendroglial cells.¹⁸ Proneural is characterized by its *IDH1* mutation, in addition to the proneural expression markers such as *SOX*, *DCX*, *DLL3*, *ASCL1*, *TCF4* and the oligodendrocytic expression markers *PDGFRA*, *OLIG2*, *TCF3*, *NKX2-2* (Figure 1.1.4).¹⁹ The neural subtype arises from astrocyte and oligodendrocyte cells and expresses high levels of EGFR, but maintains gene signatures of normal brain cells and has the neuron expression markers *NEFL*, *GABRA1*, *SYT1*, *SLC12A5* (Figure 1.1.4).^{18,19} The neural subtype is the least defined of all the subtypes. Classical GBMs have characteristics of astrocytes, while expressing markers of stem cells and neuron precursors.¹⁸ Similar to the neural subtype, classical GBM also have an *EGFR* mutation, overexpression, or amplification. The Notch and Shh pathways are also activated in the classical subtype (Figure 1.1.4).¹⁹ The mesenchymal subtype has similar characteristics as astrocytic gliomas, occurs in patients over the age of 50 and has poor prognosis which could be due to the mutation or loss of function in genes such as *TP53*, *NF1*, and *PTEN* (Figure 1.1.4).^{16,19}

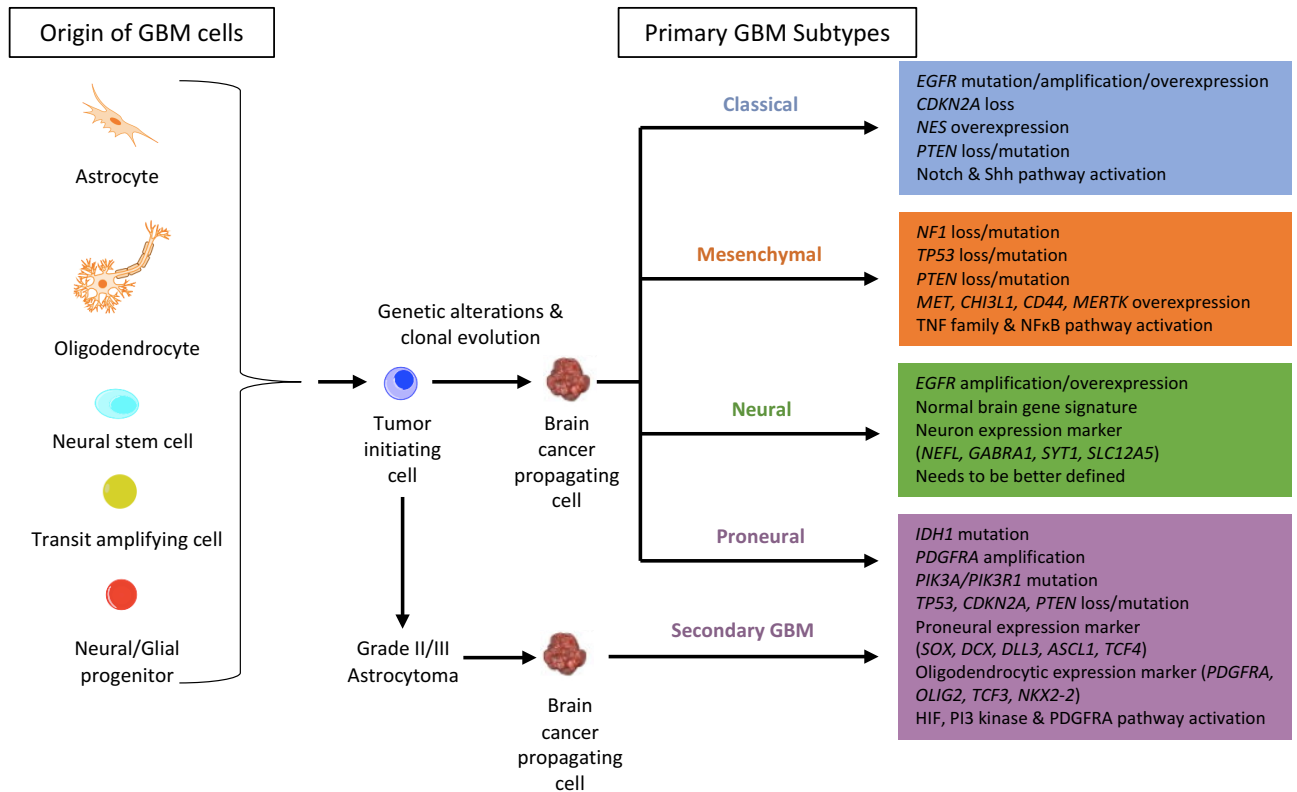


Figure 1.1.4: Common genetic changes in primary GBM Subtypes. Primary subtypes including; classical, mesenchymal, neural, and proneural subtypes. Common genetic changes in secondary GBM are also included. Adapted from Van Meir et al. 2010.¹⁹

In summary, gliomas are graded by the WHO classification, with GBM being a grade IV. GBM is then classified as primary or secondary GBM based on the progression of the tumor and the IDH mutation. Finally, GBM can be divided into the subtypes classical, mesenchymal, neural, and proneural based on genetic mutations (Full summary of GBM classification Figure 1.1.5). While being able to genetically categorize tumors may lead to more targeted therapeutics, even after 95% of tumor is removed, the invasiveness of GBM leads to formation of tumors at secondary sites. To help prevent secondary tumors from forming, more knowledge and treatment strategies to address malignant glioma, including GBM, are urgently needed.

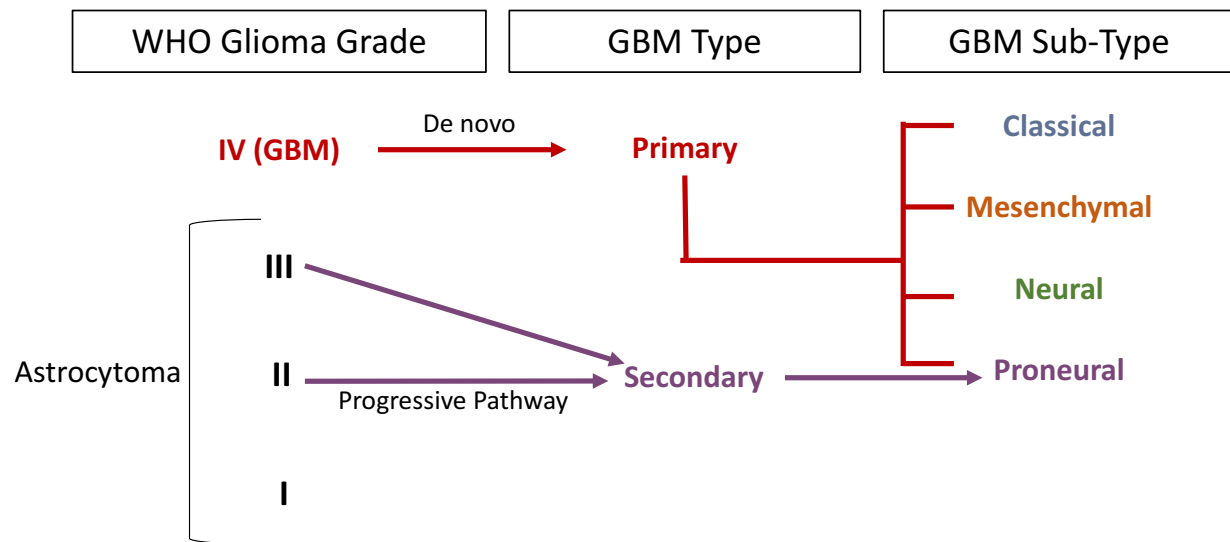


Figure 1.1.5: Summary of GBM Classification. GBM is a IV WHO glioma divided into primary or secondary. GBM is further classified as the subtype classical, mesenchymal, neural, or proneural.

1.2 Glioblastoma Multiforme Migration

Migration is a multistep process due to a combination of cellular and molecular events.^{20,21}

Typically a phenotype with stem cell likeness and the ability to degrade extracellular matrix (ECM) components results in a greater ability for invasiveness.²² For migration to occur there must be the detachment of tumor cells, the adherence of tumor cells to the ECM, and the migration of tumor cells into the surrounding tissue.²³

Invasive tumor cells will polarize, and will change shape to a spindle-like morphology, with protrusions that can attach to components of the ECM and pull the cell along.^{24,22} Proteases are involved to degrade and modify the ECM, creating space for the cell to move.²⁵ Included in these proteases are matrix metalloproteinases (MMPs) and endopeptidases that are involved in the physiological and pathological remodeling of the ECM.^{26,27} The remodeling of the ECM enhances the invasion potential of GBM.²⁵

Another factor that influences remodeling of the ECM, and thus invasion, is the hypoxic condition of the microenvironment.²⁸ Hypoxia is a state in which oxygen levels are low. Low oxygen conditions, or hypoxic conditions are common in areas that surround necrotic areas of tumors.²⁹ Often tumor hypoxia is associated with tumor progression and the aggressiveness of the tumor. Hypoxia-inducible factors (HIF-1), regulate the cell response to hypoxia by transcriptional activation of downstream genes.^{30,31} Activation of these downstream genes include genes involved with migration and invasion.³¹ HIF-1, a transcription factor, is composed of HIF-1 α (or analogs HIF-2 α , HIF-3 α) and HIF-1 β .^{32,33} HIF-1 α , the most important subunit, dimerizes with HIF-1 β , which is the constitutively active subunit, to prevent degradation of HIF-1, thus recruiting transcriptional co-activators and initiating gene transcription.^{20,34} GBM cells overexpress HIF-1 α , and glioma stem-like cells also overexpress HIF-2 α .³⁵ In normoxic conditions HIF-1 α has a half-life of approximately 5 minutes, but under hypoxic conditions is much more stable due to several pathways.³⁶ The increased activation of HIF-1, leads to increased transcription of genes associated with migration and invasion including ECM remodeling enzymes (MMPs, cathepsins) and matricellular proteins.

In addition, to the increased activation of HIF-1 hypoxic conditions can promote the reprogramming of non-stem-like cells into stem-like cells.³⁰ These changes are believed to play a critical role in the migration and invasion of GBM, including the formation of pseudopalisades or necrotic areas comprised of hypercellular zones unique to GBM.³⁰

1.2.1 Molecular Mechanisms of Cell Migration

Migration is directly connected to the microenvironment surrounding the cell. In order to migrate, the cell must modify its shape, which includes the cell becoming polarized and elongated.

Overall, there are five steps to migration: 1) The first step is the protrusion of the leading edge of the cell. (Figure 1.2.1 1) This protrusion is created by actin filaments within the cell connecting to adaptor proteins, resulting in the cell membrane being pushed outward, elongating the cell.³⁷ In addition to the leading edge of the migrating cell, necrotic areas of the tumor express cells with pseudopalisades.³⁰ These populations of pseudopalisades characteristically express more stem cell-like markers and migrate away from the hypoxic regions.^{30,38} The pseudopalisades are believed to be connected to the aggressiveness and malignancy of GBM.³⁸ Pseudopalisades overexpress HIF-1 α than compared to adjacent tumor cells.^{38,39} The HIF-1 α is localized to the leading invasive edge of the tumor and the genes regulated by HIF-1 α control the amount of ECM degradation, and therefore the invasiveness.²⁹ 2) The second step is ECM interaction and formation of focal contacts (Figure 1.2.1 2). The leading edge of the cell then comes in contact with the adjacent ECM and binds to the ECM via integrins, creating focal contacts.⁴⁰ 3) The recruitment of proteases. The involvement of integrins signals for surface proteases to become concentrated near cell-matrix interactions.^{37,41} Close to the cell surface, proteases (including MMPs) cleave ECM components such as collagen, fibronectin, laminin, etc., and pro-MMPs to generate active MMPs.³⁷ The protease ECM degradation creates space required for migration, as the cell continues moving away from the tumor, creating tube-like tracts through the ECM along its migration track.^{37,42} 4) In the fourth step of migration active myosin II binds to actin filaments

to generate the contraction of actomyosin.³⁷ The activation of myosin II by the phosphorylation of the myosin light chain by the calmodulin-dependent myosin light-chain kinase, aids in contraction.³⁷ 5) The final step of the migration process is the detachment of the trailing end of the cell. Focal contacts components at the trailing edge are cleaved by the cytoplasmic protease calpain.³⁷ Focal contacts are weakened by cleavage of adhesion receptors by proteolytic enzymes sheddases.³⁷ The accumulation of cleaved collagen fragments generated by the forward movement of the cell aids in further weakening focal contacts.³⁷ After focal contacts have been detached, integrins detach from the substrate, become internalized, and are either recycled or deposited on the substrate.³⁷

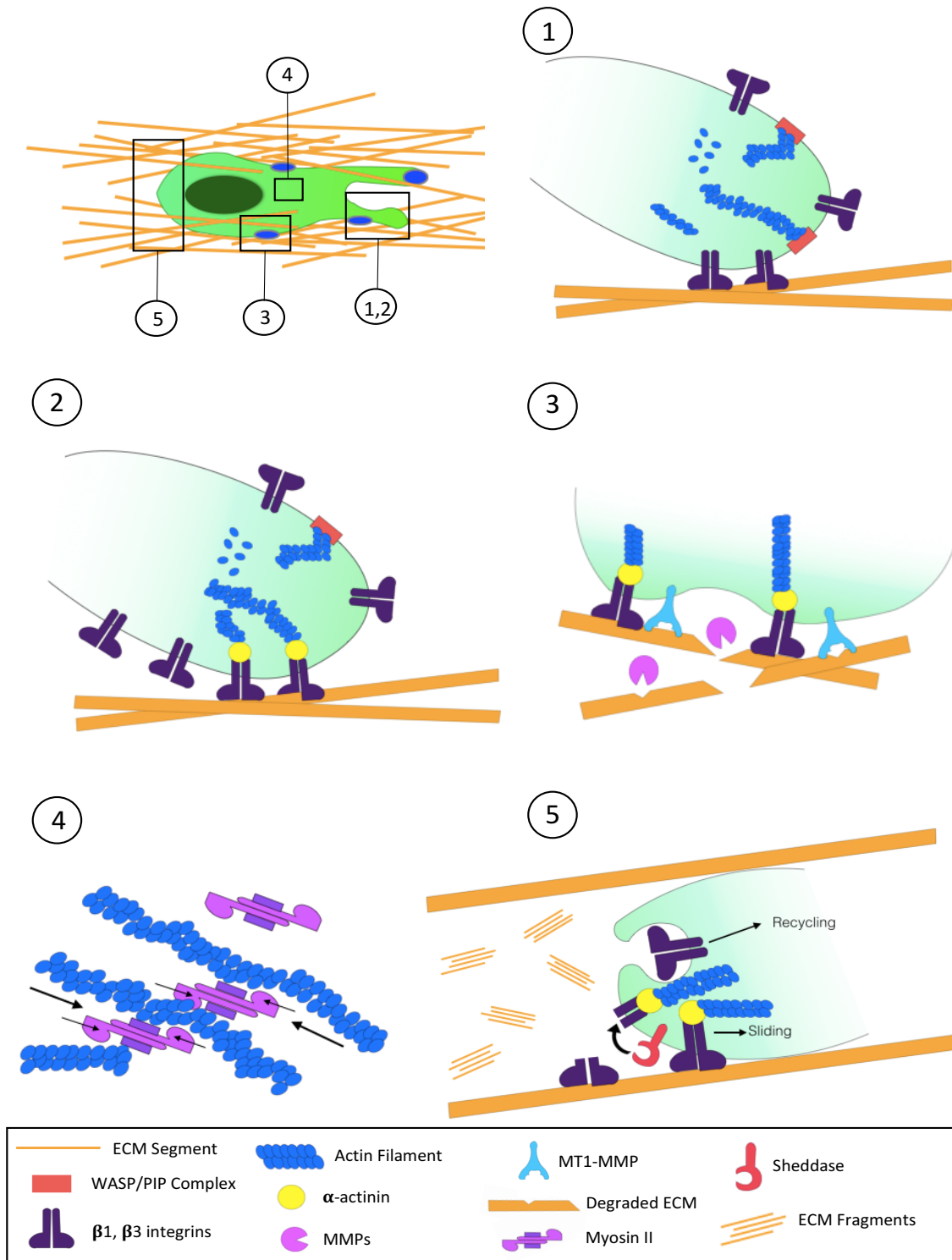


Figure 1.2.1: The five steps of migration. The top left image shows where each step of migration is occurring in relation to the cell. **1** The protrusion of the leading edge of the cell. **2** ECM interaction and formation of local contacts. **3** Recruitment of proteases (MMPs). **4** Contraction of actomyosin. **5** Detachment of trailing end. Modified from Friedl et al. 2003.³⁷

There are two types of migration that cells follow, amoeboid migration and mesenchymal migration. In amoeboid migration, there is no proteolytic ECM remodeling, cells rely on path finding and squeezing/flowing through spaces in the ECM. Cells that fit into mesenchymal migration follow the migration mechanism outlined above (Figure 1.2.1). The types of cells that follow mesenchymal migration are primarily from connective-tissue tumors, such as GBM. These type of cells have a spindle-shape morphology similar to fibroblasts due to the adhesion of integrins.³⁷ The maintenance of this phenotype and migration require the activation of MMPs.³⁷ An outline of the characteristics of a mesenchymal phenotype is located in Table 1.3.1.

Table 1.2.1: Characteristics of Mesenchymal Migration Phenotype (adapted from Friedl et al. Nature Reviews Cancer, 2003)³⁷

Characteristic	Mesenchymal Phenotype
Cancer Types	Glioblastoma, Fibrosarcoma
Cell Shape	Fibroblast-like, elongated (length 50-200µm)
Growth in Culture	Adhesive
Migration Velocity	Low (0.1-1 µm/min)
Cellular Migration Mechanism	Traction dependent
Adhesion-force generated	High, fiber bundling and pulling
Cell-matrix interactions	Integrins and proteases focalize
Proteolytic ECM Remodeling	Present to extensive
Mechanism for overcoming matrix barriers	Generating tube like deficits through ECM by proteolysis

1.2.2 Glioblastoma Multiforme Microenvironment & Extracellular Matrix

The interactions between of GBM and the microenvironment regulate invasion into healthy brain tissue to occur. Thus, the composition of exogenous factors contained within the tumour microenvironment plays an important role. In particular the ECM of brain tumors such as GBM

often consist of basement membrane proteins that line the blood vessels, including collagen IV, laminin, fibronectin, and proteins surrounding the tumor, including collagen I, tenascin-C, vitronectin, and hyaluronan (Figure 1.3.1).⁴³

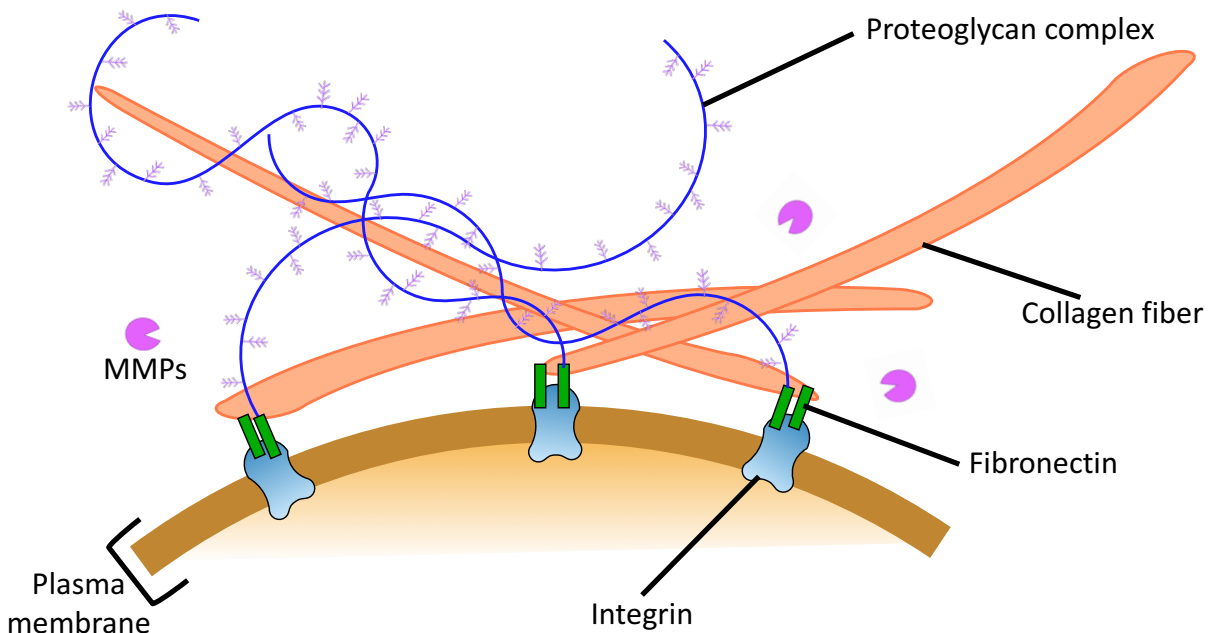


Figure 1.2.2: Model of ECM proteins. Proteins include collagen, fibronectin, integrins, and proteoglycan complexes.

Amongst these, GBM migration is stimulated by collagen IV, fibronectin, tenascin-C, and vitronectin.^{44,45} Here, the mechanical tension provided by a dense ECM environment causes GBM cells to switch to a migratory phenotype..⁴⁶ The ECM also acts as scaffold for adhesion proteins such as integrins, to promoting migration via actin dynamics.

Integrins are transmembrane glycoproteins that consist of two subunits (α and β), and are key to cell-ECM interactions, providing the adhesion for migratory cells to pull themselves along ECM components. Integrins can interact with ECM proteins such as fibrinogen, fibronectin, and vitronectin. The integrins themselves have no proteolytic activity, however the

adhesion of integrins to ECM proteins can trigger signal transduction pathways that lead to the creation of binding sites for enzymes such as matrix metalloproteinases.⁴⁴

1.3 Matrix Metalloproteinases and Collagen ECM Substrates

Matrix metalloproteinases (MMPs) are a family of structurally related zinc endopeptidases involved in both physiological and pathological remodeling of the ECM.^{26,47} The activity of MMPs was first discovered in 1962, where the ECM proteins were shown to be degraded by collagenolytic activity in the tails of tadpoles.⁴⁸ Since then, more than 26 MMPs have been identified and placed into one of five categories due to their substrate specificity or their structure/function.⁴⁹ These five categories being: collagenases, gelatinases, stromelysins, membrane-type MMPs, and others (Figure 1.3.1).⁴⁹

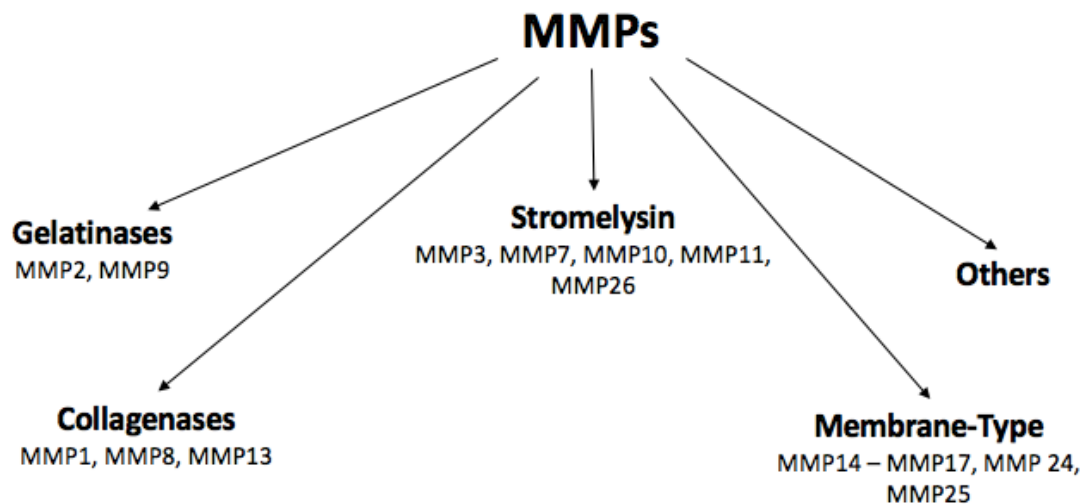


Figure 1.3.1: Five categories of matrix metalloproteinases. Categories include the gelatinases, collagenases, stromelysins, membrane-type, and others.

Invasion cannot occur without ECM remodeling, since the ECM can be both a substrate and barrier to invasion. The MMPs are the primary proteases responsible for the turnover and remodeling of the ECM.²⁷ MMPs have the ability to degrade various components of the ECM and of basement-membranes such as: aggrecan, elastin, fibronectin, gelatin, laminin and collagen.⁵⁰ In a normal adult brain, collagen levels are relatively low, however in GBM, collagen levels are elevated due to the fact that GBM cells remodel the ECM by degrading existing components and secreting new ECM proteins, including collagen.⁴³ MMPs are key proteases to the ECM remodeling and are important to collagen turnover. Out of the family of MMPs, 14 are known to degrade various types of collagens. MMPs play a role in regulating the interaction between collagen and its receptors, while also being regulated by pathways activated by collagen.⁴³

As a principle substrate of MMPs, there are 29 collagen types that can be group into three different classes. Collagen type I is one of the main type of collagens in connective tissue, with three alpha collagen chains wound together to form a superhelix structure that provides the stiff framework of collagen fibrils.⁵¹ A collagen chain is composed of four domains: the signal peptide domain, the N-terminal propeptide domain, collagen chain domain, and the C-terminal propeptide domain. Collagen type I is secreted as procollagen and thus the propeptide domains must be cleaved before the collagen can form fibrils. During invasion, collagen is believed to have three primary roles in GBM. The first role is to provide adhesion for cells, which is important in terms of migration.⁴³ Collagen can also act as a storage systems for growth factors, proteoglycans, etc. which can be released, through collagen remodeling, based upon the microenvironment.⁴³ The third role of collagen is acting as a ligand for receptors in signal

transduction pathways that are required for processes such as invasion.⁴³

Similar to collagen, fibronectin is expressed in higher levels in GBM than in normal brain tissue.⁵² Fibronectin facilitates collective invasion through fibronectin degradation.⁵² In human A375 melanoma cells, it has been shown that MMP-2 is recruited to the leading edge of leading edge of invasive cells where it cleaves fibronectin into shorter fragments.⁵³ These fragments of fibronectin facilitate adhesion and migration of tumor cells through the integrin $\alpha v \beta 3$.⁵³

Due to their ability to degrade the ECM and basement-membranes, MMPs are tightly regulated at both the transcription and protein levels.⁵⁴ Under normal conditions mRNA expression is low, however when ECM remodeling is required such as with wound healing, mRNA levels are upregulated.⁵⁴ In addition to the regulation at the transcription level, MMPs are synthesized as inactive zymogens, and can only be activated through the proteolytic cleavage of the prodomain (propeptide domain).⁵⁴ Active MMPs are further regulated by their endogenous inhibitors, tissue inhibitors of metalloproteinases (TIMPs). There are four TIMPs in total, and inhibit MMPs by binding tightly to the active site via non-covalent bonds, inactivating the enzyme.⁵⁵ Decreased levels of TIMPs and an increased expression of MMPs has been associated with tumorigenesis.^{47,55}

In order to have the greatest ability to inhibit MMPs, understanding the structure of these proteins and catalytic mechanism of the active site is key. MMPs are multi-domain proteins approximately 130-260 residues in length, that have a highly conserved propeptide and catalytic domains amongst the MMPs.^{48,54} MMPs are synthesized as inactive zymogens. This initial inactivity is due to the propeptide domain that blocks the active site. The propeptide

domain contains approximately 80 residues and has a conserved 'cysteine switch' at the N-terminal end that disrupts the interaction between the catalytic zinc ion in the active site and a cysteine residue in the propeptide domain (Figure 1.3.2).^{48,54} The sulfhydryl group of the cysteine residue coordinates to the zinc ion, keeping it inactive.⁵⁴ The removal of the propeptide domain by serine proteinases or other MMPs destabilizes the zinc-cysteine interaction, activating the MMP.⁴⁸ The substrate variation amongst MMP members is due to the specificity of subsites or subpockets.

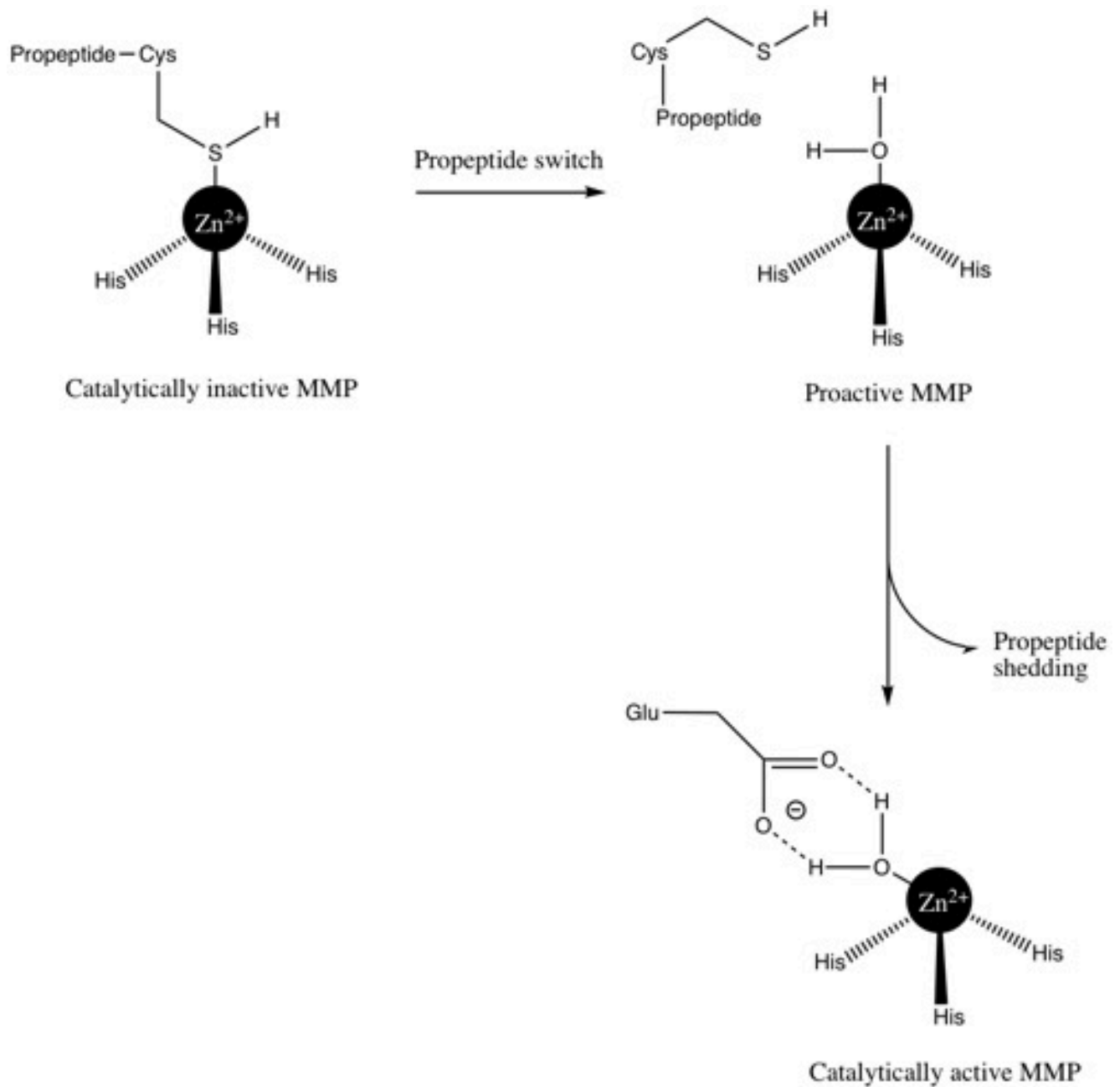


Figure 1.3.2: Propeptide cleavage and mechanism of MMP activation. MMPs are secreted in the inactive pro-MMP form with the cysteine residue coordinated to the catalytic zinc. The propeptide domain is removed by serine proteases or other MMPs, resulting in a catalytically active MMP, with a water bound to the zinc ion that can coordinate to the glutamate R-group. Modified from Rossello et al. 2009.⁵⁶

The conserved catalytic domain among MMPs contain a catalytic Zn^{2+} ion, a structural Zn^{2+} ion, and one to three Ca^{2+} ions that contribute to the stability of the MMP.⁵⁴ The catalytic zinc ion is coordinated by three histidine residues in a HEXGHXXGXXH motif.^{48,54} All MMPs also contain a conserved methionine residue with a Met-turn.⁴⁸ The active site also contains an axially coordinated water molecule that is hydrogen bonded to the carboxylate group of a glutamic acid residue that is responsible for cleaving peptide bonds (Figure 1.3.3).⁵⁴

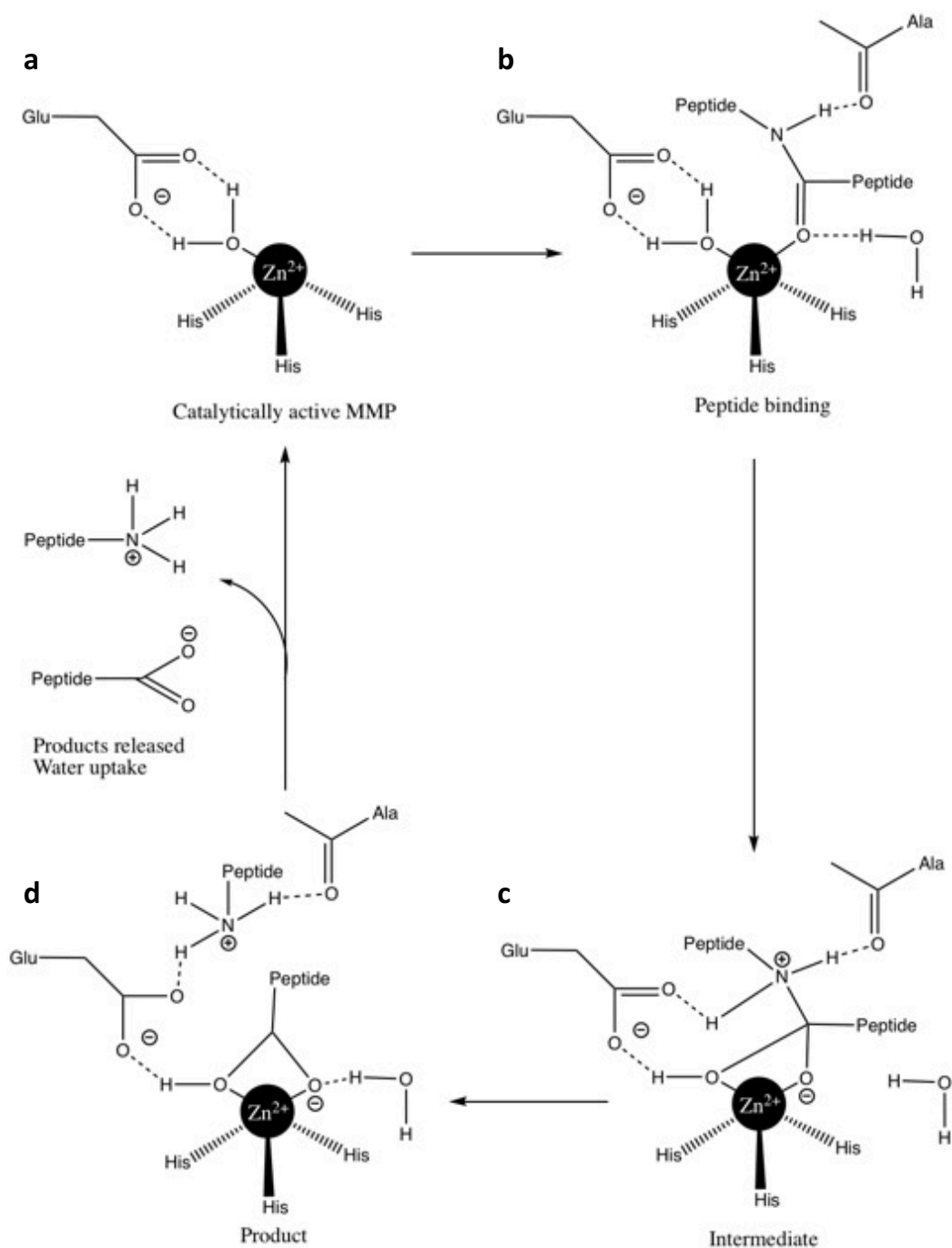


Figure 1.3.3: Mechanism of MMP peptide cleavage. (a) Catalytic zinc ion is tetrahedrally coordinated to three histidines and a water molecule. (b) Water donates proton to glutamine (Glu) peptide binds to catalytic site. (c) Proton transferred to nitrogen of scissile amid bond stabilized by alanine (Ala). (d) Generation of salt bridge between glutamine and free amine of cleaved substrate. Modified from Rossello et al. 2009.⁵⁶

The subpockets of MMPs located on either side of the active site give the selectivity for given substrates and account for the differences between MMPs. The subpockets on the 'left' side of the active site are designated S3, S2, and S1.⁵⁴ The subpockets on the 'right' side are 'primed', labelled as S3', S2', and S1'.⁵⁴ The greatest difference in the subpockets is between the S1' subpockets of the MMPs, varying in the amino acid residues and the depth.⁵⁴ The S1' subpocket can be divided based on the depth, with MMP-1 and MMP-7 having a shallow S1' subpocket; MMP-2, -8, and -9 having an intermediate depth; and MMP-3, -11, -12, -13, and -14 having a deep S1' subpocket.⁵⁴

1.4 Matrix Metalloproteinases in Cancer

The MMPs have diverse roles in cancer development and progression. Not only can MMPs be expressed by tumor cells, but they have also been found to be expressed by the stromal cells in the surrounding area, which shows that MMPs have a greater role in cancer progression than just their ability to degrade the ECM.⁵⁴ MMPs have the ability to degrade cell-adhesion molecules, modulate both cell-cell interactions and cell-ECM interactions leading to the progression of cancer.²⁶ MMPs have been associated with multiple cancer processes including: cancer cell proliferation, tumor angiogenesis and vasculogenesis, cancer cell invasion and migration.

In the early stages of tumorigenesis MMPs have been shown to contribute to the tumor microenvironment promoting cell proliferation.⁵⁵ MMPs have the ability to activate growth factors that induce cancer cell proliferation.⁵⁵ In addition, MMP-1, 2, 3, 7, 9, 11, and 19, can cleave IGF (insulin-like growth factors)-binding proteins that regulate availability of growth

factors such as epidermal growth factor receptor, further facilitating cancer cell proliferation.²⁶

The degradation of the ECM must also occur in order to generate pro-angiogenic factors that contribute to angiogenesis and vasculogenesis.²⁶ It has been shown that MMP-2, -9 and MMP-14 are the main MMPs involved in angiogenesis, but MMP-1 and -7 also play a role.²⁶ Specifically MMP-9 promotes angiogenesis because it increases the availability of vascular endothelial growth factor (VEGF), an important factor in tumor vasculature.²⁶

Cancer cell invasion and migration is capable due to the proteolytic ability of MMPs to regulate cell-cell and cell-ECM interactions.²⁶ Both MMP-2 and MMP-9 have been shown to degrade multiple components of the ECM allowing for cancer cell invasion.²⁶ The over expression of MMP-2, -3, -9, -13, -14 have been shown to allow for epithelial cell to mesenchymal cell transition, with mesenchymal cells having the increased ability to migrate.²⁶

In a study of 12 malignant human glioma cell lines, supernatant MMP-3 was expressed in the LN-18 and highly expressed in the U87MG cell line.⁵⁷ The U87MG cell line was the most migratory cell line and one of the most invasive.⁵⁷ In rat 9L glioma cells, the micro-RNA miR-152 inhibited invasion through MMP-3.⁵⁸ While there are links of MMP-3 to glioma invasiveness, more research is still needed.

1.5 A Summary: Hypothesis, Objectives and Aims

As a possible target for therapeutic design, the functions of MMP-3 in GBM progression are poorly understood. The overall ***hypothesis of this work is that MMP-3 is a key regulator of aggressive behavior in high grade glioma cells.*** **Aim 1:** We first validate the expression and activity of this protein in the connexin43 model of GBM migration/invasion⁵⁹ (Chapter 2) and

demonstrate upregulation of MMP-3 in high motility C6 glioma. Proteomic MMP-3 expression data was further supported by the use of Western Blot. A fluorescence NFF-3 protocol was established to determine MMP-3 activity. Using this cellular model and assays, **Aim 2:** we monitor the performance of commercial and novel chemically synthesized (peptidomimetics) inhibitors of MMP-3 (Chapter 3). The design of the inhibitors was based upon the active site/subsites of MMPs and the backbone of the broad spectrum MMP inhibitor Ilomastat. The sulfonyl binding groups were designed based on potential chelating to the catalytic zinc ion of MMP3. Overall, seven potential compounds were proposed. In addition to Ilomastat, three compounds were synthesized and tested. **Aim 3:** Monitor inhibition of MMP-3 effects its activity and migration ability of C6-13 cells (Chapter 4). Here, the inhibitory effect of ilomastat on MMP-3 was monitored through the NNF-3 assay to determine ilomastat concentration on the inhibition of MMP-3. Propidium iodide flow cytometry to determine the amount of cell death upon ilomastat exposure. Zymography was performed to analyze the effect of ilomastat on the expression and activity of MMP3. Scratch wound assay was performed to determine the effect of ilomastat inhibition on cell migration.

Chapter 2: MMP-3 Expression & Activity in C6 and C6-13 Cell Lines

2.1 Introduction

MMP-3 (Stromelysin 1) belongs to the stromelysin category of MMPs as it is a stromal MMP, with the same domain organization as other stromelysins. The domain organization of MMP-3 consists of a signal domain (for secretion into extracellular space), propeptide domain (cleaved to activate MMP-3), catalytic domain containing the catalytic zinc ion, a hinge/linker region to join the catalytic domain to the hemopexin C-terminal domain, which contributes to substrate specificity (Figure 2.1.2).⁵⁵

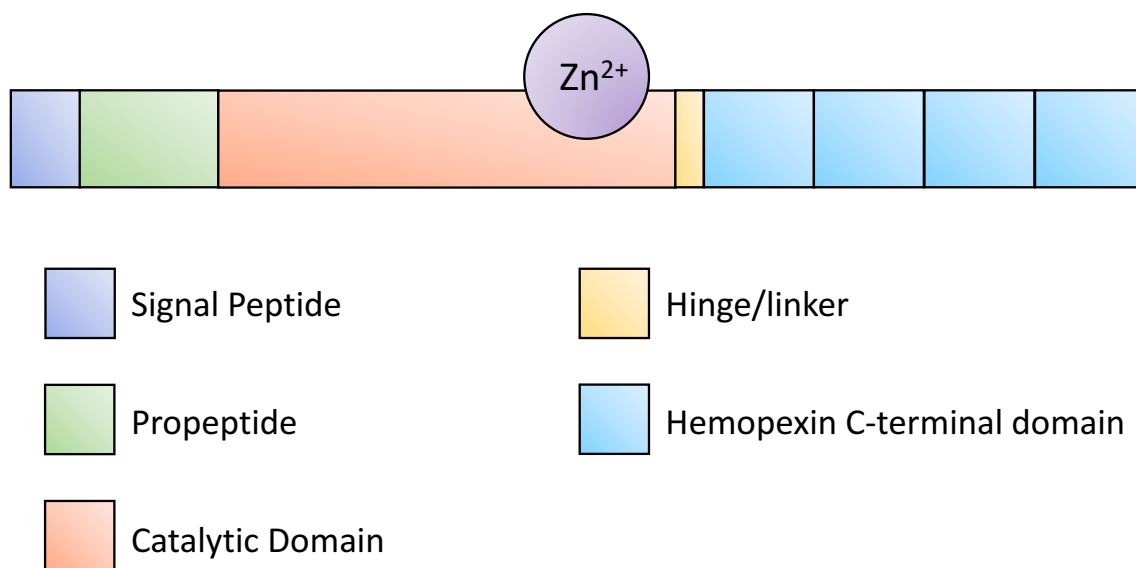


Figure 2.1.1: MMP-3 domains. Adapted from Overall et al. 2002.⁵⁵

MMP-3 has numerous substrates including ECM substrates; collagen, fibronectin, gelatin, laminin (Table 2.1.1). An important role of MMP-3 is its ability to activate pro-MMPs (Table 2.1.1), leading to more active MMPs, more ECM degradation, making MMP-3 crucial to ECM remodeling. As noted in Chapter 1, ECM degradation plays a key role in the migration and

invasion potential of GBM. In addition, MMP-3 expression has been shown to potentially have a link to the invasiveness of GBM. The C6/C6-13 rat glioma cells can be used as a model to study the link between MMP-3 expression and GBM invasiveness.

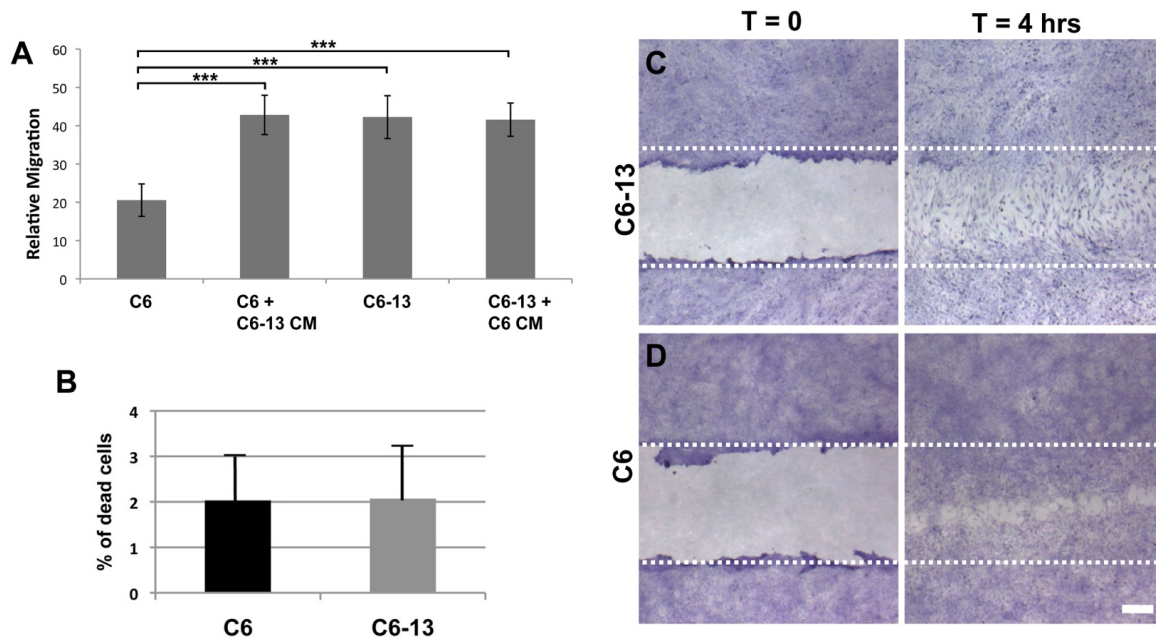
Table 2.1.1: Matrix Metalloproteinase 3 extracellular matrix substrates, non-matrix substrates, and cellular sources of MMP-3.⁶⁰

Extracellular Matrix Substrates	Non-Matrix Substrates	Cellular Sources of MMP-3
Aggrecan, Biglycan, Collagen Teloptides, Collagens (Type III, IV, V, VII, IX, X, and XI) non-triple helical regions, Decorin, Elastin, Entactin, Fibrin, Fibrinogen, Fibronectin, Fibulin, Gelatin, Laminin, Link Protein, Myelin Basic Protein, Osteonectin, Perlecan, SPARC, Tenascin, Versican, Vitronectin	α_1 -Anti-Chymotrypsin, α_2 -Antiplasmin, Carboxymethylated transferrin (Cm-Tf), Casein, Decorin, E-cadherin, endothelial growth factor (EGF), IGFBP-3, L-selectin, α_2 -Macroglobulin, Osteopontin, Plasminogen, Pro-MMP1, Pro-MMP3, Pro-MMP7, Pro-MMP8, Pro-MMP9, Pro-MMP13, urokinase-type Plasminogen Activator (uPA), vascular endothelial growth factor	Endothelial cells, Smooth muscle cells, Lymphocytes, Macrophages

The C6 cell line was produced by administering N-nitrosomethylurea to outbred Wistar rats over the course of 8 months.^{61,62} The excised and tissue cultured tumor designated as “#6” was cloned by Benda et al. and subsequently designated as C6.⁶² The C6 cell line is a glial tumor cell line with mutant p16/Cdkn2a/Ink41 locus and wildtype p53.⁶³ The genetic changes that occurred within the C6 cell line are the most similar to those that occur in human brain tumors.⁶⁴ Some frequently overexpressed genes in human GBM include PDGF β , IGF-1, EGFR, Erb3/Her3 which also show increased expression in the C6 cell line.⁶⁵ In addition to the C6 cell

line, C6 cells exogenously expressing high levels of connexin43 (Cx43) were used.⁵⁹ Referred to as C6-13, cells with increased Cx43 have been shown to express higher levels of proteins associated with migration and invasion.⁶⁶

A notable difference between the C6 cells and the C6-13 cells, is the change in mobility that occurs with the overexpression of Cx43. The C6-13 cell line has an increase in migration in comparison to the C6 cell line. In a scratch wound experiment performed by Aftab et al. 2018 (in review), there was a noticeable difference in the relative migration between the C6 and C6-13 cells (Figure 2.1.1 A), with the C6 cells filling the scratch by proliferation (dense concentration of cells indicating proliferation) and the C6-13 cells migrating into the scratch (Figure 2.1.1 C & D). In addition, when conditioned media (CM) from the C6-13 cells was applied to C6 cells, migration increased (Figure 2.1.1 A). However, when C6 CM was applied to C6-13 cells there was no change in migration. This increase in migration must be due to the differential regulation of secreted proteins by the C6-13 cell line, which includes the upregulation of proteins associated with GBM migration and invasion such as MMP-3, osteopontin, and collagens (Figure 2.1.1). An increase mechanical tension provided by the upregulation of multiple ECM proteins supports an environment in which migration occurs at a greater rate.



C6-13/C6 Fold	Symbol	Name	Location
8.5	MMP3	matrix metalloproteinase 3 (stromelysin 1, progelatinase)	Extracellular Space
7.4	SPP1	Osteopontin, secreted phosphoprotein 1	Extracellular Space
6.4	AKR1B10	aldo-keto reductase family 1, member B10 (aldose reductase)	Cytoplasm
4.1	TIMP2	TIMP metalloproteinase inhibitor 2	Extracellular Space
3.6	SPON2	spondin 2, extracellular matrix protein	Extracellular Space
3.5	VIM	vimentin	Cytoplasm
3.4	VCL	vinculin	Plasma Membrane
3.3	TAGLN2	transgelin 2	Cytoplasm
3.2	FLNA	filamin A, alpha	Cytoplasm
2.8	CTSB	cathepsin B	Extracellular Space, Cytoplasm
2.6	MYH9	myosin, heavy chain 9, non-muscle	Cytoplasm

Figure 2.1.2: Scratch wound assay and secretome changes in C6 versus C6-13 cells. (A) Relative migration of C6 cells, C6 cells with C6-13 CM applied, C6-13 cells, and C6-13 cells with C6 CM applied shows that proteins associated with migration are secreted by C6-13 cells. **(B)** Cell death was the same for C6 and C6-13 cells. **(C & D)** Scratch wound assay showing migration of C6-13 and C6 cells after 4 hours. Table at the bottom shows the top upregulated proteins in the C6-13 cells compared to the C6 cells. Figures taken with permission from Mesnil et al. 2019.⁶⁷

2.1.1 Methods to study MMPs

While it has been shown that the overall quantity of MMP-3 is upregulated in the C6-13 cells, it is unknown if this increase in expression is linked to the enzymatic activity of MMP-3. To further understand the enzymatic activity of MMP-3 in the conditioned media and how the addition of inhibitors effects MMP-3, a fluorogenic peptide substrate assay was performed. This enzyme assay is useful because low concentrations may be used and the fluorescence may be monitored continuously. The three types of fluorogenic substrates used are, aromatic amines, contact-quenched, and resonance energy transfer quenched. (Fluorometric assays of proteolytic enzymes). A common resonance energy transfer fluorophore and quencher combination is (7-methoxycoumarin-4-yl)acetyl (Mca) and *N*-2,4-dinitrophenyl (Dnp). In this combination of Mca and Dnp, the Dnp absorption spectrum overlaps the Mca fluorescence emission spectrum, essentially masking the fluorescence of the Mca.⁶⁸ Once the peptide is cleaved, the Dnp no longer masks the fluorescence of the Mca (Figure 5.1), and the amount of fluorescence measured is relative to the amount of peptide cleaved. A fluorogenic peptide that contains Mca at subsite P₆ and Lys(Dnp) at subsite P₅' can be used to detect enzymatic activity.⁶⁹ The NFF-3 [Mca-Arg-Pro-Lys-Pro-Val-Glu~Nva-Trp-Agr-Lys(Dnp)-NH₂] probe developed by Nagase et al. is very slowly hydrolyzed by the collagenase MMP-9 (k_{cat}/K_m : 10 100 s⁻¹M⁻¹) and rapidly by MMP-3 (k_{cat}/K_m : 218 000 s⁻¹M⁻¹).^{69,70} This makes the NFF-3 substrate ideal for determining the activity of MMP-3.

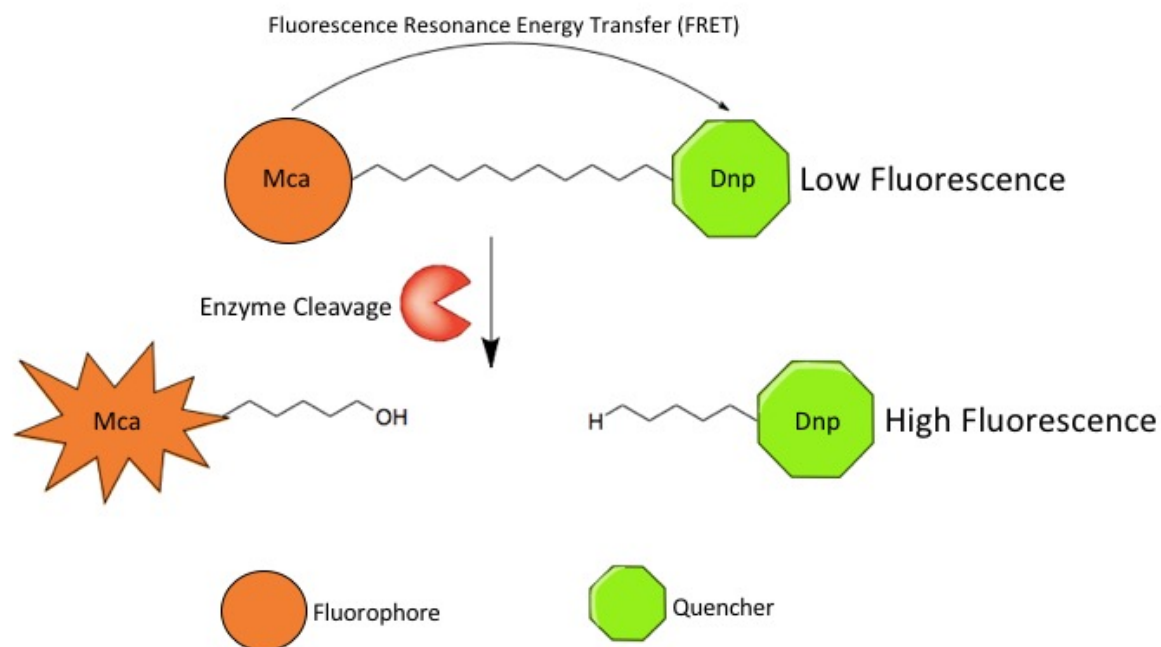


Figure 2.1.3: Mechanism behind fluorogenic substrates. The fluorophore (Mca) and quencher (Dnp) are connected through an amino acid sequence that acts as a substrate for a given MMP. When connected the Dnp absorbs the fluorescence of the Mca through fluorescence resonance energy transfer. Once cleaved by the MMP, the fluorescence of the Mca is no longer absorbed by the Dnp, and the relative absorbance can be measured.

C6-13 cells have an increase in migration compared to their C6 counterparts. This increase in migration may be due to the fact that MMP-3, an ECM protease which aids in migration, is the most upregulated secretome protein.⁶⁷ To verify that MMP-3 is upregulated in the C6-13 cells, I performed a label free mass spectrometry experiment of C6 versus C6-13 cells to identify if MMP-3 was upregulated. Western blot was used to further confirm that MMP-3 is upregulated in the C6-13 cells. Finally, the NFF-3 assay was developed to determine activity of MMP-3 in the C6-13 cells.

2.2 Materials & Methods

2.2.1 C6 Glioma Culture & Protein Precipitation

Rat glioblastoma cells (C6 and C6-13) were cultured in 4.5g/L glucose medium with 10% fetal bovine serum (FBS), with 1% antibiotics. Cells were incubated at 37°C with 4.0% CO₂. At 80-90% confluence, cells were aspirated, washed with PBS twice, washed with serum free media and were conditioned with serum free media for 24 hours. After 24 hours, the media was removed and the proteins were precipitated with ethanol followed by determining the protein concentration and in-solution digestion (trypsin) for LC-MS/MS.

2.2.2 Bicinchoninic Acid (BCA) Protein Assay

Protein concentration in each sample was determined using the bicinchoninic acid protein assay. BCA working reagent (WR) was prepared by mixing 50 parts reagent A to 48 parts reagent B to 2 parts reagent C. Into the wells of a 96-well plate, 200 µL of WR was added, followed by 25 µL of protein sample (sample may be diluted). The plate was then incubated at 37°C for 30 minutes. After the incubation period, the absorbance of each well was measured by spectrometer using the BCA Protein Quantification protocol from SoftMax Pro 7 software. A standard curve was initially constructed by measuring the absorbance of known concentrations of bovine serum albumin (BSA). Protein sample concentrations were then calculated by placing the measured absorbance into the standard curve equation.

2.2.3 Peptide Sample Preparation and Analysis

Equal amounts of C6 and C6-13 peptides were separated by a C18 stage tip, then analyzed using nanoHPLC-MS/MS (Agilent 1200) on an accurate mass QTOF mass spectrometer (Agilent, 6530).

Peptides were identified using Mascot Server (Matrix Science, UK). The following parameters were used for liquid chromatography, mass spectrometry, and the Mascot search.

Table 2.2.1: Liquid Chromatography, Mass Spectrometry, and Mascot Search Parameters

Liquid Chromatography Parameters	
Column	10cm vented trap column and 3.0 μ m C18 column (Dr. Maisch repositil-pur 20cm \times 100 μ m)
Injection Volume	5.00 μ L
Wash Solvent	Acetonitrile
Flow Rate	300 nL/min
Mass Spectrometry Parameters	
Ion Source	Nano Spray
Polarity mode	Positive
Mass range (max)	2000 (<i>m/z</i>)
Active exclusion	On, 3 spectra for 3 min
Charged state preference	2, 3
Mascot Search Parameters	
Taxonomy	Uniprot Rattus
Enzyme	semiTrypsin
Fixed Modifications	Carbamidomethyl (C)
Variable Modifications	Gln \rightarrow pyro-Glu (N-term Q), Oxidation (M)
Peptide mass tolerance	\pm 20 ppm
Fragment mass tolerance	\pm 0.6 Da
Peptide charge	2+ and 3+
Instrument	ESI-QUAD-TOF

2.2.4 Western Blot

Cells were plated on a six well plate at a concentration of 200,000 cells per well. Cells were grown to confluence (3-4 days) and conditioned with serum free DMEM media for 24 hours. After 24 hours, the conditioned media was collected in chilled 15mL falcon tubes and immediately placed on ice. Ice cold acetone (-20°C) was added to the media, 1 part conditioned media to 4 parts acetone. Tubes were incubated for 1 hour in a -20°C freezer. Proteins were pelleted by centrifuging for 12 minutes at 4800g in pre-chilled rotors. Supernatant was removed and proteins were suspended in 2x loading buffer without DTT. Proteins were incubated at room temperature, lightly vortexed, incubated for a further 20 minutes. At this time 2 µL of sample was removed and diluted in 28 µL of distilled water (15x dilution) for BCA analysis. DTT was added for a final concentration of 0.1M and samples boiled. Protein samples were loaded on a 10% SDS gel and ran at 125V for approximately 3 hours. Proteins were then transferred to the membrane ran at 30V for 3 hours at 4°C. Membrane was then washed in blocking buffer (5% nonfat dried milk in TBST (tris-buffered saline with tween 20)) for 1 hour. After the blocking step, membrane was incubated at 4°C in 1:1000 primary antibody (MMP-3 rabbit antibody) to 1% nonfat dried milk in TBST for 24 hours. After incubation, the membrane was washed three times with TBST for 5 minutes each at room temperature. Membrane was then washed for 1.5 – 2 hours with secondary rabbit antibody (1:2000 secondary antibody to 1% milk in TBST). The membrane was washed three times with TBST for 5 minutes at room temperature, then stained using ECL (enhanced chemiluminescence) stain for 1 – 2 minutes. Membrane was analyzed using a scanner to detect the signal from the ECL stain. A digital image of the membrane showing protein bands was generated and ImageJ was used for band analysis.

2.2.5 ImageJ Analysis

ImageJ software was used for both western blot analysis. Images in jpeg format were uploaded and changed to an 8-bit (black and white) image. Bands were selected using the rectangle selection tool, with the rectangle being twice as high than it is wide. The first lane (band) is selected under the “gels” section (“select first line”) of the “analyze” tab. A new rectangle is then generated and can be positioned over the next band, this band then selected under the “gels” section, “select next lane”. Band selection is continued until all bands have been selected. The lanes (bands) can then be plotted using the “plot lanes” option in the “gels” section, generating peaks for each band. The wand tool is used to select inside the peak and the area of the peak is generated by selecting “label peaks” from the “gels” section. The area of the peak, and thus the area of the band corresponds to the relative amount of MMP-3 present.

2.2.6 NFF-3 Fluorescence Assay

The NFF-3 probe is from Cayman Chemical ($\geq 95\%$ pure, MW: 1675.8) with the formal name: N²-[2-(7-methoxy-2-oxo-2H-1-benzopyran-4-yl)acetyl]-L-arginyl-L-prolyl-L-lysyl-L-prolyl-L-valyl-L- α -glutamyl-L-norvalyl-L-tryptophyl-L-arginyl-N⁶-(2,4-dinitrophenyl)-L-lysineamide. Cells were plated on a six well plate at a concentration of 200,000 cells per well. Cells were grown to confluence (3-4 days) and conditioned with serum free, phenol red free media for 24 hours. After conditioning, the media was collected. Each experimental condition had its own control condition. Using a 96 well plate 15 μ L of distilled water were added to the control wells and 15 μ L of 100 μ M NFF-3 were added to the experimental well. Then 300 μ L of the conditioned media (C6WT, C613, and DMEM media) were added to the control and experimental wells,

resulting in an overall concentration of 4.76 μ M NFF-3. The excitation wavelength of the spectrometer was set to 325nm while the emission was set to 393nm. The fluorescence was measured every ten minutes over the course of six hours, with the plate shaking for 15 seconds before each reading. The experiment was conducted at 37°C.

2.3 Results & Discussion

2.3.1 Secretome Analysis of C6 and C6-13 Cells

Initially a label free analysis of the secretome of C6 versus C6-13 cells was performed to verify that MMP-3 is in fact upregulated in the C6-13 cells. MMP-3 peptides were identified from the conditioned media. In Figure 2.3.1, a difference in the chromatographic (XIC) peak area of the MMP-3 peptide SANAELMYPVYK from the C6 secretome to the C6-13 secretome can be seen. Peak areas were generated using Skyline. While this is only N=1, there is a notable visual difference between the peak of the MMP-3 peptide in the C6 and the C6-13. There is no visible peak in the C6 secretome, indicating that the relative amount of MMP-3 is undetectable from the baseline, whereas in the C6-13 there are clear peaks in the precursor ion and $[M+2H]^{2+}$ ion at the retention time of 84.0 minutes, which corresponds to the retention time of the SANAELMYPVYK peptide. This secretome analysis confirms that MMP-3 is upregulated in the C6-13 as found in the Mesnil et al. 2019 study.

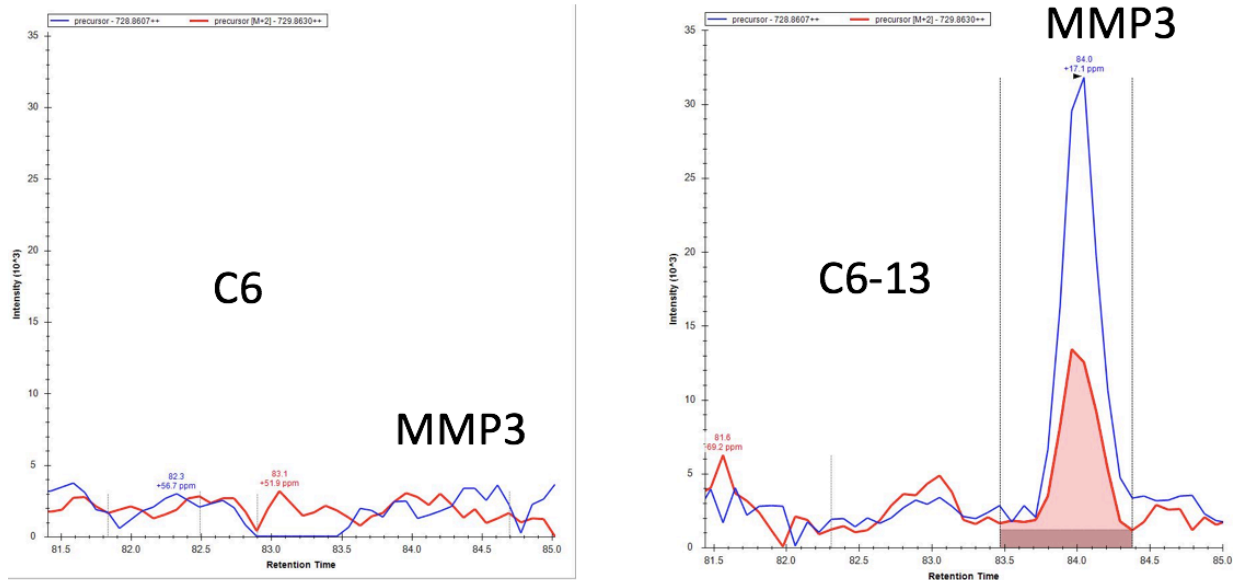


Figure 2.3.1: Comparison of MMP-3 chromatographic (XIC) peak areas of peptide SANAELMYPVYK (retention time 84.0) from secretome of C6 & C6-13.

2.3.2 Western Blot of C6 and C6-13

Western blot analysis was performed to further verify the upregulation of MMP-3 in C6-13 cells. MMP-3 has a molecular weight of 54 kDa (Figure 2.3.2 a). From Figure 2.3.2 a it is clearly visible that MMP-3 is significantly upregulated in the C6-13 as opposed to the C6 where no detectable band is present. From ImageJ analysis, quantified area of the C6-13 bands is statistically significantly greater than that of the C6 bands (Figure 2.3.2 b). This western blot data supports the mass spectrometry data in which C6-13 cells express higher levels of MMP-3 than the C6 cells.

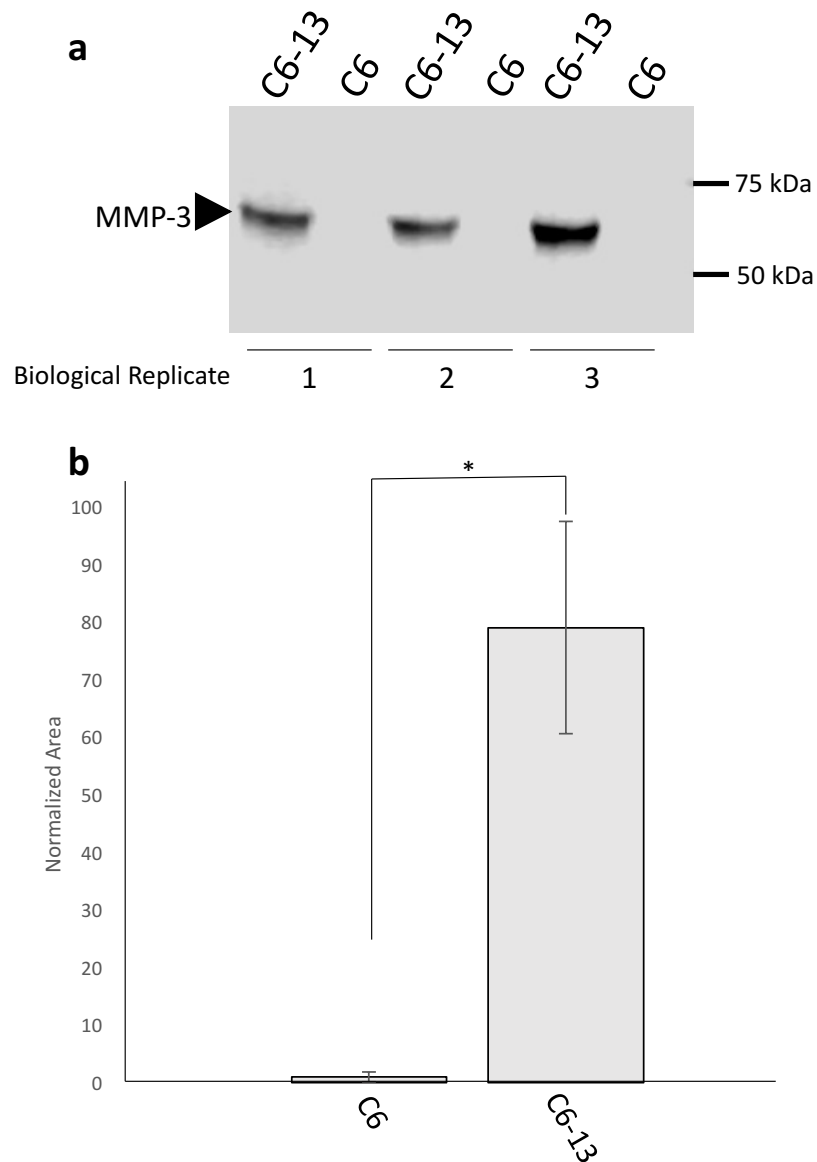


Figure 2.3.2: Western blot analysis of MMP-3 in C6 and C6-13 secretome. (a) Detection of MMP-3 in C6-13 versus C6 (N=3). **(b)** Normalized area of the detected bands by Western blot showing a statistically significant difference between the C6 and C6-13. Bands normalized to C6 area.

2.3.3 C6 and C6-13 NFF-3 Fluorescence Assay

Knowing that the overall expression of MMP-3 is upregulated from the C6 cells to the C6-13 cells, next we wanted to determine if there is a correlation between expression and activity. If increased expression corresponds to increased activity, it would further emphasize the use of C6-13 cells as a model to study MMP-3. To test the activity of MMP-3, the NFF-3 assay was utilized.

The majority of NFF-3 assays are used on the MMP-3 protein itself or on whole cells lysates. However, it would be difficult to isolate MMP-3 from the conditioned media and we are only concerned with MMP-3 in the conditioned media, not in the cells. Therefore, we designed an NFF-3 assay to be used on the conditioned media itself. The NFF-3 substrate concentration was set at 4.76 μM , which is in the recommended range of 2.5 – 75 μM .⁷¹ A time point of six hours was set, due to the leveling off of fluorescence around this time.

This study was designed to have three conditions: the control; unconditioned DMEM media, and two experimental; conditioned C6 media and C6-13 conditioned media. There was no change in the relative fluorescence of the unconditioned DMEM media (Figure 2.3.3). If increased expression correspond to activity, then a significant change in RFU over time should be apparent for the C6-13 condition based upon the Western data. From the NFF-3 data, the C6-13 conditioned media does have significantly higher MMP-3 activity than the C6 (Figure 2.3.3). Therefore, not only do the C6-13 cells have a higher expression of MMP-3, but also higher activity.

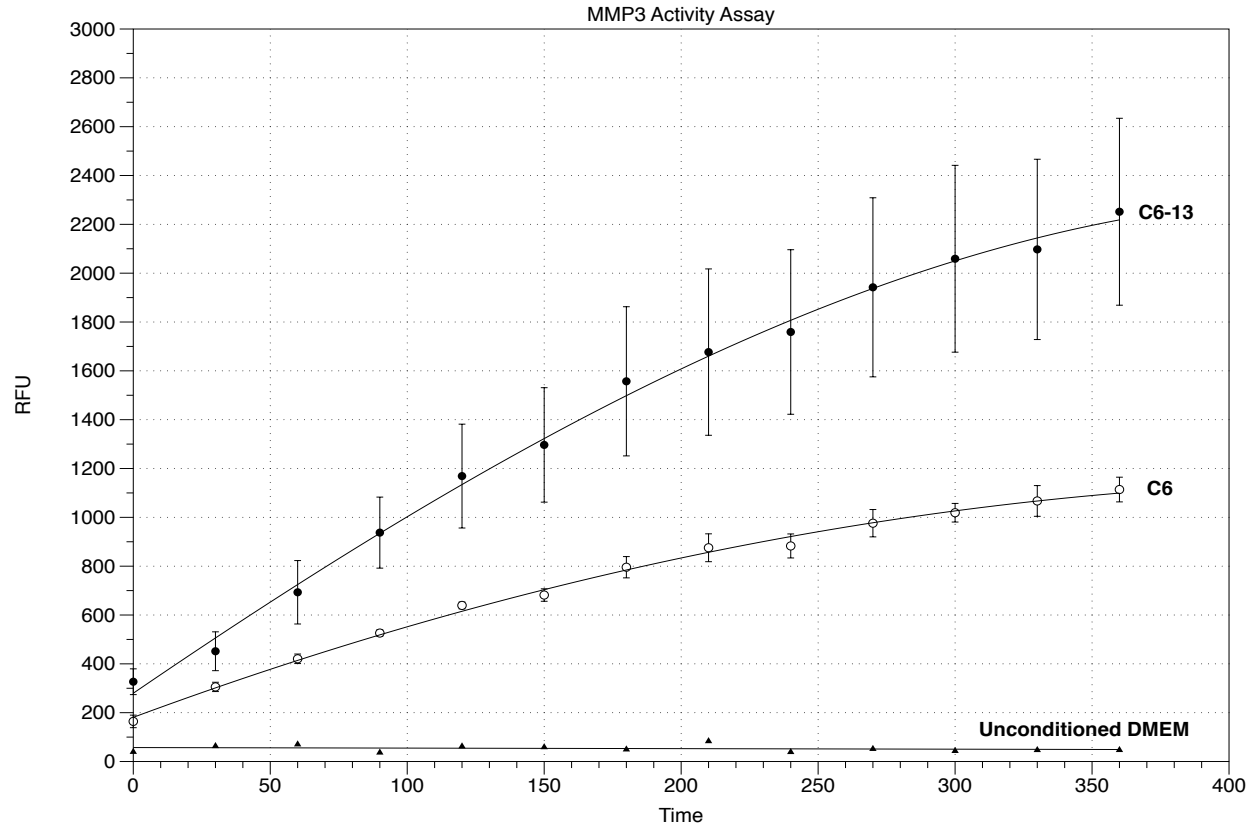


Figure 2.3.3: NFF-3 assay of MMP-3 activity in C6 and C6-13 secretome. The change in relative fluorescence units was measured over the course of six hours and plotted for the conditions: unconditioned DMEM media, C6 CM, and C6-13 CM.

2.4 Conclusion

The mass spectrometry secretome analysis of C6 versus C6-13 cells performed indicated that MMP-3 is upregulated in C6-13 cells. Western blot analysis provided further confirmation that the expression of MMP-3 is upregulated in C6-13 and validated the mass spectrometry data. Not only is the expression of MMP-3 upregulated, but from the NFF-3 assay, the activity of MMP-3 is also upregulated. The increased expression and activity of MMP-3 in the C6-13 cells, provides a model to study the link between MMP-3 and invasiveness.

Chapter 3: Synthesis of Matrix Metalloproteinase 3 Inhibitors

3.1 Introduction

Inhibiting MMPs may negate some of the invasiveness of GBM. Currently, various inhibitors for MMPs have been designed based on the catalytic zinc ion in the active site and the subpockets of the MMPs. The majority of the MMP inhibitors to date that have been developed are peptidomimetics. The idea of using endogenous peptides as therapeutics began in the 1920's, purified insulin from bovine pancreas was used to treat diabetes. Use of peptides as a therapeutic option over small molecules was initially difficult due to challenges faced with peptide synthesis, including low yields, reduced purity, poor stability of the peptides, and the delivery method.⁷² Generally peptides are unstable, have poor oral bioavailability, low membrane permeability, and linear peptides have short half-lives that may reduce the dosage that reaches the target.⁷² Thus the limitations that accompany peptides, may be overcome by using peptidomimetics.⁷² Peptidomimetics are any small molecules that are modified from an existing peptide, or mimics the structure of a peptide.⁷³ Peptidomimetics may be better therapeutic compounds compared to small molecule compounds and antibodies due to their similarity to endogenous substrates.⁷² This similarity can be exploited to interfere with protein-protein interactions and modulate protein signaling.⁷⁴ In addition, peptide-based therapeutics can be synthesized in larger quantities, generally are non-immunogenic, usually do not have tertiary or quaternary structures (as with antibodies) making them more stable, and have greater specificity for the protein target over their antibody counterparts.⁷⁴

In HER2-positive breast cancer, monoclonal or combination antibodies, alongside

chemotherapy is the traditional treatment route.⁷⁵ Kanthala *et al.* have shown that peptidomimetic compounds can inhibit the protein-protein interaction of HER2:HER3, having antiproliferative activity, without the limitations of antibody treatment.⁷⁵ In approximately 50% of invasive prostate cancers, the androgen-regulate promoter *TMPRSS2* is fused to the coding region of *ERG*.⁷⁶ ERG derived peptides and peptidomimetics destabilize the ERG interaction, decreasing invasion and metastasis.⁷⁶ While peptidomimetic MMP inhibitors have not been greatly explored in cancer treatment, the majority of MMP inhibitors designed for other diseases have utilized the peptidomimetic-based strategy.

MMPs were first introduced as therapeutic targets over 30 years ago. The goal of matrix metalloproteinase inhibitors (MMPIs) was to control the synthesis, regulation, activation, and enzyme activity.²⁶ The first generation of MMPIs were peptidomimetics, mimicking the structure of collagen at cleavage site of MMP.²⁶ Collagenases preferentially cleave N-terminal to hydrophobic side chains, such as leucine, with the leucine residing in the S1' subsite to the right of the catalytic zinc ion.⁷⁷ In a study of 7 MMPs (MMP-1,2,3,7,8,9,1), collagen was most frequently cleaved at the N-terminal end of leucine.⁷⁸ These first generation MMPIs were designed as a competitive inhibitor, chelating to the catalytic zinc ion by using the hydroxamic acid zinc binding group (ZBG).^{26, 54} As more MMPs were identified and the structure of MMPs was determined using crystallographic methods and X-ray diffraction, second and third generation MMPIs were developed.⁵⁴

All MMPIs that have been developed share two general characteristics: a ZBG and a side chain that interacts with MMP subpockets surrounding the zinc ion.⁴⁹ The MMPI design

generally includes a ZBG, because the catalytic zinc ion in the MMP active site facilitates the cleavage of substrates.⁵⁴ The zinc bound water molecule in the active site is responsible for cleaving peptide bonds (Figure 1.3.3). The ZBG is used to displace this water molecule, deactivating the enzyme.⁵⁴ Additionally, the ZBG helps to direct side chains of the peptidomimetic backbone into the subpockets of the MMP, furthering its inhibition.⁵⁴

The first generation of MMPis used the following as ZBGs: hydroxamic acids, carboxylates, thiols, and phosphoric acids.⁵⁴ However, the hydroxamic acids as a ZBG were favoured because of their ability to chelate well to the Zn^{2+} ion forming a trigonal-bipyramidal geometry around the Zn^{2+} and their simple synthesis.^{54,48} Good chelation to the zinc ion was aided by the fact that the NH group and deprotonated OH group of the hydroxamic acid were able to hydrogen bond to the alanine and glutamic acid residues in the active site (Figure 3.1.1).⁵⁴

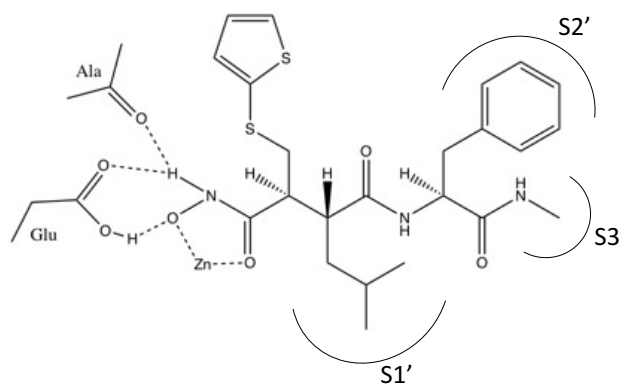


Figure 3.1.1: Interaction of Batimastat with the MMP active site. Diagram shows the bidentate binding of the hydroxamic acid to the zinc ion, as well as the hydrogen bonding to the alanine and glutamic acid residues of the active. This binding directs the peptide backbone and side chain into the S1', S2', and S3' subsites. Modified from Jacobsen et al. 2010.⁵⁴

The first MMPI to enter clinical trials was batimastat, a collagen-based hydroxamic acid peptidomimetic.²⁶ Other peptidomimetic hydroxamates include marimastat and ilomastat. Batimastat was the first broad spectrum MMPI to enter clinical trials in patients with malignant ascites and malignant pleural effusion, inhibiting the activity of most major MMPs such as MMP-1, -2, -3, -7, and -9.^{27,50} The hydroxamate chelates to the zinc ion, while the leucine side chain occupies the S1' site (Figure 3.1.1).⁴⁷ Preclinical studies showed that Batimastat had good potential as an anti-cancer agent.⁴⁸ However, the compound was almost completely insoluble, had poor oral bioavailability and had to be administered directly into body cavities or intravenously.⁵⁰

Marimastat is another broad-spectrum inhibitor that has better oral bioavailability than Batimastat.²⁷ When Marimastat was used in combination with temozolomide in patients with glioblastoma multiforme, there was an improvement in progression-free survival at six months in these patients and an overall survival of 45 weeks.⁵⁵ In addition, Marimastat had positive results in patients with gastric carcinoma and pancreatic carcinoma.⁵⁵ However, it was ineffective at doses associated with musculoskeletal toxicity.⁴⁸

Ilomastat also is a broad-spectrum inhibitor (inhibiting MMP-1, MMP-2, MMP-3, MMP-7, MMP-8, MMP-9, MMP-12, MMP-14, and MMP-26) that uses the hydroxamic acid as a ZBG, with a backbone consisting of the amino acids leucine and tryptophan.⁷⁹ Ilomastat was initially used as a topical treatment for corneal ulcers.⁸⁰ Although Ilomastat reached phase III clinical trials, it also has the poor bioavailability associated with hydroxamate peptidomimetics.⁷⁹

Currently no hydroxamate-based MMPI have been approved by the FDA.⁵⁴ There are

many limitations associated with hydroxamate-based MMPis that have hindered their potential as clinically viable compounds. These limits include low oral bioavailability, poor in vivo stability, and undesired side effects, such as musculoskeletal pain due to the broad spectrum inhibition.⁸¹ The biggest limitation of hydroxamate MMPis is that drug metabolism can lead to ZBG loss.⁴⁸ The first MMPis were developed when only several MMPs were identified and their structure was poorly understood due to the lack of crystallographic studies. The second and third generations of MMPis took into account the limitations of hydroxamate ZBG and the structural information of MMPs from crystallographic studies.

Second and third generation MMPis include non-hydroxamate and reverse hydroxamate (hydroxamate group is substituted on nitrogen instead of carbon) ZBG inhibitors were developed to overcome the limitations of hydroxamate inhibitors.⁴⁸ Non-hydroxamate and reverse hydroxamate ZBG include: carboxylates, hydrocarboxylates, sulhydryls, phosphoric acid, and hydantoins.⁴⁸ Non-hydroxamate MMPis do have some similarities to the hydroxamate versions, including the ability to form five-member chelates, but may have better affinity for the catalytic zinc than their hydroxamate counterparts.⁸¹ However, there is still an issue of broad MMP inhibition.

To reduce broad inhibition that occurs with MMPis due to the structural similarity between MMPs, it may be more effective to target sites such as the S1' subpocket, that are less conserved from one MMP to another.⁴⁸ As stated before, the S1' site has the most variation among MMPs, varying in both depth and amino acid sequence. Greater selectivity for one MMP over another may be accomplished by exploiting variations among the S1' sites.

Ilomastat was chosen as the compound to benchmark further derivatives because ilomastat has been shown to block hypoxia-induced invasion in breast carcinoma.⁸² The design of these derivatives began with using the same backbone as Ilomastat, including the leucine residue and tryptophan residue. This backbone was kept the same because MMP-3 has a preference for leucine in the S1' subsite and aromatics such as tryptophan in the S2' subsite.⁷⁸ The tryptophan residue has a methylamine at the C-terminal end as opposed to a carboxylic acid. We propose using sulfonyl derivatives as the zinc binding group because of the potential chelating ability of sulfur to zinc. This stems from the fact that the sulfhydryl group of the propeptide domain coordinates to the zinc in the inactive zymogen of MMPs (Figure 1.6.1). In addition, zinc/thiolate coordination is generally thermodynamically stable.⁸³ To test the thermodynamic stability of each compound, *in silico* molecular docking was utilized.

In silico molecular modelling has become a useful tool in drug discovery/development due to the advances in computational methods and increased number of protein structures deposited in the Protein Data Bank (PDB).^{84,85} Molecular docking can be applied to screen for top potential drug candidates, thus reducing the number of *in vitro* tests.⁸⁵ A molecular docking algorithm takes the receptor (protein) and the ligand (compound) then predicts the interactions that may occur, specifically whether the ligand will interact with the receptor, and the binding affinity.⁸⁵ Binding affinity scores are obtained using an energy function, which approximates the real energy value.⁸⁵

This study uses MOE (molecular operating environment) as the *in silico* molecular docking software. MOE gives binding energy scores based on the strength of binding interactions that exist between the compound and active site of MMP-3. The software also

indicates the types of molecular interactions that occur between the compound and active site, such as electronegative interactions, pi bonding, hydrogen bonding.

3.2 Materials & Methods

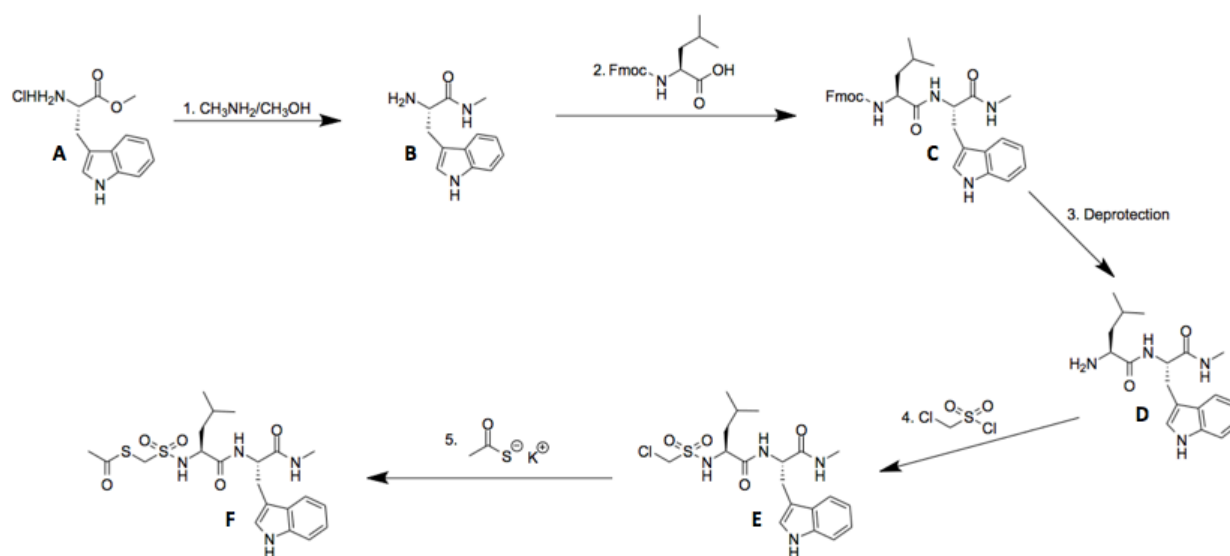


Figure 3.2.1: General synthesis scheme for derivatives: (1) **A** (1.0 eq.), $\text{CH}_3\text{NH}_2/\text{CH}_3\text{OH}$ (33% CH_3NH_2 by wt., 10 eq.); (2) **B** (1.0 eq.), Fmoc-Leu-OH (2.0 eq.), DIC (2.0 eq.), Oxyma Pure (2.0 eq.), *N,N*-Diisopropylethylamine (2.0 eq.); (3) **C** (1.0 eq.), 20% piperidine in DMF; (4) **D** (1.0 eq.), chloromethane sulfonyl chloride (7.0 eq.), *N,N*-Diisopropylethylamine (7.0 eq.); (5) **E** (1.0 eq.), potassium thioacetate (5.0 eq.), THF.

The sulfonyl ilomastat derivatives were synthesized following Figure 2.2.1. All compounds were synthesized using in solution peptide coupling and have the same leucine-tryptophan backbone. The zinc binding group chloromethane sulfonyl chloride was added by $\text{S}_{\text{N}}2$ reaction. The addition of thioacetate to **E**, again, was a $\text{S}_{\text{N}}2$ substitution.

3.2.1 Chemistry: General Procedures

All starting materials and reagents were commercially available and used without further purification. Reactions were monitored via TLC with 210 – 270 μm silica gel plates (EMD Chemicals Inc., 5715-7) using UV light and potassium permanganate. Flash column chromatography was performed using 230 – 400 mesh ultra pure silica gel, with a pore diameter of 60 Å (Silicycle). Proton NMR of compound **D** was performed on a Bruker spectrometer (400 MHz) with $\text{DMSO-}d_6$ as the solvent (see appendix). NanoHPLC-MS/MS was performed, analysis of the synthesized compounds was done using a QTOF mass spectrometer (Agilent, 6530) (appendix).

3.2.1.1 Compound B:

0.5062 g (1.963 mmol) L-tryptophan methyl ester hydrochloride (**A**) in 2.5 mL of $\text{MeNH}_2/\text{MeOH}$ (33% MeNH_2 by wt.) was mixed overnight under nitrogen. Product was then placed on rotovap to evaporate MeOH and MeNH_2 to yield L-tryptophan methyl amide (**B**) as a yellow oil (0.4126 g, 95.6%).

3.2.1.2 Compound C:

1.387 g (3.926 mmol) Fmoc-Leucine-OH was dissolved in 8 mL of 1:1 $\text{DMF}:\text{CH}_2\text{Cl}_2$ and mixed with 0.61 mL of DIC, 0.557 g of Oxyma Pure, and 0.70 mL of *N,N*-Diisopropylethylamine under nitrogen at room temperature for 10 minutes. The solution was then added to 0.4126 g (1.899 mmol) compound **B** and mixed for 48 hours under nitrogen. Compound **C** was purified by flash

column chromatography using 2:1 chloroform to methanol as the mobile phase. Fractions were collected, and solvent evaporated to yield a yellow-orange oil (0.8126 g, 77.4%).

3.2.1.3 Compound D (Leu-Trp):

0.08126 g (0.147 mmol) Fmoc-Leucine-Tryptophan was mixed with 4 mL of 20% piperidine in DMF for two hours. Compound **D** was purified by the same flash column chromatography as Compound **C**. Fractions were collected, and solvent evaporated to yield a yellow-orange oil (0.041 g, 83.9%, LC-MS/MS m/z : 331.2177 (M+H), NMR 400 MHz: ~11 ppm H on N of Trp five carbon ring, ~7 ppm Trp aromatic H, ~1 ppm H on methyl groups of Leu).

3.2.1.4 Compound E (AP-1):

0.78 mL (8.627 mmol) of chloromethane sulfonyl chloride was added to 0.4097 g (1.23 mmol) of Compound **D**. 1.55 mL (8.627 mmol) of *N,N*-Diisopropylethylamine was then added and the mixture was refluxed under nitrogen overnight. Compound **E** was purified by the same flash chromatography method as the previous compounds. Fractions were collected, and solvent evaporated to yield a reddish-orange oil (0.5154 g, 94.5%, LC-MS/MS m/z : 443.1669 (M+H)).

3.2.1.5 Compound F (AP-2):

0.09855 g (0.8629 mmol) potassium thioacetate was mixed with 8 mL of THF until dissolved. The solution was then added to 0.0764 g (0.1726 mmol) of Compound **E** and refluxed under nitrogen for 48 hours. Purification of Compound **F** was performed by the same flash column

chromatography as previous compounds. Fractions were collected, and solvent evaporated to yield a reddish-brown oil (0.0443 g, 54.9%, LC-MS/MS m/z : 467.1723 (M+H)).

3.2.2 In Silico Molecular Docking

First the MMP3 protein (PDB:4G9L), co-crystallized with the inhibitor NNGH, was prepared for the molecular dynamics simulation by deleting alpha chains, adding protons, and ensuring that the protonation states of the crystalline structure were correct. MMP3 (PDB:4G9L) was solvated using periodic boundary conditions with NaCl counter ions. Amber10: EHT was the forcefield used to minimize energy with rigid water constraints to an optimization gradient of 0.1 kcal/mol Å².

The molecular dynamics simulation was performed using the NPA algorithm and Amber10: EHT forcefield. In the simulation, the system was heated up to 310K for 220ps, then ran at a constant temperature of 310K for 800ps to allow for the protein to anneal. During the simulation, the phase space was sampled every 0.5ps, all light bonds constrained and rigid water molecules used with the time step being 2 fs. Compounds were docked using the last trajectory.

MMP-3 active site was set to the entire protein as well as the catalytic zinc ion and active site bound water molecule. Compounds with an acidic proton were deprotonated and charges fixed before compounds were docked. Generation of random poses for each compound was performed using the proxy triangle algorithm. Each conformer was scored using the London dG scoring function, with the top thirty poses rescored using induced fit refinement

algorithm. Top five poses were ranked by the Gibbs binding energy, scored using the Generalized-Born Volume Integral/Weighted Surface Area (GBVI/WSA) algorithm.

3.2.3 NFF-3 Fluorescence Assay

Cells were plated on a 20cm plate and grown to confluence (3-4 days). The plate was washed twice with PBS, once with serum free phenol red free media and conditioned with 15 mL of serum free phenol red free media for 24 hours. After 24 hours, the conditioned media was collected and 1400 μ L portioned out into 9 Eppendorf tubes. Inhibitors were added resulting in a final concentration of 50 μ L or 100 μ L. Each experimental condition had its own control condition. Using a 96 well plate 15 μ L of distilled water were added to the control wells and 15 μ L of 100 μ M NFF-3 were added to the experimental well. Then 300 μ L of the conditioned media with inhibitors were added to the control and experimental wells, resulting in an overall concentration of 4.76 μ M NFF-3. The excitation wavelength of the spectrometer was set to 325 nm while the emission was set to 393 nm. Fluorescence was measured every ten minutes over the course of six hours, with the plate shaking for 15 seconds before each reading. The experiment was conducted at 37°C.

3.3 Results & Discussion

3.3.1 Synthesis of Ilomastat Derivatives

Sulfonyl ilomastat derivatives were designed based on the backbone of ilomastat, but using a sulfonyl ZBG in place of hydroxamic acid. Of the seven compounds proposed (Figure 3.3.1), the

leucine-tryptophan backbone was the first synthesized. AP-1 was produced by coupling the backbone with chloromethane sulfonyl chloride. Finally, AP-2 was synthesized using an S_N2 substitution with thioacetate. Synthesis and evaluation of MMP inhibitors were limited to 3 compounds.

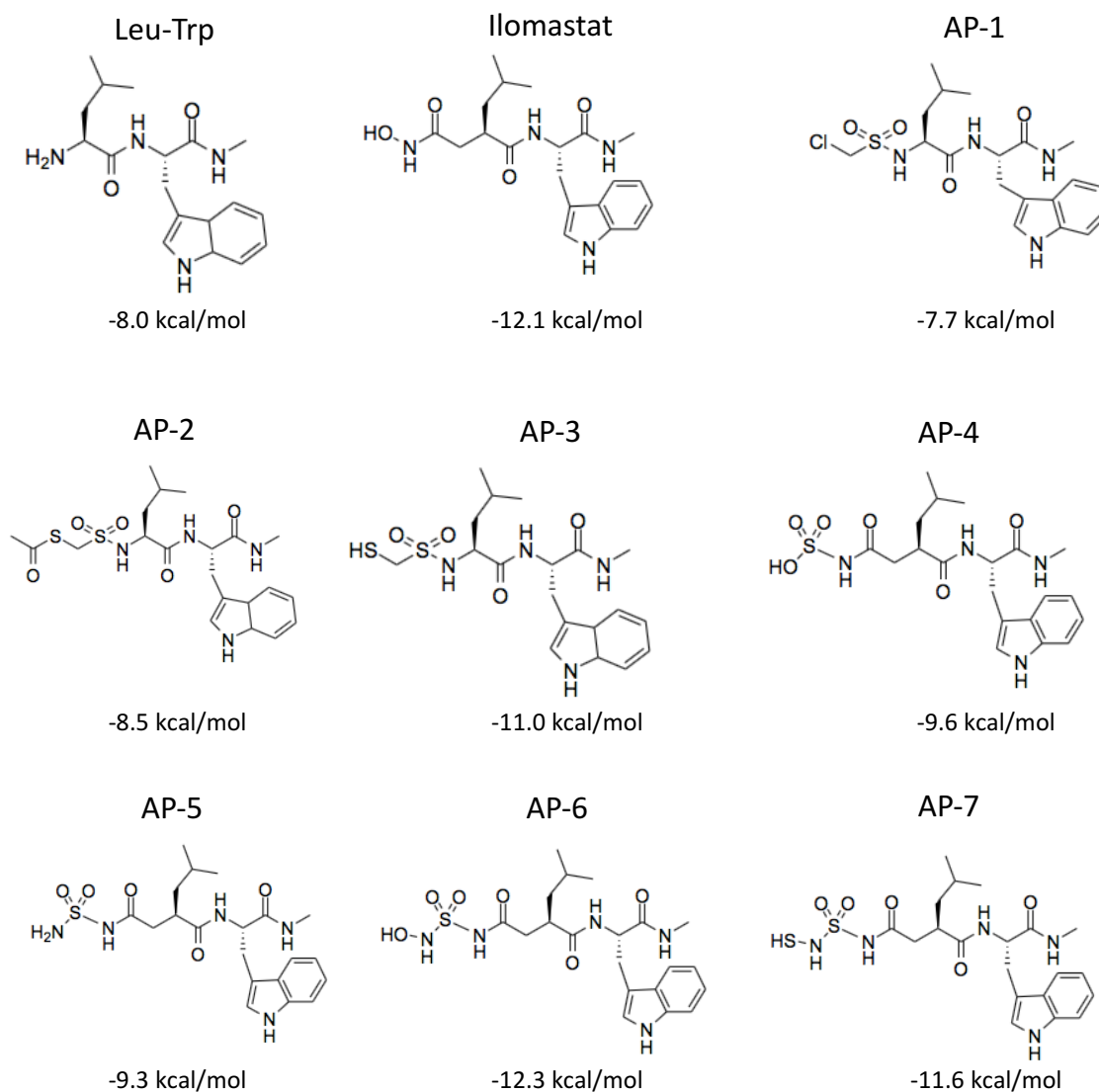


Figure 3.3.1: Proposed ilomastat derivatives. Compounds include the leucine-tryptophan backbone, and ilomastat (commercially available). Below each compound is the binding energy score calculated for the MMP-3 active site using the MOE software.

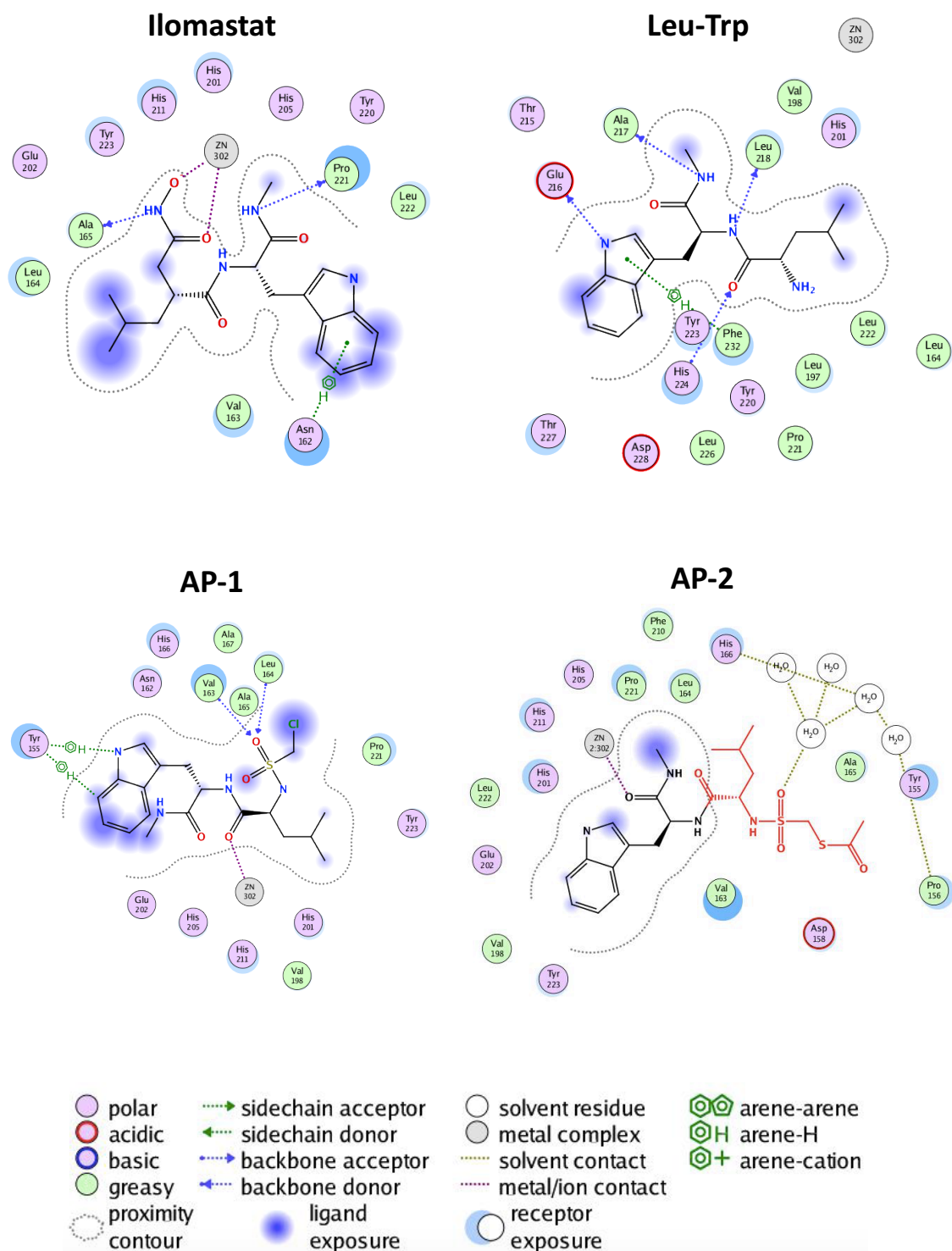


Figure 3.3.2: Interaction diagrams for ilomastat, Leu-Trp, AP-1, and AP-2. Shown are the most favourable interaction diagrams for synthesized compounds leucine-tryptophan backbone, AP-1, AP-2, and ilomastat.

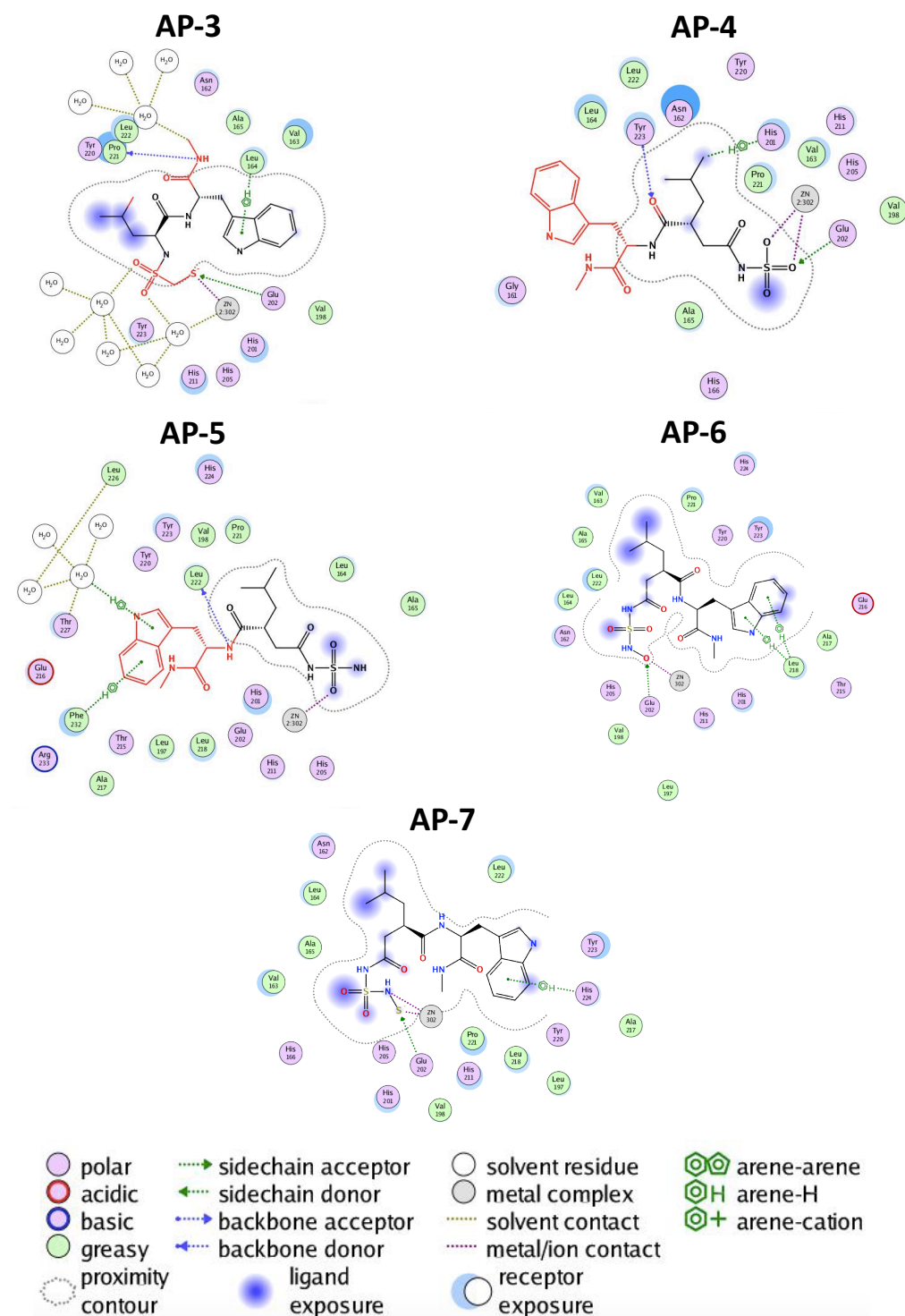


Figure 3.3.3: Interaction diagrams for AP-3, AP-4, AP-5, AP-6, and AP-7. Shown are the most favourable interaction diagrams for proposed compounds AP-3, AP-4, AP-5, AP-6, and AP-7.

3.3.2 Molecular Docking of Ilomastat Derivatives

All proposed compounds (Figure 3.3.1) were subjected to molecular docking to predict their interaction with the MMP-3 active site. In the MOE software, assigned overall best scores (binding energy), the most negative, based on interactions such as ionic bonds, hydrogen bonds, and hydrophobic interactions. When bonds are formed, energy is released, resulting in a decrease in entropy, for a more thermodynamically stable system. Thus, lower binding energy is a predictor for the stability of the interaction between the compound and active site of MMP-3. Furthermore, all compounds examined here demonstrated ligand exposure, indicating each compound had regions that did not interact with the active site of MMP-3 (Figure 3.3.2 and Figure 3.3.3). As competitive inhibitors, a reduction in ligand exposure was used as predictive measure that the compound would be a better inhibitor of MMP-3. Majority of the compounds display the indole ring of tryptophan with an arene-H interaction to the amino acids of the active site, which would stabilize the compound. However, the indole ring also is a destabilizing factor in most of the proposed compounds due to ligand exposure.

All proposed compounds have the same leucine-tryptophan backbone, but with varying ZBGs. As expected, Leu-Trp, which lacks a ZBG, has no interaction with the active site zinc ion. The backbone does have favourable interactions with the active site, giving Leu-Trp a higher score than AP-1. The ZBG of both AP-1 and AP-2 is predicted not bind to the zinc ion, but the ketone portion of the amino acid backbone does coordinate to the zinc, resulting in a lower score than the backbone and ilomastat.

It is expected that ZBGs that form a bidentate interaction and more bonds with the zinc ion would result in a lower binding energy, and thus would be a higher scoring candidate for

catalytic inhibition. An increase in bonds, leads to a decrease in entropy in the system, and an overall more stability. Two of the top scoring compounds, ilomastat and AP-7, are both predicted to have bidentate binding to the zinc ion. However, AP-4 a middle scoring compound also exhibits bidentate binding. The remaining compounds all have monodentate binding to the zinc ion, including AP-6, which is the highest scoring proposed compound. Considering that the highest scoring compound has monodentate binding, both the chelating ability of the ZBG and peptide backbone have to be considered when designing compounds to interact with the MMP-3 active site.

3.3.3 NFF-3 of Ilomastat and Synthesized Compounds

The synthesized compounds Leu-Trp, AP-1, AP-2, and ilomastat were subjected to the NFF-3 assay to determine the biological inhibition of MMP-3. All compounds were tested at a concentration of 50 μ M and 100 μ M, then compared to a control of serum free phenol red free DMEM media. For all these compounds, 100 μ M concentration was better at inhibiting MMP3 than the 50 μ M concentration (Figure 3.3.4 a). Synthesized compounds and ilomastat with the best predicted scores molecular docking were: ilomastat, AP-2, Leu-Trp, and AP-1. However, NFF-3 data shows that AP-1 performs better than Leu-Trp at inhibiting MMP-3. While all compounds do show some inhibition of MMP-3, only the 100 μ M of ilomastat was found to be significant ($p \leq 0.05$).

NFF-3 results coupled with generated binding energy scores for each proposed compound provide valuable input to predict biological compound performance. The change in RFU value for each compound was normalized to the control, resulting in a value of less than 1.

These normalized values were plotted against compound binding energy (Figure 3.3.4). A line of best fit was generated with an R^2 value of 0.98997 for the inhibitors at 50 μM and 0.85178 for inhibitors at 100 μM , indicating a good correlation between the normalized RFU and binding energy scores. Normalized RFU values were calculated for the remaining proposed compounds that were not synthesized, and these compounds were included on the graph (Figure 3.3.4 **d** and **e**). The ability to predict the biological performance of a compound based on the generated binding energy allows for more specific inhibitor design.

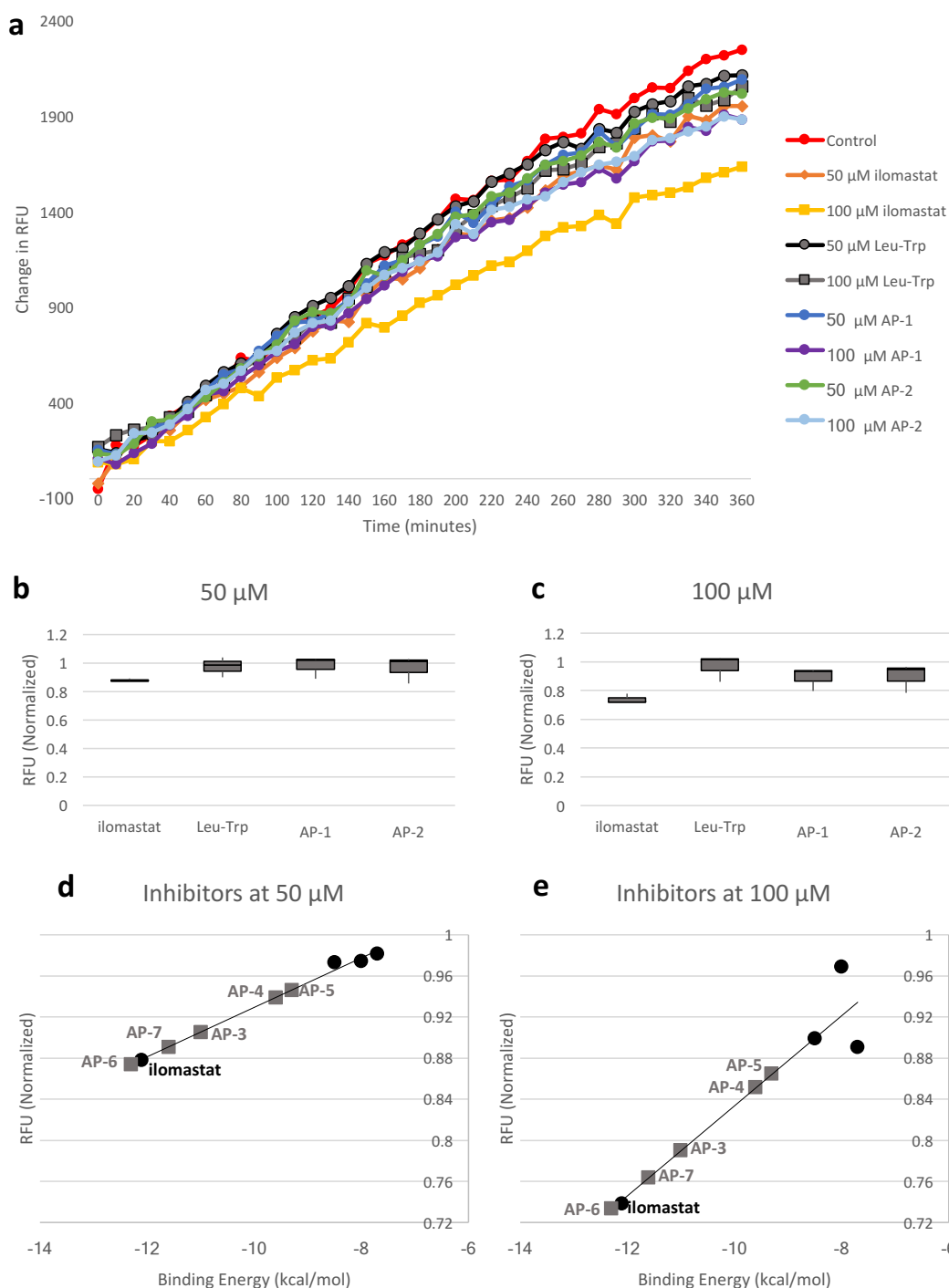


Figure 3.3.4: Inhibition of MMP-3 activity detected by NFF-3 assay. (a) NFF-3 assay over six hours for all synthesized compounds and ilomastat at 50 μ M and 100 μ M concentration. **(b & c)** Box and whisker plot of the change in relative fluorescence units at six hours for inhibitors at a concentration of 50 μ M and 100 μ M. **(d & e)** The binding energy of the synthesized compounds and ilomastat were plotted versus the RFU values normalized to the control at 50 μ M and 100 μ M.

3.4 Conclusion

Seven ilomastat derivative compounds were proposed, MMP-3 active site interaction diagrams and binding energy provided for each compound. Due to time constraints and ease of synthesis, the leucine-tryptophan backbone, AP-1, and AP-2 were synthesized. All synthesized compounds were analyzed by mass spectrometry. The NFF-3 assay was used to determine the inhibition of MMP-3 activity for ilomastat and each of the synthesized compounds. Ilomastat performed better than the synthesized compounds; Leu-Trp, AP-1, and AP-2, therefore, was chosen for further biological studies.

Chapter 4: Biological Effects of MMP-3 Inhibition by Ilomastat

4.1 Introduction

The activity of MMP-3 can be inhibited by the peptidomimetic compound ilomastat. However, further studies into the biological effect of MMP-3 inhibition by ilomastat were required to determine the effect *in vitro*. Different assays were performed using C6-13 cells conditioned with ilomastat to further test the effect on MMP-3 activity, the cytotoxicity of ilomastat, and C6-13 migration. These assays included flow cytometry death assay to determine the cytotoxicity of the ilomastat by measuring cells stained with propidium iodide (PI); NFF-3 assay, and zymography, to monitor the inhibition of increasing ilomastat concentrations on MMP-3 activity. Scratch wound assay was used to assess the relative migration of the cells once exposed to ilomastat.

Flow cytometry is a spectroscopy technique that can be used to distinguish characteristics of cell populations. The advantage of this technique is the ability to analyze large populations of cells, often thousands of cells per second.^{86,87} The majority of flow cytometers use hydrodynamic focusing to narrow the sample stream down to the diameter of an average cell by enclosing the sample stream in a faster flowing sheath stream.⁸⁶ Since the sample stream is the diameter of a cell, the cell will displace most of the sample stream surrounding it, allowing for the fluorophores associated with each individual cell to be excited by the laser beam and be detected (Figure 4.1.1).⁸⁶ The ability to detect characteristics of a single cell, provide cell populations to be grouped based upon defined characteristics, such as apoptosis.

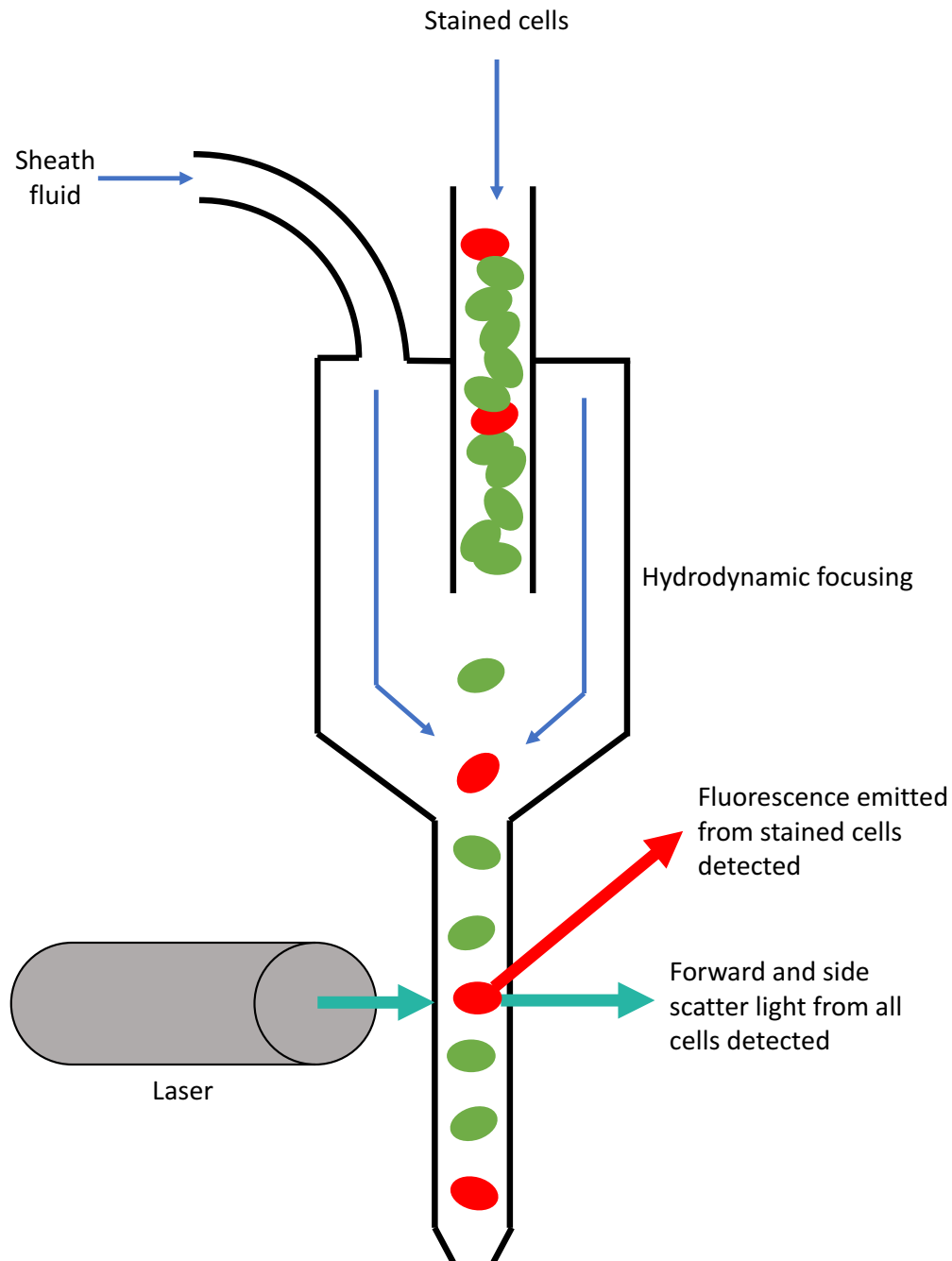


Figure 4.1.1 Flow cytometry mechanism. Sample of PI stained cells are hydrodynamically focused into a single cell stream using sheath fluid. As cells pass the laser, the light beam is disrupted causing detectors to measure the amount of forward and side scattered light. If a cell is stained with PI, PI will fluoresce red and will be detected by the red fluorescence detectors. Adapted from Abcam protocol.⁸⁸

A change in cell morphology is standard for the recognition of apoptotic cells.⁸⁹ A defining feature of apoptotic cells is a permeable plasma membrane that is no longer intact, allowing them to be distinguished from alive cells via fluorescent molecules such as propidium iodide (PI). PI is a small molecule that intercalates to nucleic acids, and thus cannot enter cells that have an intact membrane.^{90,91} Once bound to nucleic acids, PI can be excited by wavelengths between 400 – 600nm, and displays red fluorescence between 600 – 700nm.⁹¹ The ability to distinguish apoptotic cells from live cells, allows for the cytotoxicity of a compound (in this thesis ilomastat) to be determined and a concentration range to be established for additional assays.

Zymography is an electrophoretic technique based on SDS-PAGE in which MMP activity can be detected. In zymography, enzymatic substrates such as gelatin, casein, and collagen are co-polymerized with the sodium dodecyl sulfate (SDS) polyacrylamide gel. In the electrophoretic step MMPs are separated based upon molecular weight. In addition to separating various MMPs, the electrophoretic step also separates MMP-TIMP complexes.⁹² This is important to note because TIMPs are the endogenous inhibitors of MMP; in order to see MMP activity the enzymes must not be inhibited. Proteins are loaded onto the gel using a standard denaturing SDS loading buffer. However, the proteins are not boiled or treated with a reducing agent such as DTT, in order to limit the amount of degradation and denaturing of the protein.⁹² The SDS causes denaturation and inactivation of MMPs, although this is reversible, and the enzymes partially renature and recover part of the initial activity.^{92,93} Activation of pro-MMPs is believed to be due to the cysteine switch being removed during denaturation, exposing the catalytic zinc ion.⁹⁴

After the electrophoresis, the MMPs are partially renatured by washing the gel with a non-ionic detergent such as Triton X-100, which removes the SDS from the gel.⁹² The gel is then incubated overnight in buffer containing Ca^{2+} , since MMPs are calcium dependent.⁹² The MMPs can then degrade the substrate added to the gel. After incubation overnight, the gel is stained with Coomassie Blue and MMP activity is detected as clear bands.

Cell migration is essential to many biological processes such as cell growth, differentiation, inflammation, wound healing, but is also involved in cancer.⁹⁵ Migration is the movement of individual cells or cell sheets from one place to another, whereas invasion is the migration of cells in 3-dimensional space as they move through the ECM.⁹⁵ *In vitro* scratch wound assays are a standard, simple, inexpensive technique to measure collective cell migration that somewhat mimics *in vivo* cell migration.^{96,97} A cell free area, or “scratch”, is created on the confluent cell monolayer, the exposure to the scratch induces cells at the edge to migrate into the gap until new cell-cell connections are formed.^{96,97} The advantages of using the scratch wound assay include: the assay can be performed on any plate, usually a multi-well plate; cells move in a defined direction; the surface can be coated with ECM proteins of choice; movement and morphology of cells can be easily visualized; it is a simple and inexpensive assay to perform.⁹⁵ Due to its many advantages, the scratch wound assay is used widely to study *in vitro* migration.

4.2 Materials & Methods

4.2.1 Flow Cytometry Cell Death Assay

At 80-90% confluence, cells were aspirated, washed twice with PBS and treated with serum free DMEM containing various concentrations of ilomastat (no ilomastat, 50 μ M, 100 μ M, 200 μ M) for 24 hours. After 24 hours, conditioned media was collected, cells were removed from the wells using trypsin and added to the conditioned media. Wells were washed with PBS twice, with washes added to the cells/CM, and centrifuged at 500g for 5 minutes. The supernatant was removed and the cell pellet was resuspended in 2mL of PI-FACS buffer. Cells were conditioned in PI-FACS buffer for 15 minutes at room temperature, in the dark, then pelleted again at 500g for 5 minutes. Cells were washed with 2mL of PBS, pelleted again, and resuspended in 4mL PBS. For analysis 1mL of the cell suspension was added to 2mL of PBS. The percentage of dead cells was quantified by flow cytometry (CyAn ADP, Beckman Coulter).

A second flow cytometry sample preparation was performed to limit the cell death by trypsin in the cell removal stage mentioned above and measure cell death over a longer period of time. Cells were grown to 80-90% confluence, washed twice with PBS, conditioned with serum free DMEM, and treated with the following ilomastat concentrations: no ilomastat, 25 μ M, 50 μ M, 75 μ M, 100 μ M. After 72 hours, the conditioned media was collected and incubated in the dark at 37°C for 15 minutes in 1mL of PI-FACS. The cells were conditioned at the same time in 2mL of PI-FACS for 15 minutes at 37°C, in the dark. After the incubation time, cells were removed with trypsin, added to the conditioned media, wells were washed twice with PBS, with the washes added to the conditioned media/cell suspension. Cells were pelleted at 500 x g for 5 minutes, the supernatant removed, resuspended in 2 mL of PBS, pelleted again,

then resuspended in 4mL of PBS. For analysis 1mL of the cell suspension was added to 2mL of PBS. The percentage of dead cells was quantified by flow cytometry (CyAn ADP, Beckman Coulter).

4.2.2 NFF-3 Fluorescence Assay

Cells were plated on a 20cm plate and grown to confluence (3-4 days). The plate was washed twice with PBS, once with serum-free/phenol-red free media and conditioned with 15mL of serum free phenol red free media for 24 hours. After 24 hours, the conditioned media was collected and 2500 μ L were portioned out into five 15 mL falcon tubes. Ilomastat was added to have tubes with the final following concentrations: 25 μ M, 50 μ M, 75 μ M, and 100 μ M. Each experimental condition had its own control condition. Using a 96 well plate 15 μ L of distilled water were added to the control wells and 15 μ L of 100 μ M NFF-3 were added to the experimental well. Then 300 μ L of the conditioned media with inhibitors were added to the control and experimental wells, resulting in an overall concentration of 4.76 μ M NFF-3. The excitation wavelength of the spectrometer was set to 325nm while the emission was set to 393nm. The fluorescence was measured every ten minutes over the course of six hours, with the plate shaking for 15 seconds before each reading. The experiment was conducted at 37°C.

4.2.3 Gelatin Zymography

Cells were plated on a six well plate at a concentration of 200,000 cells per well. Cells were grown to confluence (3-4 days) and conditioned with serum free DMEM. Ilomastat was then added to the media to a final concentration of 25 μ M, 50 μ M, 75 μ M, or 100 μ M. Cells were

conditioned for 24 hours. After 24 hours, the conditioned media was collected and immediately placed on ice. The conditioned media was concentrated using spin filters, with the tubes being centrifuged at 4800g for 12 minutes in pre-chilled rotors. Protein concentration was determined by BCA assay. Protein samples were loaded on a 10% SDS gel containing 0.1% gelatin and ran at 125V for approximately 3 hours. The gel was then washed twice in the incubation buffer with Triton X-100 for a minimum of 45 minutes each. The gel was washed for 10 minutes in the incubation buffer, new incubation buffer was added and the gel was placed in a 37°C incubator for 20 hours. After incubation, the gel was stained in Coomassie blue for 1 hour. The gel was then washed in destaining solution until bands appeared. Photos were then taken of the gel and analyzed using ImageJ.

4.2.4 ImageJ Analysis

ImageJ software was used for both western blot and zymography analysis. Images in jpeg format were uploaded and changed to an 8-bit (black and white) image. Bands were selected using the rectangle selection tool, with the rectangle being twice as high than it is wide. The first lane (band) was selected under the “gels” section (“select first line”) of the “analyze” tab. A new rectangle was then generated and positioned over the next band, this band was then selected under the “gels” section, “select next lane”. Band selection is continued until all bands have been selected. The lanes (bands) can then be plotted using the “plot lanes” option in the “gels” section, generating peaks for each band. For zymography the peaks were inverted and thus a straight line must be drawn from the baseline to baseline to enclose the peak. Once peaks are enclosed the wand tool is used to select inside the peak and the area of the peak is

generated by selecting “label peaks” from the “gels” section. The area of the peak, and thus the area of the band corresponds to the relative amount of MMP-3 present.

4.2.5 Scratch Wound Assay

Cells were plated on a six well plate at a concentration of 200,000 cells per well. Cells were grown to confluence (3-4 days), then a 1 mm scratch was made through the center of the wells using a P1000 pipette tip. Cells were then washed twice with PBS, once with low glucose (serum free phenol red free media) or high glucose (serum free) media and conditioned with 1.5mL of low glucose or high glucose media. Ilomastat was then added to the media to have a final concentration of 25 μ M, 50 μ M, 75 μ M, or 100 μ M. Images of the scratch were taken (t=0) using the Zeiss Axio Zoom.V16 microscope at 68x magnification and 78% amplification, using the Zen Blue Lite software. Images were taken again at t=24 hours and t=48 hours. Images were then analyzed using ImageJ, the 20 furthest moving cells were measured and the relative migration was calculated.

4.3 Results & Discussion

4.3.1 Flow Cytometry Cell Death Assay

Ilomastat cytotoxicity was tested to determine ilomastat concentrations for further biological studies such as NFF-3, zymography, and scratch wound. Initially, ilomastat concentrations of 50 μ M, 100 μ M, and 200 μ M were used to measure the amount of cell death after 24 hours of conditioning. Cells were then removed and stained with propidium iodide. More PI uptake results in higher PI fluorescence, which is detected using PE CD38Log, a red fluorescence

detector. PI fluorescence was measured against the side scatter of the cells (Figure 4.3.1 a & b). PI fluorescence versus the event count, total number of cells, was measured for additional cell death data. Percentage of cell death was determined by gating the two cell populations (Figure 4.3.1 a & b), apoptotic cells will appear in the top gate because of the higher PI fluorescence, whereas alive cells will appear in the bottom gate. The percentage of cell death for each condition can be seen in Figure 4.3.1 c. Amount of cell death measured for each condition is high for a 24-hour conditioning period. Cell death normalized to the control gives more reasonable values, although the 200 μ M treatment still has considerable cell death.

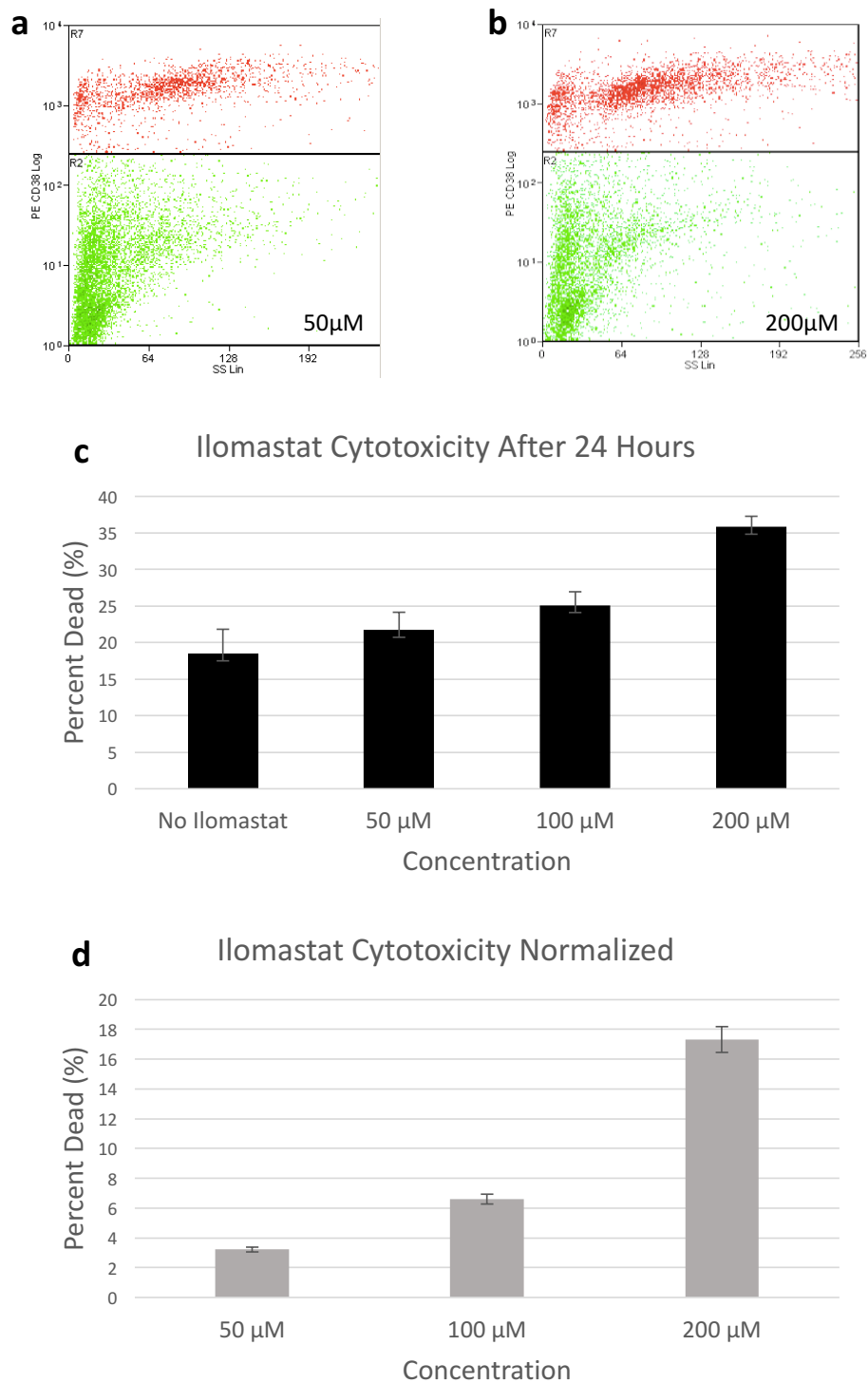


Figure 4.3.1: Cytotoxicity of ilomastat after 24 hours. (a & b) After conditioning for 24 hours, cells stained with propidium iodide were measured using flow cytometry, 50 μM and 200 μM . **(c)** Cell death after 24 hours. **(d)** Cell death normalized to the no ilomastat treatment.

The amount of cell death occurring in this procedure may be due to the sample prep itself. C6-13 are very adherent cells, and thus can be more difficult to detach from the plate. During incubation with trypsin to detach cells, additional cell death may have occurred if the cells were incubated for too long, adding to the cell death from ilomastat. A substantial amount of cell death occurs in the control sample (Figure 4.3.1 c), indicating that this cell death is due to natural processes or sample preparation. The control sample does contain DMSO, but DMSO contribution to cell death can be ruled out because concentrations below 1% are safe for most cell lines. Therefore, the majority of the cell death must be due to sample preparation, specifically the incubation of trypsin. In addition, visually there was little to no cell death in these samples.

A secondary protocol was tested using a gentler cell approach and staining the cells before removal from the plate. Experimental time period was changed from 24 hours to 72 hours because little cell death should occur after 72 hours and the maximum time point in the scratch wound assay would be 48 hours. Concentration of ilomastat used was changed to 25 μ M, 50 μ M, 75 μ M, and 100 μ M. Cell death from applying 200 μ M in the first protocol was relatively high and it is not recommended to use concentrations above 100 μ M⁷⁹. Using the secondary protocol, there was a significant decrease in cell death across all ilomastat concentrations and control. All conditions have less than 1% cell death (Figure 4.3.2 b), signifying that at these concentrations, ilomastat is not cytotoxic over a 72-hour time period. Ilomastat concentrations 25 μ M, 50 μ M, 75 μ M, and 100 μ M was used in further biological studies.

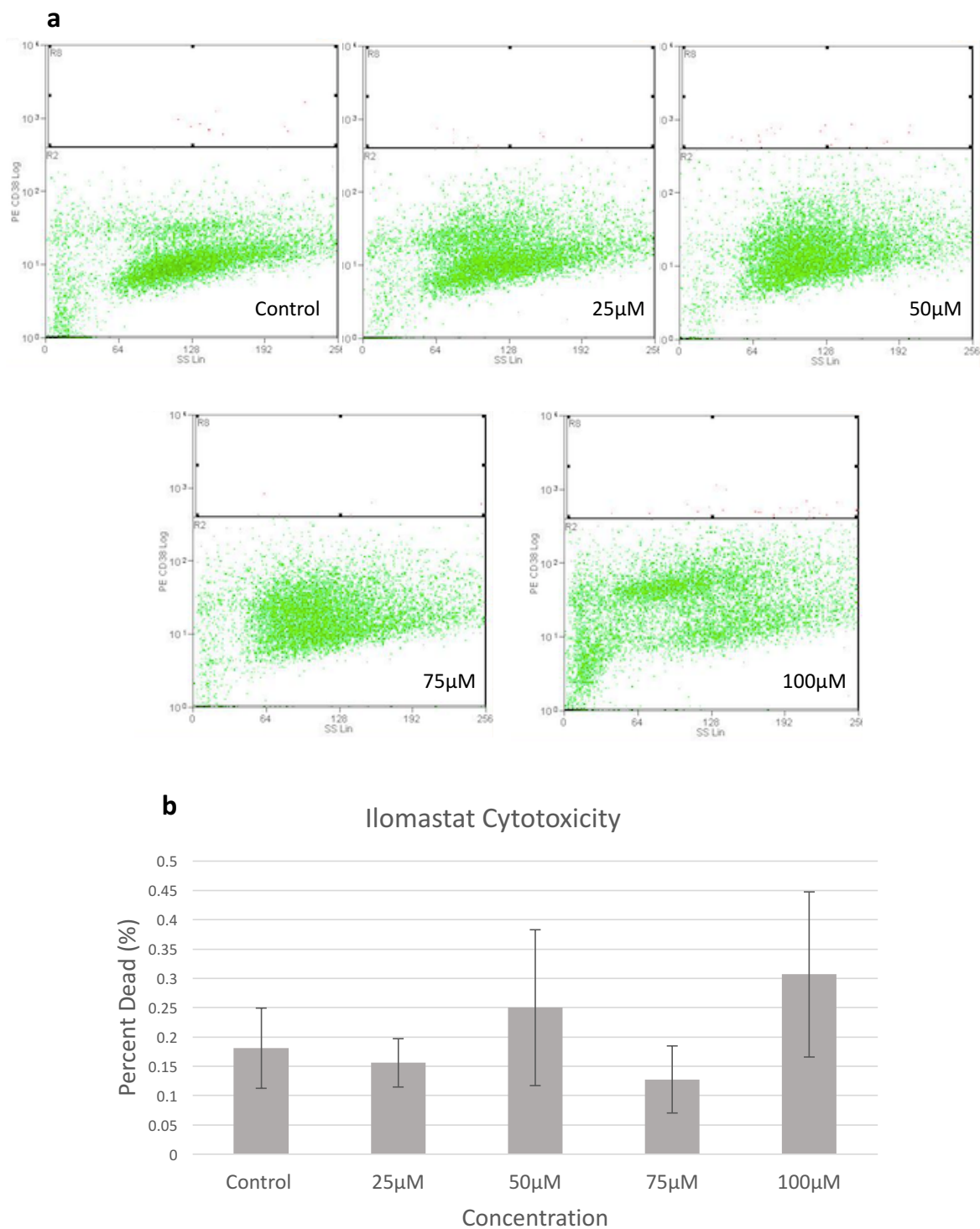


Figure 4.3.2: Cytotoxicity of ilomastat after 72 hours. (a) Flow cytometry of red fluorescence detector PECD38 Log versus side scatter for each experimental condition. **(b)** Cell death after 72 hours for each condition.

4.3.2 NFF-3 Fluorescence Assay

Inhibition of MMP-3 by ilomastat was tested using the NFF-3 assay (same as in chapter 2 & 3).

As determined by the flow cytometry experiment, ilomastat concentrations used were 25 μM , 50 μM , 75 μM , and 100 μM . A significant difference occurs between the control and all four of the ilomastat treatments, with significance increasing as the ilomastat concentration increases.

Thus, all treatment concentrations had an inhibitory effect on MMP-3.

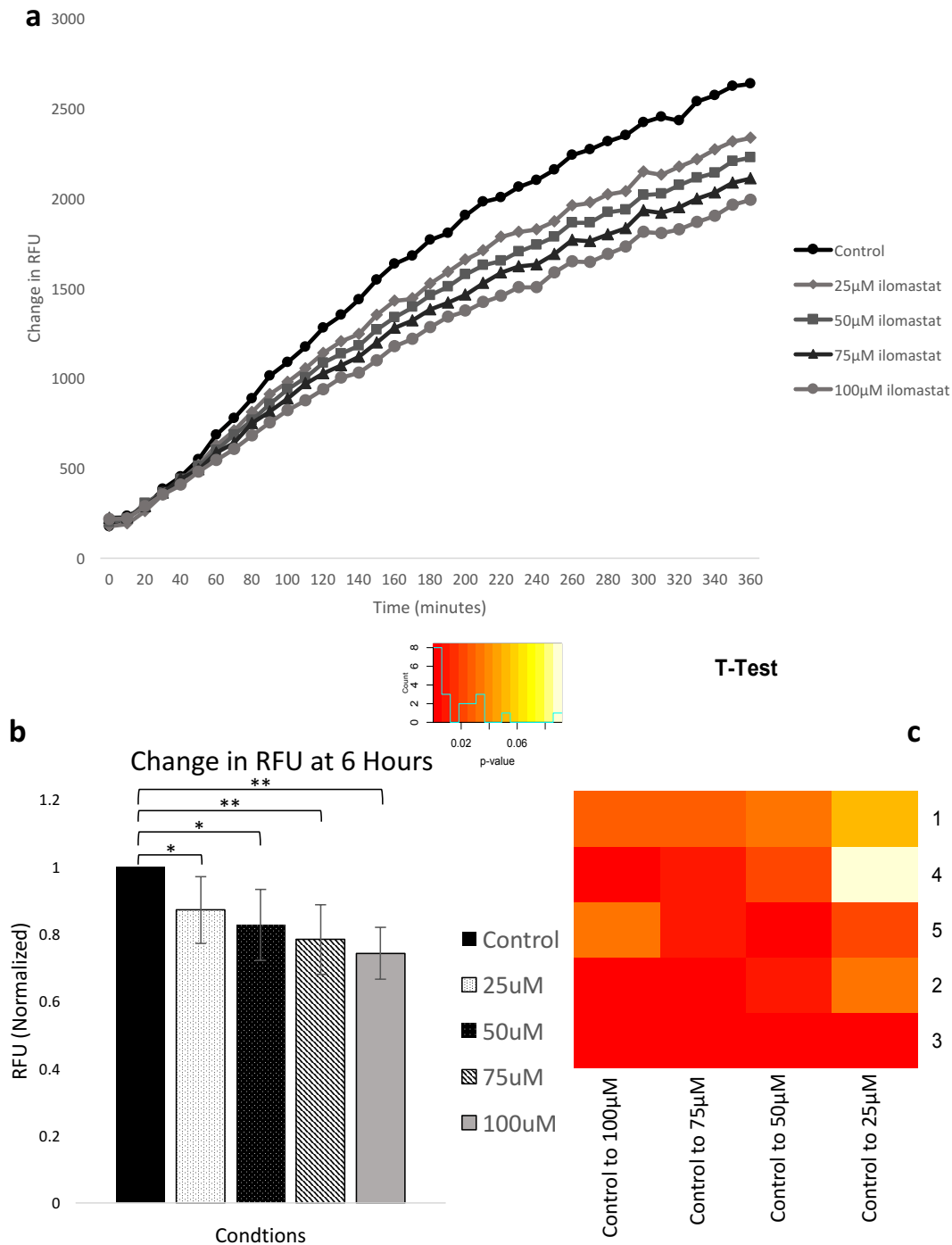


Figure 4.3.3: Inhibition of MMP-3 activity by varying ilomastat concentrations. (a) Change in RFU for each concentration of ilomastat. **(b)** Normalized RFU of all biological replicates, showing significance for each condition. **(c)** T-test comparison of all biological replicates showing statistical significance for all replicates.

4.3.3 Gelatin Zymography

A further insight into MMP-3 activity was performed using gelatin zymography. As mentioned in Chapter 2, gelatin is a substrate of MMP-3, thus gelatin zymography was performed to monitor the effect of MMP-3 inhibition by ilomastat on a natural substrate of MMP-3. MMP-3 has a molecular weight of 54 kDa and can be seen just below the 60 kDa protein marker (Figure 4.3.4a). As can be seen in Figure 4.3.4a, increases in ilomastat concentration result in decrease of thickness and visibility of MMP-3 bands, indicating that less gelatin is being degraded. The decrease in degradation of gelatin is noteworthy, because it signifies that MMP-3 inhibition does have an effect on degradation of its substrates and, thus, may have an effect on MMP-3 involvement in migration. All the concentrations of ilomastat had a significant effect on the inhibition of MMP-3, with the greatest significance occurring at the highest concentration of ilomastat. The MMP-3 zymography data further supports the results from the NFF-3 assay.

In addition to the MMP-3 results, multiple bands appeared between the 90 kDa and 70 kDa protein markers indicating the presence of more gelatin degrading enzymes. These bands most likely belong to MMP-9, which has a molecular weight of 92 kDa in its pro-MMP form and 82 kDa in its active form. Gelatin zymography is most commonly used for the gelatinases MMP-9 and MMP-2. Pro-MMP-9 is also a substrate of MMP-3, thus it is likely that the additional bands appearing in the zymography belong to MMP-9. The bands of MMP-9 do appear fainter as ilomastat concentration increases, which could be due to MMP-3 being inhibited, leading to a reduction in the activation of pro-MMP-9 to MMP-9, or simply ilomastat inhibiting MMP-9 itself.

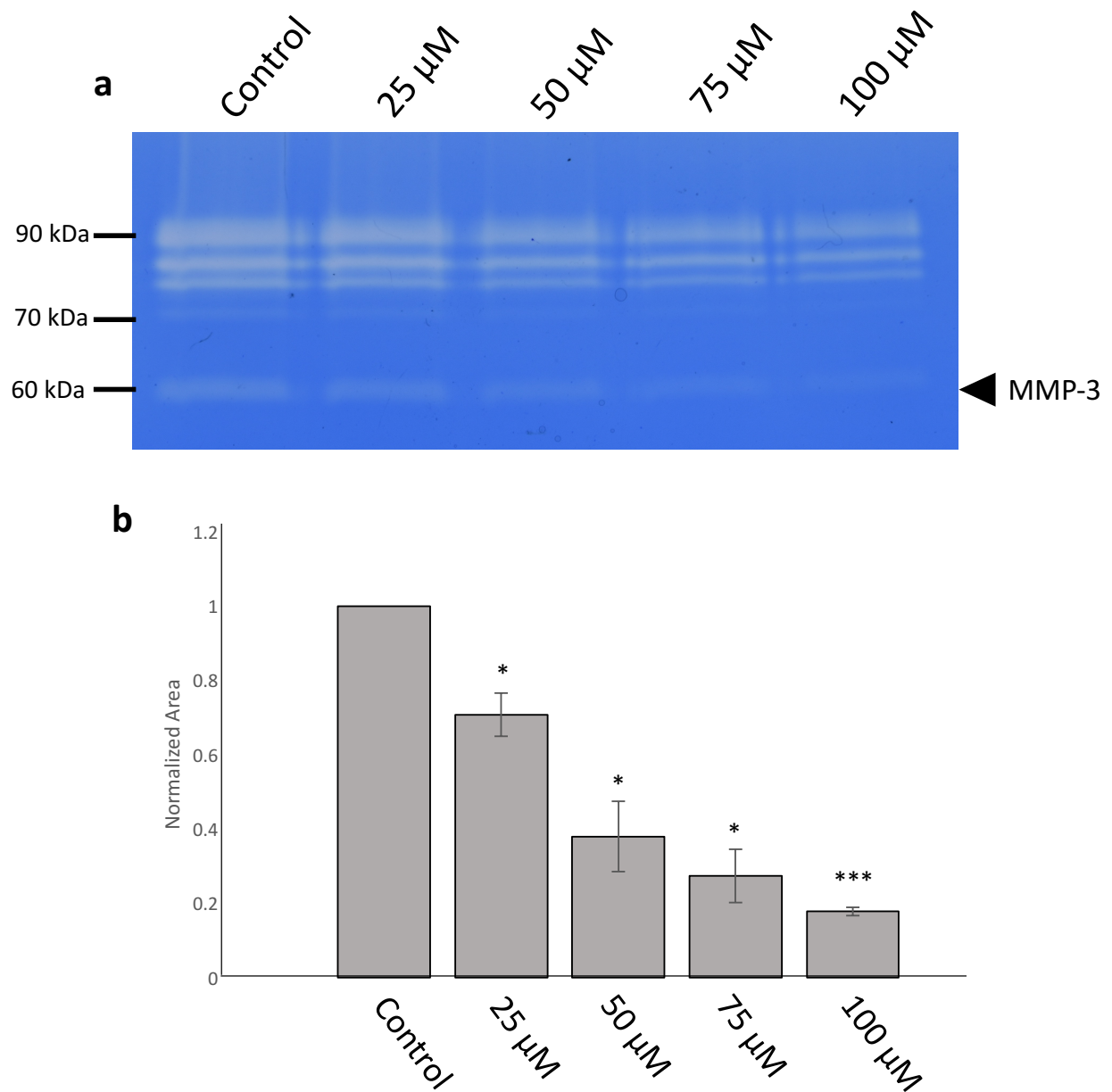


Figure 4.3.4: Gelatin zymography of varying ilomastat treatments. (a) MMP-3 appears just below the 60 kDa protein marker. **(b)** Normalized band area of MMP-3 normalized to the control, with each ilomastat treatment showing statistical significance, and 100 μ M having the highest significance.

4.3.4 Scratch Wound Assay

To understand the effect of ilomastat on the migration of C613 cells, the scratch wound assay was performed. In these studies, C613 cells were conditioned with either low glucose (1000mg/L glucose) or high glucose (4500mg/L glucose). Ilomastat concentrations were set at 25 μ M, 50 μ M, 75 μ M, or 100 μ M based on the NFF-3 results.

The relative migration of the top 20 most migratory cells were taken for comparison from control to ilomastat treatments (Figure 4.3.5 - 4.3.8). There was an insignificant decrease in migration from the control to the treatments, but the decrease in migration was not dependent on the concentration of ilomastat. In addition, corresponding to the literature^{98,99}, cells conditioned with low glucose media had a higher relative migration in comparison to cells conditioned with high glucose media (Figure 4.3.9).

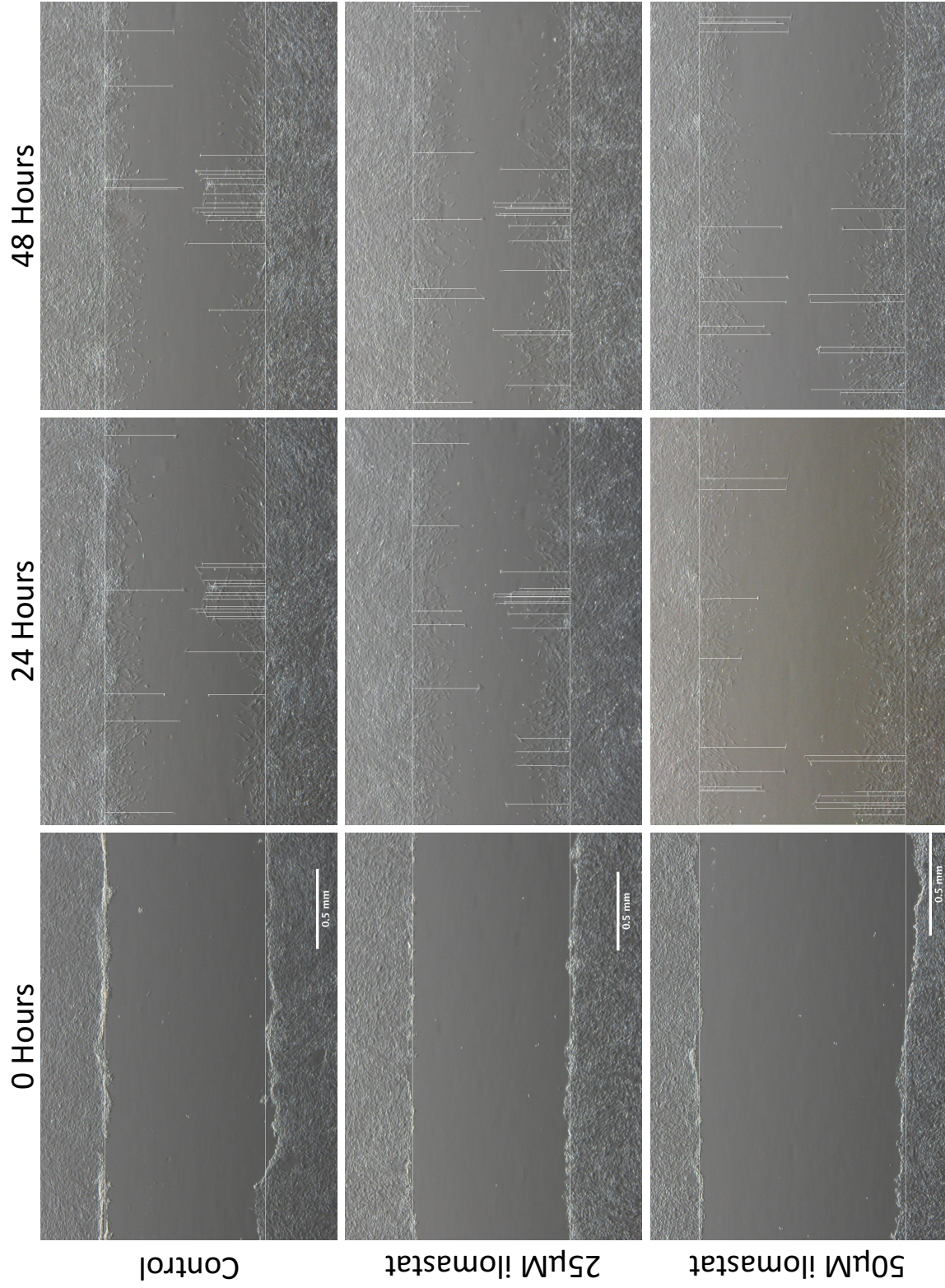


Figure 4.3.5: Low glucose media migration for control, 25 μ M, and 50 μ M at 0, 24, and 48 hours.

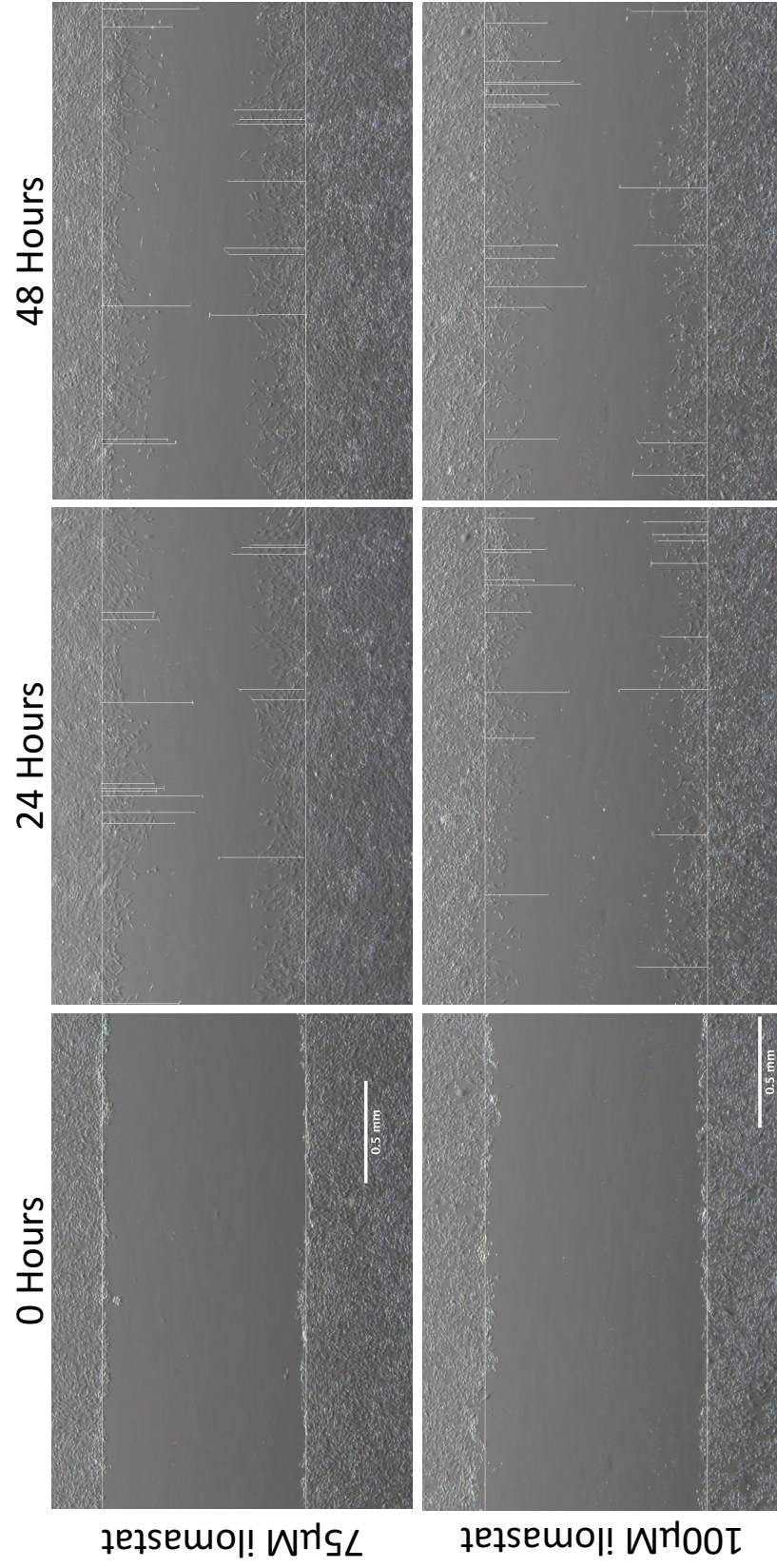


Figure 4.3.6: Low glucose media migration for 75 μM and 100 μM at 0, 24, and 48 hours.

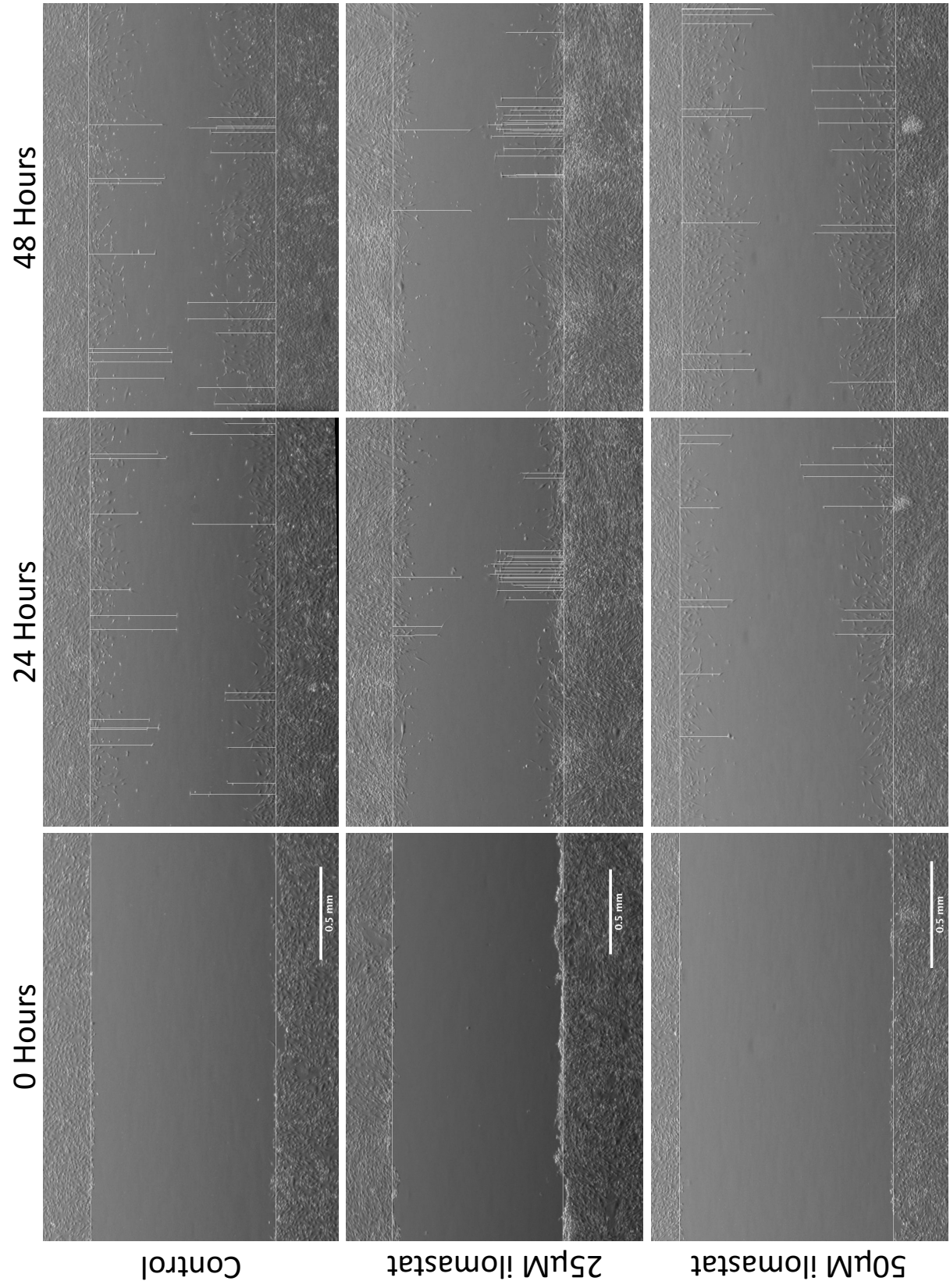


Figure 4.3.7: High glucose media migration for control, 25 µM, 50 µM at 0, 24, and 48 hours.

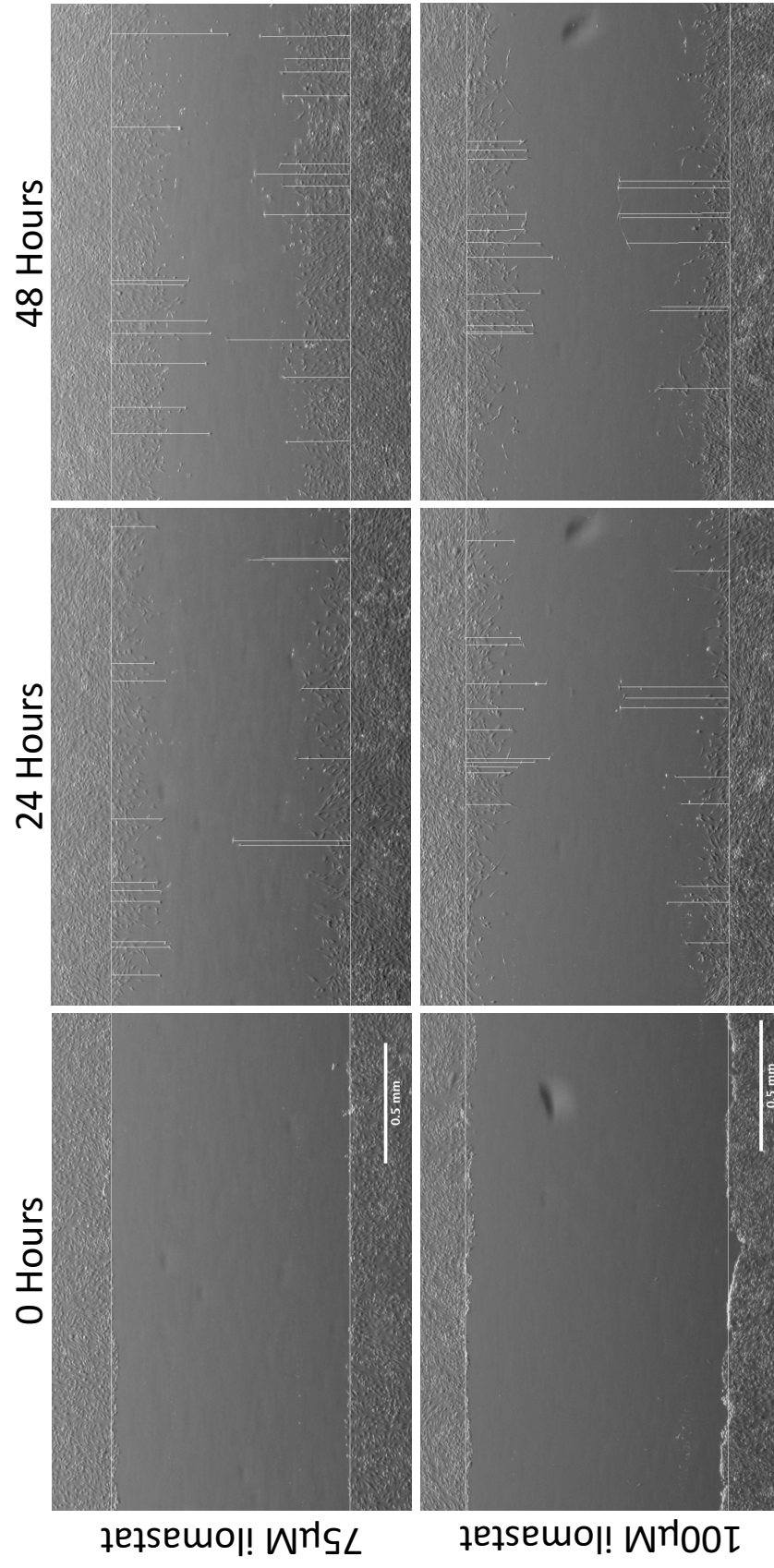


Figure 4.3.8: High glucose media migration for 75 μM and 100 μM at 0, 24, and 48 hours.

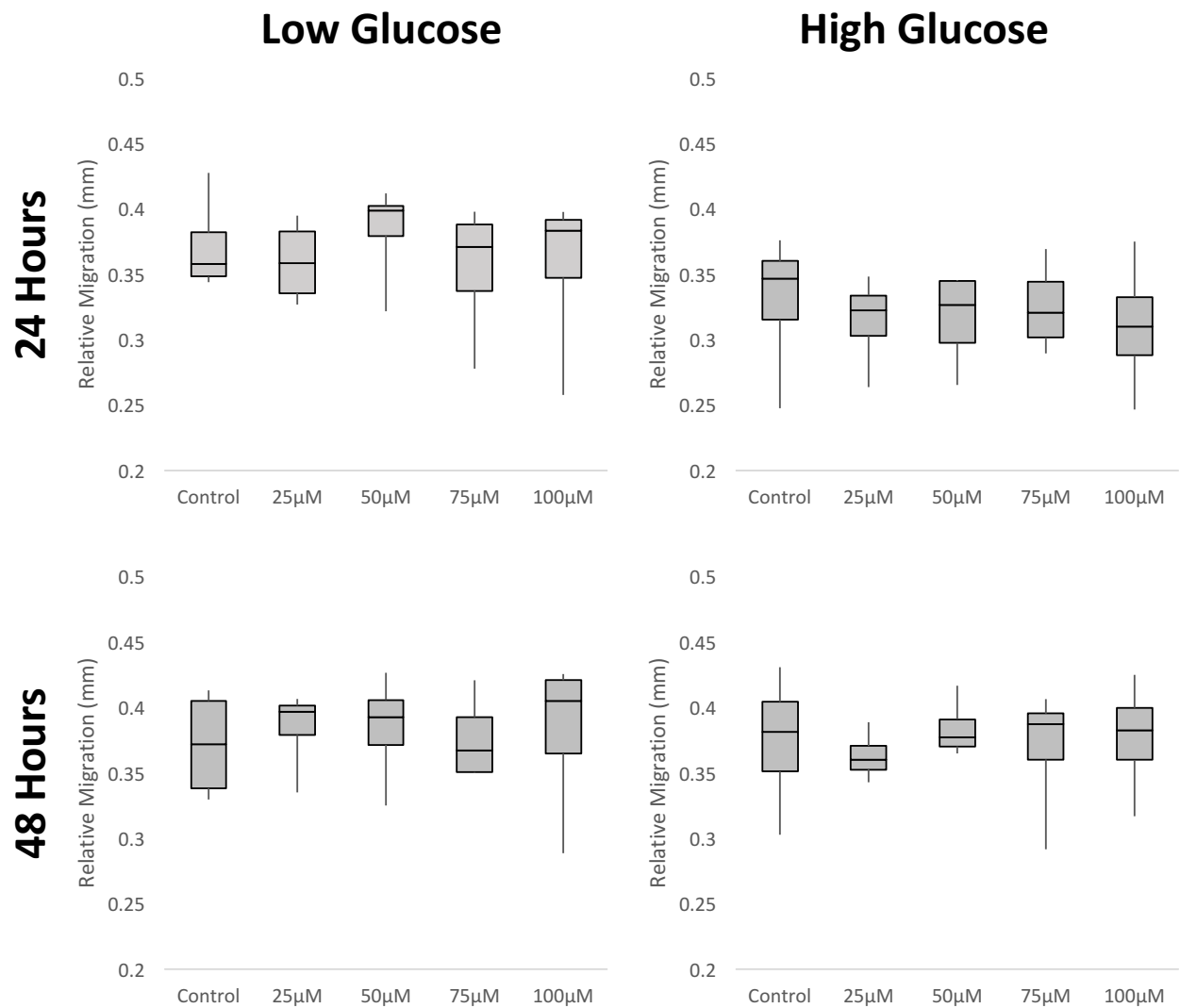


Figure 4.3.9: Relative migration of each ilomastat treatment for low glucose and high glucose media at 24 and 48 hours.

The fact that there was no change between the control and experimental conditions in the migration of cells in the scratch wound assay may be attributed to the disadvantages to the assay itself. Some of the disadvantages of the scratch wound assay include: the size and shape of the scratch can vary from well to well; monolayer confluence from control to experimental conditions may not be the same; the ECM and ECM proteins can be damaged by the scratching of the monolayer.⁹⁵ In addition, the edges of the scratch often retract indicating that cells on the edge of the scratch may have lost their original morphology and function due to the physical stress from the scratch.¹⁰⁰

As mentioned above the scratch wound assay has many disadvantages that may contribute to the inconsistency in results. This may be overcome by increasing the number of biological replicates or trying to further minimize any variation that may occur from well to well. Another factor that may have contributed to non-significant results, is the fact that ilomastat is an MMP inhibitor, and MMPs aid migration in cleaving the ECM. If the ECM produced by the cells was damaged due to the scratch, there would be no mechanical resistance preventing the cells from migrating, therefore the addition of ilomastat would be ineffective. This could be overcome by adding artificial ECM, such as matrigel to the wells providing the mechanical resistance.

Another assay to try would be the tumor spheroid invasion assay. In this assay cells are grown in vitro in a low-adhesion, round bottom well to promote the formation of spheroids. Matrigel is added and the cell migration out of the tumor spheroid. This assay is a better representation of how migration away from a tumor occurs and may be a better assay to investigate MMP-3 in this cell system.

In a study by Yan et al. 2016, it was shown that GBM cells treated with ilomastat may be able to overcome the loss of protease-dependent migration by switching to an amoeboid-like migration. Ilomastat caused the activation of RhoA/ROCK/MLC signal causing mesenchymal-amoeboid transition in the cells, inducing amoeboid-type cell migration.¹⁰¹ The combination of ilomastat and a RhoA/Rho kinase inhibitor decreased the invasiveness of cells.¹⁰¹ Therefore, a combination of inhibitors may be needed to have a beneficial effect on migration and invasion.

4.4 Conclusion

Ilomastat was used for further biological studies on the inhibition of MMP-3. First, the cytotoxicity of ilomastat was determined using propidium iodide flow cytometry. From the flow cytometry data, it was determined that the highest concentration of ilomastat for biological assays would be 100 μ M. The NFF-3 assay was then performed to see if there was a correlation between increasing ilomastat concentration and the inhibition of MMP-3. Gelatin zymography data further support the NFF-3 data in that increasing ilomastat concentration does in fact lead to an inhibition of MMP-3 and a decrease in its activity. Finally, scratch wound assays were performed to monitor the effect of MMP-3 inhibition on migration. While no significant change was noticed in the scratch wound assays performed, it cannot conclusively be said that MMP-3 does not play a role in migration, further investigation into this area is needed.

Chapter 5: Overview of Research and Future Directions

5.1 Overview of Research

The overall objective of this thesis was to analyze the enzymatic inhibition of MMP-3 through the use of peptidomimetic inhibitors. The initial step of this thesis was to further confirm the upregulated expression of MMP-3 in C6-13 cells through my own mass spectrometry secretome experiment and Western blot analysis. Both experiments showed an increased expression of MMP-3 in the C6-13 cells over the C6 cells. Knowing that the expression of MMP-3 is upregulated, the next step was to determine if the activity of MMP-3 is correlated to expression through the use of the fluorescent NFF-3 assay. It was found that in addition to the expression of MMP-3 being upregulated so is the activity.

The third chapter of the thesis focused on the design, synthesis, and molecular docking of peptidomimetic MMP-3 inhibitors. Inhibitors were proposed and synthesized based on ease of synthesis. Leu-Trp, AP-1, AP-2, were synthesized and analyzed by mass spectrometry. AP-3 was in the process of being synthesized but was not identified by mass spectrometry, thus needs further work. All proposed inhibitors and ilomastat were docked into the active site of MMP-3 using in silico molecular docking. The top scoring inhibitors, and thus the best potential inhibitors would be AP-6 and AP-7. Inhibitory effect of synthesized compounds and ilomastat were tested using the NFF-3 assay. The best performing compounds were AP-6 and ilomastat. However, since AP-6 has not yet been synthesized, ilomastat was chosen for further analysis on MMP-3 activity.

The final aim of this thesis was to analyze how inhibition of MMP-3 effected its activity and if MMP-3 is involved with C6-13 migration. The cytotoxicity of ilomastat was determined using propidium iodide flow cytometry. From the concentrations of ilomastat tested, it was determined that 100 μ M would be the highest concentration used. Next various ilomastat concentrations were tested using the NFF-3 assay to determine if increasing concentration led to increasing MMP-3 inhibition and if there was a maximum inhibitory concentration. It was found that all concentrations had a significant effect on the inhibition of MMP-3, and that the significance increased as the concentration increase. There was no maximum inhibitory concentration determined for the concentrations used. Gelatin zymography was used to determine the effect of MMP-3 inhibition on a natural substrate of MMP-3. As with the NFF-3 assay, increasing concentration of ilomastat, led to an increase of MMP-3 inhibition, and therefore a decrease in gelatin degradation. The zymography showed that by inhibiting MMP-3, you can reduce the degradation of its natural substrates, and may be able to reduce its contribution to migration.

To test MMP-3 inhibition on migration, the scratch wound assay was used. Both high glucose and low glucose DMEM media was used to see if increased migration could be induced by using low glucose media. While cells conditioned in the low glucose media did have a higher relative rate of migration, there was no significant difference between the migration in the ilomastat treated cells and the control.

5.2 Future Research into MMP-3 and the C6-13 Secretome

Like all cancers, the mechanisms and pathways of GBM tumors are highly complex. While gaining more knowledge of these tumors is necessary, it is as equally important to study the environment surrounding the tumor. The tumor microenvironment consists of cells, proteins, ECM, and mechanical cues that protect the tumor from host immunity, provide therapeutic resistance, promote growth and invasion.¹⁰² Thus, studying the tumor microenvironment, or secretome, will provide better insight into the mechanism of invasion and could provide better therapeutic targets.

An area that needs further attention are secretome studies on the C6-13 cells. Originally this thesis was going to include mass spectrometry secretome analysis comparing peptide cleavages with and without MMP-3 inhibition, to compare how these peptide cleavages change and to get a better understanding of the role of MMP-3 in the tumor microenvironment of C6-13 cells. By inhibiting MMP-3 we would be able to analyze the effects of MMP-3 inhibition not only on peptide cleavage, but the proteins upstream and downstream from MMP-3 itself. Being able to monitor the effects upstream and downstream of MMP-3 may offer alternative therapeutic targets than MMP-3.

While we did attempt TAILS (terminal amine isotopic labeling of substrates) and secretome studies, we were unable to get a working protocol to give consistent results. This would be an excellent area for future studies due to some of the ground work already being in place. Better understanding of the role of MMP-3 in the tumor microenvironment of C6-13 cells may provide insight into new therapeutics and MMP-3 inhibitors.

The inhibitors synthesized in this thesis did not perform better than the commercially available ilomastat. However, the proposed compound AP-6 did have a better score than ilomastat in the molecular docking simulations and was projected to have better MMP-3 inhibition by the NFF-3 assay. Thus, it may be worthwhile to synthesize AP-6 to determine if it does outperform ilomastat. In addition, it would be worthwhile to do more molecular docking simulations, varying both the zinc binding group and the peptide backbone, to determine the zinc binding group with the best chelating ability and the backbone that fits the best in the MMP-3 subpockets.

While very few MMP-3 specific inhibitors exist, a study including a reversed 4-biaryl piperidine sulfonamide core, located next to the ZBG, bound specifically to the S1' subsite of MMP-3.⁵⁶ The inclusion of the sulfonamide core may help direct the remainder of the backbone into additional subpockets. When designing future backbones of MMP-3 inhibitors it will be important to take into consideration the amino acids that fit most favorably into each subpocket. From Eckhard et al. the most favorable amino acids for the MMP-3 active site are shown in Figure 5.2.1.

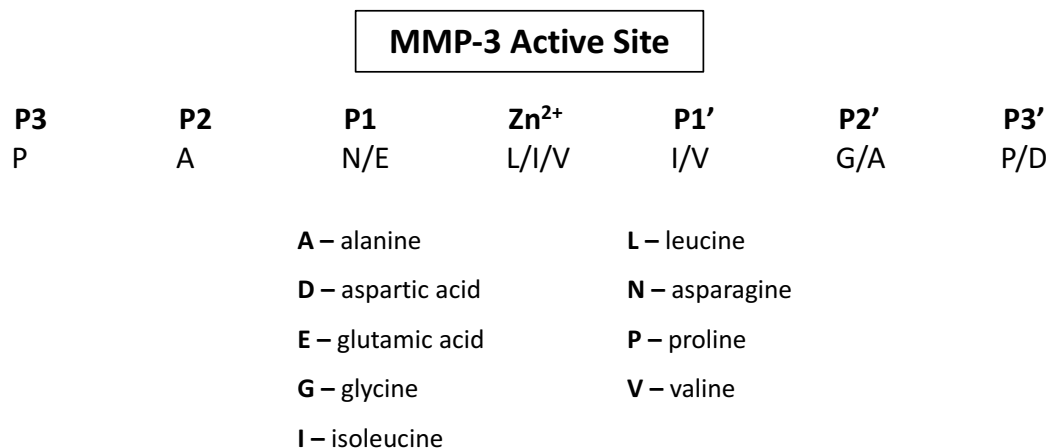


Figure 5.2.1: MMP-3 active site with amino acid preference for each subsite. Adapted from Eckhard et al. 2016.¹⁰³

This thesis showed that MMP-3 inhibition is capable in C6-13 cells, but we were unable to demonstrate whether MMP-3 inhibition has an impact on migration. Further studies into MMP-3 inhibition on migration and invasion are needed. Such studies could include a scratch wound assay incorporating Matrigel, 3D spheroid invasion assay, or a transwell assay, all of which would be better representations of migration and invasion due to the synthetic ECM environment. The 3D spheroid assay and transwell assay are both better *in vitro* models to simulate the process that occurs *in vivo*.

Studies on MMP-3 should be continued because MMP-3 upregulation is not only seen in the C6-13 GBM cells. MMP-3 upregulation also occurs in breast, gastric, and lung cancer, corresponding to increased cancer progression and metastasis.¹⁰⁴ Further understanding of MMP-3, the pathways upstream and downstream, may offer insight into the mechanism of cancer while providing new avenues for development of therapeutics to inhibit the disease.

References

1. Pan American Health Organization. Available at:
http://www.paho.org/hq/index.php?option=com_content&view=article&id=292&Itemid=3904&lang=en.
2. Canadian Cancer Society. Available at: <http://www.cancer.ca/en/cancer-information/cancer-101/cancer-statistics-at-a-glance/?region=mb>.
3. Yuan, X. *et al.* Isolation of cancer stem cells from adult glioblastoma multiforme. *Oncogene* **23**, 9392–9400 (2004).
4. Lieberman, F. Glioblastoma update: molecular biology, diagnosis, treatment, response assessment, and translational clinical trials. *F1000Research* **6**, 1–8 (2017).
5. McLendon, R. *et al.* Comprehensive genomic characterization defines human glioblastoma genes and core pathways. *Nature* **455**, 1061–1068 (2008).
6. Holland, E. C. Glioblastoma multiforme: The terminator. *Proc. Natl. Acad. Sci.* **97**, 6242–6244 (2000).
7. TCGA-GBM. Available at: https://portal.gdc.cancer.gov/projects/TCGA-GBM?genesTable_size=60.
8. Louis, D. N. *et al.* The 2007 WHO classification of tumours of the central nervous system. *Acta Neuropathol.* **114**, 97–109 (2007).
9. WHO Grading System. Available at: <https://www.braintumour.ca/4901/who-grading-system>.
10. Louis, D. N., Holland, E. C. & Cairncross, J. G. Glioma classification: A molecular

- reappraisal. *Am. J. Pathol.* **159**, 779–786 (2001).
11. Buczkowicz, P. & Hawkins, C. Pathology, Molecular Genetics, and Epigenetics of Diffuse Intrinsic Pontine Glioma. *Front. Oncol.* **5**, (2015).
 12. Louis, D. N. *et al.* The 2016 World Health Organization Classification of Tumors of the Central Nervous System: a summary. *Acta Neuropathol.* **131**, 803–820 (2016).
 13. Cancer Browser. Available at:
http://cancer.sanger.ac.uk/cosmic/browse/tissue?wgs=off&sn=central_nervous_system&ss=all&hn=glioma&sh=astrocytoma_Grade_IV&in=t&src=tissue&all_data=n.
 14. Cohen, A., Holmen, S. & Colman, H. IDH1 and IDH2 Mutations in Gliomas. *Curr. Neurol. Neurosci. Rep.* **13**, 345. (2013).
 15. Association, A. B. T. Glioblastoma (GBM). (2018). Available at:
https://www.abta.org/tumor_types/glioblastoma-gbm/. (Accessed: 29th October 2018)
 16. Phillips, H. S. *et al.* Molecular subclasses of high-grade glioma predict prognosis, delineate a pattern of disease progression, and resemble stages in neurogenesis. *Cancer Cell* **9**, 157–173 (2006).
 17. Roel G.W. Verhaak, Katherine A. Hoadley, Elizabeth Purdom, Victoria Wang, Yuan Qi, Matthew D. Wilkerson, C. Ryan Miller, Li Ding, Todd Golub, Jill P. Mesirov, Gabriele Alexe, Michael Lawrence, Michael O’Kelly, Pablo Tamayo, Barbara A. Weir, Stacey Gabriel, and T. C. G. A. R. N. An integrated genomic analysis identifies clinically relevant subtypes of glioblastoma characterized by abnormalities in PDGFRA, IDH1, EGFR and NF1. *Cancer Cell* **17**, 1–25 (2010).
 18. Soomro, S. H., Ting, L. R., Qing, Y. Y. & Ren, M. Molecular biology of glioblastoma:

- Classification and mutational locations. *J. Pak. Med. Assoc.* **67**, 1410–1414 (2017).
19. Van Meir, E. G. *et al.* Exciting New Advances in Neuro-Oncology: The Avenue to a Cure for Malignant Glioma. *CA. Cancer J. Clin.* **60**, 166–193 (2010).
 20. Xu, Y. *et al.* Procollagen-lysine 2-oxoglutarate 5-dioxygenase 2 promotes hypoxia-induced glioma migration and invasion. *Oncotarget* **8**, 23401–23413 (2017).
 21. Formolo, C. a *et al.* Secretome signature of invasive glioblastoma multiforme. *J Proteome Res.* **10**, 3149–3159 (2011).
 22. Paw, I., Carpenter, R. C., Watabe, K., Debinski, W. & Lo, H.-W. Mechanisms Regulating Glioma Invasion. *Cancer* **362**, 1–7 (2015).
 23. Sangar, V. *et al.* Quantitative proteomic analysis reveals effects of EGFR on invasion-promoting proteins secreted by glioblastoma cells. *Mol. Cell. Proteomics* 2618–2631 (2014). doi:10.1074/mcp.M114.040428
 24. Friedl, P. & Wolf, K. Tube travel: The role of proteases in individual and collective cancer cell invasion. *Cancer Res.* **68**, 7247–7249 (2008).
 25. Friedl, P. & Alexander, S. Cancer invasion and the microenvironment: Plasticity and reciprocity. *Cell* **147**, 992–1009 (2011).
 26. Gialeli, C., Theocharis, A. D. & Karamanos, N. K. Roles of matrix metalloproteinases in cancer progression and their pharmacological targeting. *FEBS J.* **278**, 16–27 (2011).
 27. Rasmussen, H. S. & Mccann, P. P. Matrix Metalloproteinase Inhibition as a Novel Anticancer Strategy : A Review with Special Focus on Batimastat and Marimastat. *Pharmacol. Ther.* **75**, 69–75 (1997).
 28. Schito, L. & Semenza, G. L. Hypoxia-Inducible Factors: Master Regulators of Cancer

- Progression. *Trends in Cancer* **2**, 758–770 (2016).
29. Joseph, J. V. *et al.* Hypoxia enhances migration and invasion in glioblastoma by promoting a mesenchymal shift mediated by the HIF1 α -ZEB1 axis. *Cancer Lett.* **359**, 107–116 (2015).
 30. Roos, A., Ding, Z., Loftus, J. C., Tran, N. L. & Forrendinis, C. J. Molecular and Microenvironmental Determinants of Glioma Stem-Like Cell Survival and invasion. *Frontiers (Boulder)*. **7**, 1–8 (2017).
 31. Masoud, G. N. & Li, W. HIF-1 α pathway: Role, regulation and intervention for cancer therapy. *Acta Pharm. Sin. B* **5**, 378–389 (2015).
 32. Wang, G. L., Jiang, B. H., Rue, E. A. & Semenza, G. L. Hypoxia-inducible factor 1 is a basic-helix-loop-helix-PAS heterodimer regulated by cellular O₂ tension. *Proc. Natl. Acad. Sci.* **92**, 5510–5514 (1995).
 33. Søndergaard, K. L., Hilton, D. a, Penney, M., Ollerenshaw, M. & Demaine, a G. Expression of hypoxia-inducible factor 1 α in tumours of patients with glioblastoma. *Neuropathol. Appl. Neurobiol.* **28**, 210–7 (2002).
 34. Wu, X., Qiao, B., Liu, Q. & Zhang, W. Upregulation of extracellular matrix metalloproteinase inducer promotes hypoxia-induced epithelial-mesenchymal transition in esophageal cancer. *Mol. Med. Rep.* **12**, 7419–7424 (2015).
 35. Colwell, N. *et al.* Hypoxia in the glioblastoma microenvironment: Shaping the phenotype of cancer stem-like cells. *Neuro. Oncol.* **19**, 887–896 (2017).
 36. Kallio, P. J., Pongratz, I., Gradin, K., McGuire, J. & Poellinger, L. Activation of hypoxia-inducible factor 1 α : posttranscriptional regulation and conformational change by

- recruitment of the Arnt transcription factor. *Proc. Natl. Acad. Sci. U. S. A.* **94**, 5667–72 (1997).
37. Friedl, P. & Wolf, K. Tumour-cell invasion and migration: Diversity and escape mechanisms. *Nat. Rev. Cancer* **3**, 362–374 (2003).
 38. Brat, D. J. *et al.* Pseudopalisades in Glioblastoma Are Hypoxic, Express Extracellular Matrix Proteases, and Are Formed by an Actively Migrating Cell Population. *Cancer Res.* **64**, 920–927 (2004).
 39. Inukai, M. *et al.* Hypoxia-mediated cancer stem cells in pseudopalisades with activation of hypoxia-inducible factor-1 α /Akt axis in glioblastoma. *Hum. Pathol.* **46**, 1496–1505 (2015).
 40. Hynes, R. O. Integrins: Bidirectional, allosteric signaling machines. *Cell* **110**, 673–687 (2002).
 41. Mueller, S. C. *et al.* A novel protease-docking function of integrin at invadopodia. *J. Biol. Chem.* **274**, 24947–24952 (1999).
 42. Friedl, P. *et al.* Migration of highly aggressive MV3 melanoma cells in 3-dimensional collagen lattices results in local matrix reorganization and shedding of $\alpha 2$ and $\beta 1$ integrins and CD44. *Cancer Res.* **57**, 2061–2070 (1997).
 43. Payne, L. S. & Huang, P. H. The pathobiology of collagens in glioma. *Mol Cancer Res* **11**, 1–21 (2013).
 44. Demuth, T. & Berens, M. E. Molecular mechanisms of glioma cell migration and invasion. *J. if Neuro-Oncology* **70**, 217–228 (2004).
 45. Ohnishi, T. *et al.* Fibronectin-mediated cell migration promotes glioma cell invasion

- through chemokinetic activity. *Clin. Exp. Metastasis* **15**, 538–546 (1997).
46. Mahesparan, R. *et al.* Extracellular matrix-induced cell migration from glioblastoma biopsy specimens in vitro. *Acta Neuropathol.* **97**, 231–239 (1999).
 47. Botos, I., Scapozza, L., Zhang, D., Liotrat, L. a & Meyer, E. F. Batimastat, a potent matrix metalloproteinase inhibitor, exhibits an unexpected model of binding. *Proc. Natl. Acad. Sci.* **93**, 2749–2754 (1996).
 48. Vandenbroucke, R. E. & Libert, C. Is there new hope for therapeutic matrix metalloproteinase inhibition ? *Nat. Publ. Gr.* 1–24 (2014). doi:10.1038/nrd4390
 49. Zhang, J. *et al.* Design, synthesis and preliminary evaluation of α -sulfonyl γ -(glyciny-amino)proline peptidomimetics as matrix metalloproteinase inhibitors. *Bioorg. Med. Chem.* **22**, 3055–3064 (2014).
 50. Li, N. G., Tang, Y. P., Duan, J. A. & Shi, Z. H. Matrix metalloproteinase inhibitors: a patent review (2011 - 2013). *Expert Opin. Ther. Pat.* **24**, 1039–1052 (2014).
 51. Alberts, B. *et al.* *Molecular Biology of The Cell.* (2002).
 52. Serres, E. *et al.* Fibronectin expression in glioblastomas promotes cell cohesion, collective invasion of basement membrane in vitro and orthotopic tumor growth in mice. *Oncogene* **33**, 3451–3462 (2014).
 53. Jiao, Y. *et al.* Matrix metalloproteinase-2 promotes avb3 integrin-mediated adhesion and migration of human melanoma cells by cleaving fibronectin. *PLoS One* **7**, (2012).
 54. Jacobsen, J. A., Major Jourden, J. L., Miller, M. T. & Cohen, S. M. To bind zinc or not to bind zinc: An examination of innovative approaches to improved metalloproteinase inhibition. *Biochim. Biophys. Acta - Mol. Cell Res.* **1803**, 72–94 (2010).

55. Overall, C. M. & López-Otín, C. Strategies for MMP inhibition in cancer: innovations for the post-trial era. *Nat. Rev. Cancer* **2**, 657–672 (2002).
56. Rossello, A. & Nuti, E. Drug Design of Sulfonylated MMP Inhibitors. *Drug Des. Zinc-Enzyme Inhib. Funct. Struct. Dis. Appl.* 549–589 (2009).
doi:10.1002/9780470508169.ch25
57. Wild-Bode, C., Weller, M. & Wick, W. Molecular determinants of glioma cell migration and invasion. *J. Neurosurg.* **94**, 978–84 (2001).
58. Zheng, X., Chopp, M., Lu, Y., Buller, B. & Jiang, F. MiR-15b and miR-152 reduce glioma cell invasion and angiogenesis via NRP-2 and MMP-3. *Cancer Lett.* **329**, 146–154 (2013).
59. Zhu, D., Caveney, S., Kidder, G. M. & Naus, C. C. G. Transfection of C6 glioma cells with connexin43 cDNA : analysis of intercellular coupling. *J. Cell Biol.* **111–5(2)**, 154a (1990).
60. Supplement Table S1: List of mammalian MMPs and their major substrates. Available at: https://erj.ersjournals.com/content/erj/suppl/2012/07/10/09031936.00209911v1.DC1/Supplement_file_ERJ-02099-2011.pdf.
61. Benda, P., Lightbody, J., Sato, G. Differentiated rat glial cell strain in tissue culture. *Science (80-.)*. 370–371 (1968).
62. Schmidek, H., Nielsen, S. & Schiller, A. Morphological studies of rat brain tumors induced by N-nitrosomethylurea. *J Neurosurg.* 335–340 (1971).
63. Asai, A., Miyagi, Y., Sugiyama, A. & et al. Negative effects of wild-type p53 and s-myc on cellular growth and tumorigenicity of glioma cells. Implication of the tumor suppressor genes for gene therapy. *J Neurooncol.* 259–268 (1994).
64. Sibenaller, Z., Etame, A., Ali, M. & Al., E. Genetic characterization of commonly used

- glioma cell lines in the rat animal model system. *Neurosurg Focus* (2005).
65. Barth, R. F. & Kaur, B. Rat brain tumor models in experimental neuro-oncology: the C6, 9L, T9, RG2, F98, BT4C, RT-2 and CNS-1 gliomas. *Neuro. Oncol.* **94**, 299–312 (2010).
 66. Zhang, W. *et al.* Increased invasive capacity of connexin43-overexpressing malignant glioma cells. *J. Neurosurg.* **99**, 1039–46 (2003).
 67. Mesnil, M. *et al.* Cx43-associated secretome and interactome reveal synergistic mechanisms for glioma migration and MMP3 activation (In Review). *Front. Neurosci.* (2019).
 68. Knight, C. G., Willenbrock, F. & Murphy, G. A novel coumarin-labelled peptide for sensitive continuous assays of the matrix metalloproteinases. *FEBS Lett.* **296**, 263–266 (1992).
 69. Nagase, H., Fields, C. G. & Fields, G. B. Design and characterization of a fluorogenic substrate selectively hydrolyzed by stromelysin 1 (matrix metalloproteinase-3). *J. Biol. Chem.* **269**, 20952–20957 (1994).
 70. Fields, G. B. Using Fluorogenic Peptide Substrates to Assay Matrix Metalloproteinases. *Methods Mol Biol* **151**, 495–518 (2001).
 71. Giricz, O., Lauer, J. L. & Fields, G. B. Comparison of Metalloproteinase Protein and Activity Profiling. *Anal Biochem* **409**, 37–45 (2011).
 72. Qvit, N., Rubin, S. J. S., Urban, T. J., Mochly-Rosen, D. & Gross, E. R. Peptidomimetic therapeutics: scientific approaches and opportunities. *Drug Discov. Today* **00**, (2016).
 73. Boyden, T., Niosi, M. & Vaz*, A. Chapter 8. Peptidomimetics and Peptides as Drugs: Motifs Incorporated to Enhance Drug Characteristics. *Structure* **0**, 370–389 (2010).

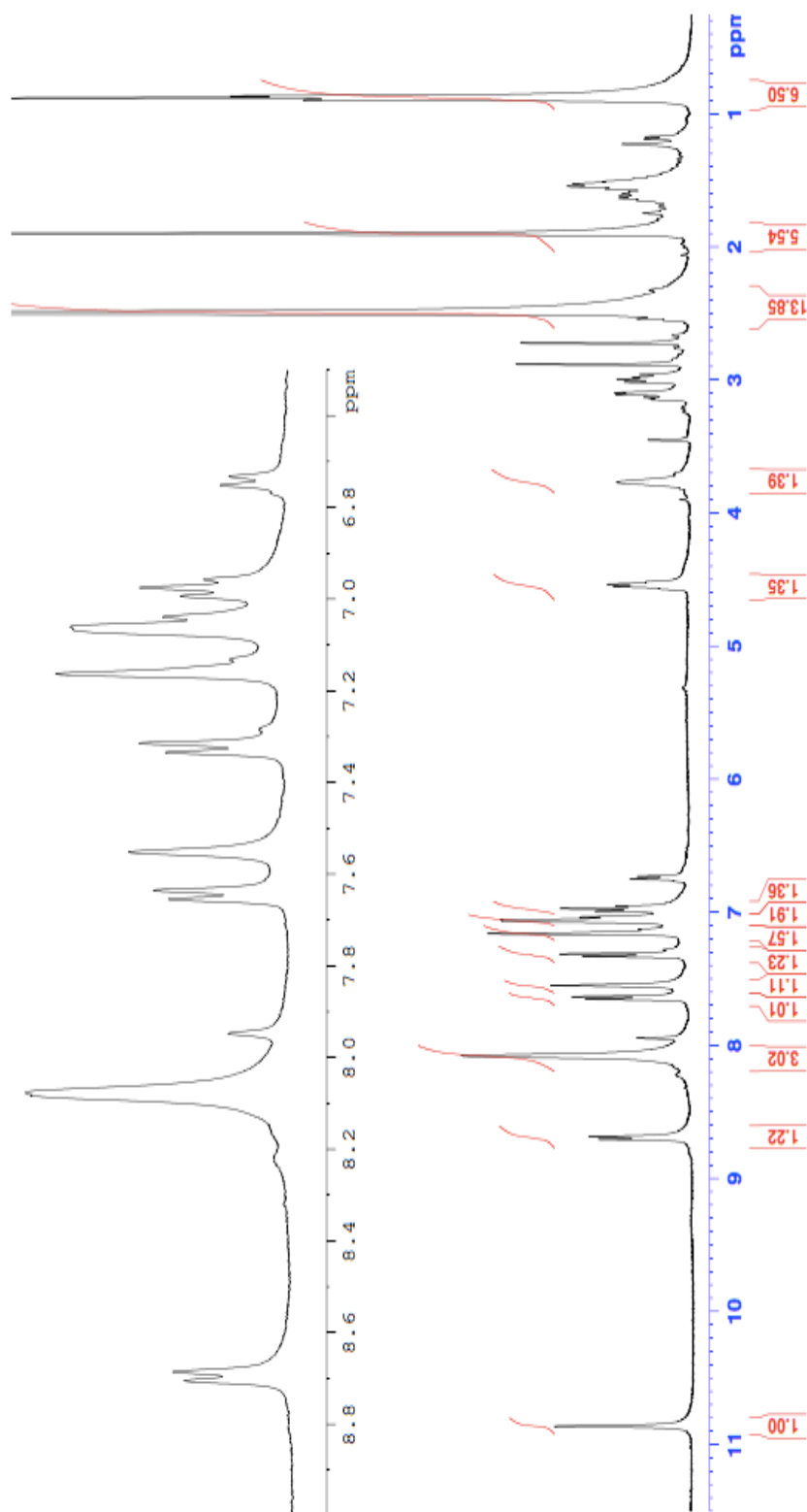
74. Gokhale, A. S. & Satyanarayanajois, S. Peptides and peptidomimetics as immunomodulators. *Immunotherapy* **6**, 755–774 (2014).
75. Kanthala, S. *et al.* Novel Peptidomimetics for Inhibition of HER2:HER3 Heterodimerization in HER2-Positive Breast Cancer. *Chem Biol Drug Des.* **85**, 702–714 (2015).
76. Wang, X. *et al.* Development of peptidomimetic inhibitors of the ERG gene fusion product in prostate cancer. *Cancer Cell* **31**, 532–548 (2017).
77. Betz, M. *et al.* 1.8-Å Crystal Structure of the Catalytic Domain of Human Neutrophil Collagenase (Matrix Metalloproteinase-8) Complexed With a Peptidomimetic Hydroxamate Primed-Side Inhibitor With a Distinct Selectivity Profile. *Eur. J. Biochem.* **247**, 356–363 (1997).
78. Nagase, H. & Fields, G. B. Human matrix metalloproteinase specificity studies using collagen sequence-based synthetic peptides. *Biopolymers* **40**, 399–416 (1996).
79. Song, J. *et al.* Selective non-zinc binding MMP-2 inhibitors: Novel benzamide Ilomastat analogs with anti-tumor metastasis. *Bioorganic Med. Chem. Lett.* **26**, 2174–2178 (2016).
80. Brown, P. D. Clinical studies with matrix metalloproteinase inhibitors. *Apmis* **107**, 174–180 (1999).
81. Giustiniano, M. *et al.* Amino Acid derivatives as new zinc binding groups for the design of selective matrix metalloproteinase inhibitors. *J. Amino Acids* **2013**, 178381 (2013).
82. Muñoz-Nájjar, U. M., Neurath, K. M., Vumbaca, F. & Claffey, K. P. Hypoxia stimulates breast carcinoma cell invasion through MT1-MMP and MMP-2 activation. *Oncogene* **25**, 2379–92 (2006).
83. Chen, Y. & Maret, W. Catalytic oxidation of zinc/sulfur coordination sites in proteins by

- selenium compounds. *Antioxid Redox Signal* **3**, 651–656 (2001).
84. Ekins, S., Mestres, J. & Testa, B. In silico pharmacology for drug discovery: Methods for virtual ligand screening and profiling. *Br. J. Pharmacol.* **152**, 9–20 (2007).
 85. Duhovny, D. S., Nussinov, R. & Wolfson, H. J. Predicting molecular interactions in silico: II. Protein-protein and protein-drug docking. *Curr Med Chem* **11**, 91–107 (2004).
 86. Edwards, B. S. & Sklar, L. A. Flow Cytometry: Impact on Early Drug Discovery. *J Biomol Screen* **20**, 689–707 (2015).
 87. Wlodkowic, D., Skommer, J. & Darzynkiewicz, Z. Flow cytometry-based apoptosis detection. *Methods Mol Biol.* **559**, 1–14 (2009).
 88. Abcam. Introduction to Flow Cytometry. (2018). Available at: <https://www.abcam.com/protocols/introduction-to-flow-cytometry>. (Accessed: 25th October 2018)
 89. Darzynkiewicz, Z., Bedner, E. & Smolewski, P. Flow cytometry in analysis of cell cycle and apoptosis. *Semin. Hematol.* **38**, 179–193 (2001).
 90. Rieger, A. M., Nelson, K. L., Konowalchuk, J. D. & Barreda, D. R. Modified Annexin V/Propidium Iodide Apoptosis Assay For Accurate Assessment of Cell Death. *J. Vis. Exp.* 3–6 (2011). doi:10.3791/2597
 91. Crowley, L. C. *et al.* Measuring cell death by propidium iodide uptake and flow cytometry. *Cold Spring Harb. Protoc.* **2016**, 647–651 (2016).
 92. Kupai, K. *et al.* Journal of Pharmacological and Toxicological Methods Matrix metalloproteinase activity assays : Importance of zymography. *J. Pharmacol. Toxicol. Methods* **61**, 205–209 (2010).

93. Snoek-van Beurden, P. A. M. & Von den Hoff, J. W. Zymographic techniques for the analysis of matrix metalloproteinases and their inhibitors. *Biotechniques* **73**–83 (2005).
94. Springman, E. B., Angleton, E. L., Birkedal-Hansen, H. & Van Wart, H. E. Multiple modes of activation of latent human fibroblast collagenase: evidence for the role of a Cys73 active-site zinc complex in latency and a ‘cysteine switch’ mechanism for activation. *Proc. Natl. Acad. Sci.* **87**, 364–368 (1990).
95. Hulkower, K. I. & Herber, R. L. Cell migration and invasion assays as tools for drug discovery. *Pharmaceutics* **3**, 107–124 (2011).
96. Liang, C. C., Park, A. Y. & Guan, J. L. In vitro scratch assay: A convenient and inexpensive method for analysis of cell migration in vitro. *Nat. Protoc.* **2**, 329–333 (2007).
97. Jonkman, J. E. N. *et al.* An introduction to the wound healing assay using livecell microscopy An introduction to the wound healing assay using live cell microscopy. *Cell Adh. Migr.* **8**, 440–451 (2014).
98. Peng, J., Zheng, H., Wang, X. & Cheng, Z. Upregulation of TLR4 via PKC activation contributes to impaired wound healing in high-glucose-treated kidney proximal tubular cells. *PLoS One* **12**, 1–18 (2017).
99. Ishida, T. *et al.* Investigation of the influence of glucose concentration on cancer cells by using a microfluidic gradient generator without the induction of large shear stress. *Micromachines* **7**, (2016).
100. Kam, Y., Guess, C., Estrada, L., Weidow, B. & Quaranta, V. A novel circular invasion assay mimics in vivo invasive behavior of cancer cell lines and distinguishes single-cell motility in vitro. *BMC Cancer* **8**, 1–12 (2008).

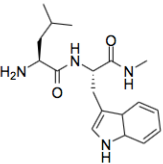
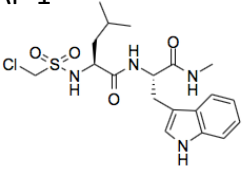
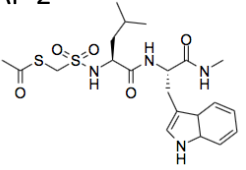
101. Yan, S. *et al.* MMP inhibitor Ilomastat induced amoeboid-like motility via activation of the Rho signaling pathway in glioblastoma cells. *Tumor Biol.* **37**, 16177–16186 (2016).
102. Swartz, M. a *et al.* Tumor Microenvironment Complexity: Emerging Roles in Cancer Therapy. *Cancer Res.* **72**, 2473–2480 (2012).
103. Eckhard, U. *et al.* Active site specificity profiling of the matrix metalloproteinase family: Proteomic identification of 4300 cleavage sites by nine MMPs explored with structural and synthetic peptide cleavage analyses. *Matrix Biol.* **49**, 37–60 (2016).
104. Jiang, Y. N. *et al.* Interleukin 6 triggered ataxia-telangiectasia mutated activation facilitates lung cancer metastasis via MMP-3/MMP-13 up-regulation. *Oncotarget* **6**, 40719–40733 (2015).

Appendix 1



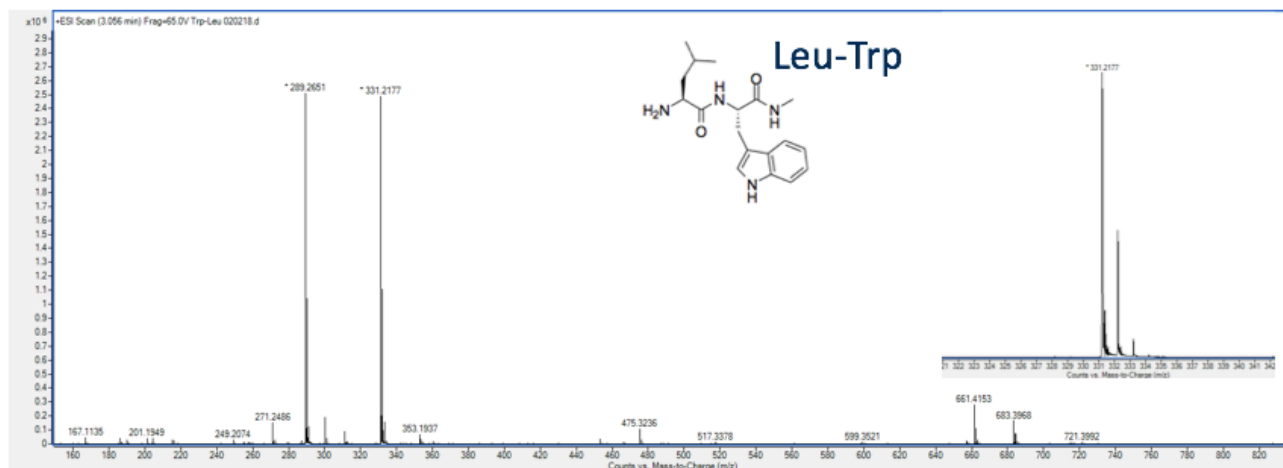
Appendix 1: ^1H -NMR of tryptophan-leucine backbone. The peak at ~11 ppm corresponds to the H on the N of the Trp five carbon ring. The peaks around ~7 ppm correspond to Trp aromatic H. The peak just before ~1 ppm corresponds to the H on the methyl groups of leucine.

Appendix 2

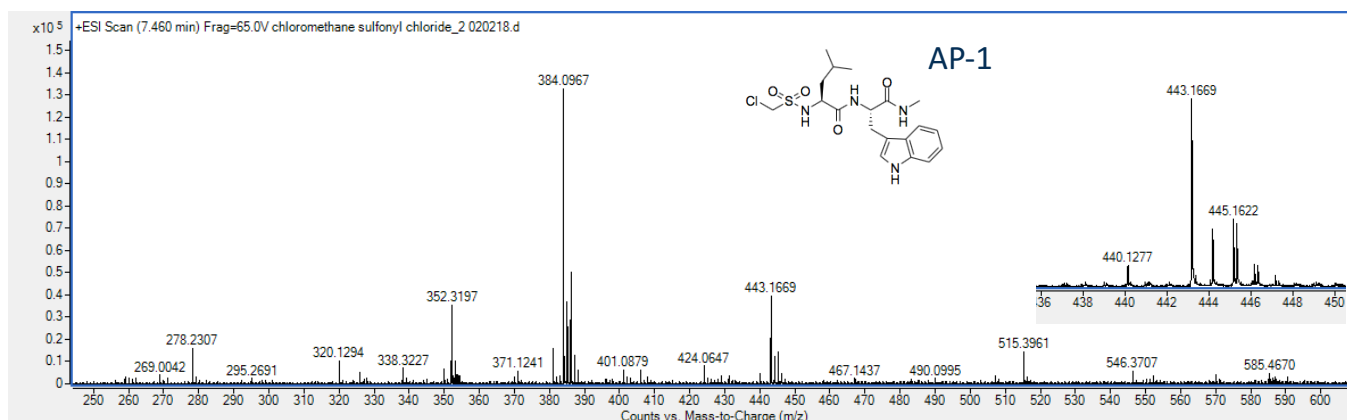
Compound	Monoisotopic (M) Mass	Theoretical M+H	Experimental M+H
Leu-Trp 	330.2056	331.2056	331.2177
AP-1 	442.1442	443.1442	443.1669
AP-2 	466.1708	467.1708	467.1723

Appendix 2: Monoisotopic (M) mass, theoretical M+H mass, and the experimental M+H determined by LC-MS/MS for the compounds Leu-Trp, AP-1, and AP-2.

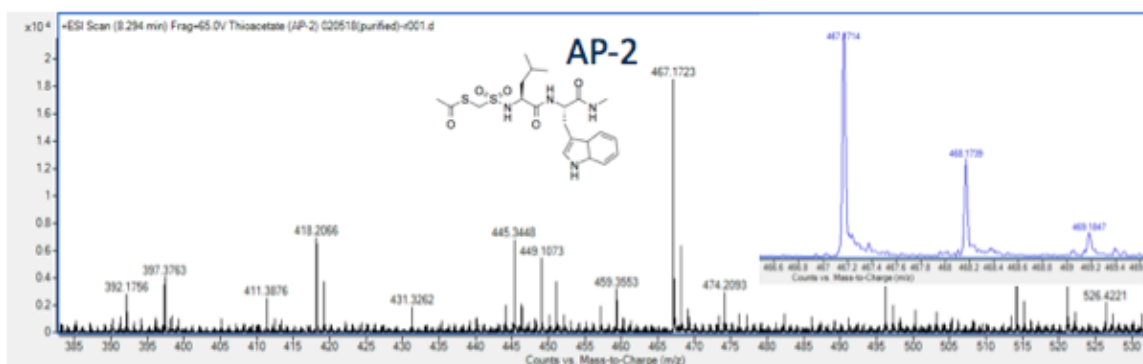
Appendix 3



$[M+H]^+$: 331.2056



$[M+H]^+$: 443.1442



[M+H]⁺: 467.1708

Appendix 3: Mass spectrometry results for Leu-Trp, AP-1, and AP-2. Experimental M+H values located under each spectra correspond to the peaks determined by mass spectrometry for each compound.